THE PROPAGATION OF ELECTROMAGNETIC WAVES

IN AN OVERDENSE PLASMA

by

ROBERT JOHN LA HAYE

A dissertation submitted to the Graduate Faculty in Physics in partial fulfillment of the requirements for the degree of Doctor of Philosophy, The City University of New York.

1975

This manuscript has been read and accepted for the Graduate Faculty in Physics in satisfaction of the dissertation requirement for the degree of Doctor of Philosophy.

7/10/75
date

L. A. Ferrari
Chairman of Examining Committee

7/18/75
date

Myriam P. Sarachik
Executive Officer

Norman H. Tolk

Lee Bernheim

C. R. Fischer

Supervisory Committee

The City University of New York

ABSTRACT

Linearly polarized electromagnetic waves with power densities up to 12 W/cm^2 (f=2.45 GHz) are propagated along an external static magnetic field in a cylindrical waveguide. The power is pulsed with a duration of about 4 msec. Plasma with density $n \approx 2 \times 10^{11}$/cc, $T_e \approx 8$ ev, and axial length ≈ 22 cm (defined by the length of the region for which $\omega_p/\omega \geq 1$) is produced by electron cyclotron resonance.

At this density the left component of the incident wave is nominally cut off. We find that approximately 25% of the left wave power is transmitted through the plasma while a linear theory predicts that less than 0.01% of the incident power should tunnel through. Dynamic measurements of the plasma density and electromagnetic field profiles during the transmission period were made and both show a transition from peaked on axis to annular configurations.

Transmission of the left wave occurs for a time τ after the beginning of the microwave pulse until at $t=\tau$ it abruptly ceases and the plasma becomes opaque to both the left and right handed incident electromagnetic waves.

ACKNOWLEDGEMENTS

I would like to acknowledge the guidance and assistance of Prof. Lawrence A. Ferrari, without whom this thesis would not have been possible.

Paul A. Schaedler turned many of the author's crude drawings into instruments with which this work could be done. Charles J. Spiteri provided assistance with many of the electronic devices. Walter B. Koch showed the author how to do the ink drawings and acted as purchasing agent for many of the devices and materials used to do this work.

Finally, I would like to thank Arthur W. McQuade with whom the author spent so many afternoons on the experiment accumulating the data.

TABLE OF CONTENTS

I. INTRODUCTION

The general problem of the interaction of high power electromagnetic waves with plasma is of current topical interest because of its application to plasma heating. The power densities available, either from lasers or microwave tubes, are large enough so that non-linear processes are usually encountered in schemes that use electromagnetic (EM) wave power for heating.

In this thesis we are concerned with the non-linear penetration of EM waves in a magnetized plasma. We report what we believe to be the first clear unambiguous observation of EM wave penetration into and through an overdense plasma. We also report what we believe to be the first detailed dynamic measurements of the plasma density and EM field distributions in the plasma during the penetration or transmission phase. In addition, after a period of transmission, the incident EM wave is observed to be almost completely absorbed with a subsequent increase in the electron temperature.

The bulk of the experiments on non-linear wave propagation have been done in the U.S.S.R. in unmagnetized plasmas in oversized waveguides (guide radius much larger than the free space wavelength.) In our experiment we study the interaction of electromagnetic waves in a magnetized plasma contained in a cylindrical conducting waveguide whose radius is less than half of the free space wavelength. In vacuo only the dominant TE_{11} mode can propagate. This reduces two problems: the ambiguity in which modes are excited in the waveguide and the attenuation of the wave amplitude by beam spreading.

Plasma is produced by electron cyclotron resonance. The external D.C. magnetic field is in a mirror configuration. The left handed component of the incident linearly polarized electromagnetic wave is of principal interest in this study and in the absence of collisions at the frequency used here plays no role in plasma production or heating according to the linear theory. A disadvantage of the experimental configuration is that the small amplitude linear behavior of the left wave is difficult to study, as reducing the left wave incident power greatly also reduces the right wave incident power which maintains

the plasma by electron cyclotron resonance (ECR.) Plasma production by ECR procedes in the following way: the electric field vector of the right handed electromagnetic wave rotates in the same sense about the static magnetic field as the electrons do. If the wave frequency ω is adjusted to equal the local electron cyclotron frequency $|\omega_c|$, then in a coordinate system fixed to the electrons, the electrons are acted on by a static electric field, are accelerated, and make ionizing collisions with the neutral gas present. The technique is well known.

The method of electron cyclotron resonance as a technique to produce and maintain a hot electron plasma has been used at Oak Ridge[1,2] in the EPA mirror machine (50 kw at 10.6 GHz producing an electron temperature Te of about 120 kev and a density n of about 4 - 7 x 10^{11}/cc) and the PTF mirror machine (5 kw at 10.6 GHz yielding plasmas of Te $<$ 200 ev and similar density.) Similar machines have been used effectively for producing hot electron plasmas at Kurchatov[3] and at Princeton[4]. The emphasis in these experiments was to produce a hot electron plasma as the first stage of forming a dense hot ion plasma and also to study instabilities (in particular the production of x-rays and neutrons) during and after the heating phase. Little interest was shown in these experiments on the wave propagation characteristics of the plasma.

In 1969 Gekker and Sizukhin[5] directed linearly polarized electromagnetic waves at an overdense unmagnetized plasma (the wave frequency ω is less than the plasma frequency ω_p.) For incident electric fields Eo well below 100 V/cm, they observed complete reflection of the incident wave as predicted by linear theory. However for Eo $>$ 100 V/cm, both reflection and transmission of the wave went to zero indicating strong absorption. No probing of the plasma density distribution or distribution of fields in the plasma was made in this experiment. This appears to be the first of a series of experiments in recent years that deal with the non-linear effects of wave propagation in plasmas.

Kaw, Valeo, and Dawson[6] (1970) interpreted the absorption as being caused by a parametric instability in which the EM wave of frequency ω decays into an electron plasma wave of frequency ω_p and an ion acoustic wave of frequency ω_{ia}. The transfer of EM wave energy to the plasma is completed by the subsequent collisionless Landau damping[7] of

the electron plasma wave. The selection rules for such decay are

$$\omega = \omega_p + \omega_{ia} \tag{1}$$

$$\vec{K} = \vec{K}_p + \vec{K}_{ia} \tag{2}$$

$$m = m_p + m_{ia} \tag{3}$$

where the $\vec{k}$ are the wavenumbers and the m are the azimuthal orders.[8] The threshold power for the instability is governed by the growth rate which is found to be[6] proportional to Eo^2 minus a term proportional to the appropriate collision frequency ν . Thus a critical field

$$E_c \sim \nu^{1/2} \tag{4}$$

exists below which the instability does not grow and linear behavior holds. This interpretation of the anomalous absorption has not been verified as no observation of the excited plasma and ion acoustic waves was reported by Gekker and Sizukhin. It is not clear from their paper that they even searched for such a decay process.

Anomalous transmission of intense electromagnetic waves through a nominally overdense unmagnetized plasma has been reported by Brodskii et al[9] (1971) and by Batanov and Silin[10] (1971.) In the first case the neutral density is high; the EM wave heats the plasma through collisions by the oscillating electrons with the neutrals. The increased plasma pressure due to the local heating where the fields are strongest drives plasma out of these regions. The wave is then refracted into these lower density regions, thereby increasing the process. This process is called self-focusing. As a result a waveguide channel was

thought to open up which allowed propagation. However, no direct measurement of the change in the plasma density distribution was made.

In the experiment of Batanov and Silin, the transmission was believed to be caused by the large amplitude temporal density modulations ($\Delta n/n \gtrsim 1$) induced by the parametric decay of the strong pump EM wave into electron and ion plasma waves. The time averaged density was believed to be too high for strong transmission but the large slow density modulations caused by the ion wave were thought to allow the density to fall low enough every cycle for transmission to occur. However, no dynamic measurements of the plasma density were made to support this hypothesis.

Note that in both the anomalous transmission experiments just described what starts out as an overdense plasma is believed to eventually become at some point in space or time underdense through the non-linear action of the electromagnetic wave with the plasma.

Another experiment in which anomalous transmission through a nominally overdense unmagnetized plasma has been reported is that by Motz (1975.)[11] Power densities of up to 10^4 watts per sq. cm were used. No explanation of the phenomenon was offered and no probing of the density or field distributions within the plasma was mentioned.

One way in which an electromagnetic wave can rearrange the plasma density distribution is through its radiation pressure (ponderomotive force.) In general the establishment of a localized region of high fields sets up a radiation pressure which can maintain a low plasma density in this region against the higher plasma pressure outside.

Such an effect has been observed by Kim, Stenzel, and Wong[12] (1974) where a "caviton" of low plasma density grows where the EM fields are high. The effect is enhanced by occuring near the plasma cutoff ($\omega \approx \omega_p$) where the fields are strong.

Minami et al[13] (1974) have observed a non-linear skin depth in a collisionless magnetized plasma overdense to both the right and left handed electromagnetic waves used. The skin depth increased with increasing incident microwave power (up to 6×10^3 W/cm^2.) The effect was explained as being caused by the ponderomotive force of the in-

cident wave rearranging the plasma density distribution so as to allow deeper penetration. However, all measurements were made external to the plasma and thus the change in the density distribution was only assumed.

Self-focusing or filamentation of EM radiation in a plasma can be caused either by the ponderomotive force (in collisionless plasmas) or by ohmic heating (thermal deposition) in collision dominated plasmas where the mean free path for collisions is much shorter than both the wavelength and the size of the plasma.

The ponderomotive force was interpreted to be the mechanism which caused self-focusing of EM waves in a weakly ionized unmagnetized plasma in the experiment of Eremin and Litvak[14] (1971.) The change in the field distribution was measured external to the plasma and no accompanying measurement of the change in the density distribution was made at all.

Thome and Perkins[15] (1974) have observed the production of ionospheric striations by self-focusing of intense radio waves in the collision dominated magnetized ionosphere. Power densities up to 0.5 W/cm^2 were used. The heating of the plasma by collisional damping of the wave was interpreted by Perkins and Valeo[16] to cause the effect. The density change was inferred from the distribution of the reflected wave fields external to the plasma with no direct internal measurement of the change in density distribution. Of course in this case local probing is difficult if not impossible.

In this thesis a linearly polarized electromagnetic wave of power density up to 12 W/cm^2 is incident upon a longitudinally magnetized inhomogeneous overdense plasma ($\omega_{p\,MAX}^2/\omega^2 \approx 3$.) Anomalously high left handed wave power transmission is reported; on the basis of a linear theory less than 0.01% of the incident left wave power should tunnel through the overdense region while approximately 25% transmission is observed.

Dynamic measurements of the axial and radial plasma density distributions in which the wave propagates are presented as well as the time evolution of the distribution of the electromagnetic fields with-

in the plasma. By comparing the field and density distributions we show that the wave power is transmitted through an annular region in the plasma and that the transmission is not due to leakage around the plasma at the waveguide walls.

In addition, after a period of transmission, the left handed component of the incident electromagnetic wave is observed to be almost completely non-resonantly absorbed with a concurrent increase in the electron temperature. The dependence of the anomalous absorption on incident microwave power and on neutral hydrogen pressure is reported as well as the observation of radiation excited near the electron plasma frequency ($\gtrsim$ 4 GHz) upon the absorption taking place.

After a brief discussion of the experimental apparatus and a review of the pertinent plasma parameters for this experiment, the detailed experimental results are presented. The theoretical linear wave propagation characteristics for this experiment are discussed in appendix A. The methods of measuring the various plasma parameters are explained in appendix B.

1. REFERENCES

1. R.A. Dandl et al, Nuclear Fusion 4, 344 (1964.)

2. W.B. Ard et al, Physical Review Letters 10, 87 (1963.)

3. V.V. Alikaev et al, Plasma Physics 10, 753 (1968.)

4. L.A. Ferrari and A.F. Kuckes, Physics of Fluids 8, 2295 (1965.)

5. I.R. Gekker and O.V. Sizukhin, JETP Letters 9, 243 (1969.)

6. P. Kaw, E. Valeo, and J.M. Dawson, Phys. Rev. Letters 25, 430 (1970.)

7. L. Landau, J. Phys. U.S.S.R. 10, 25 (1946.)

8. G. Van Hoven and D.A. Phelps, Physics of Fluids 16, 495 (1973.)

9. Yu. Ya. Brodskii et al, JETP Letters 13, 95 (1971.)

10. G.M. Batanov and V.A. Silin, JETP Letters 14, 303 (1971.)

11. H. Motz, Annals of the New York Academy of Sciences 251, 89 (1975.)

12. H.C. Kim, R.L. Stenzel, and A.Y. Wong, Phys. Rev. Letters 33, 866 (1974.)

13. K. Minami et al, Phys. Rev. Letters 33, 740 (1974.)

14. B.G. Eremin and A.G. Litvak, JETP Letters 13, 430 (1971.)

15. G.D. Thome and F.W. Perkins, Phys. Rev. Letters 32, 1238 (1974.)

16. F.W. Perkins and E.J. Valeo, Phys. Rev. Letters 32, 1234 (1974.)

II. DESCRIPTION OF THE EXPERIMENT

1. APPARATUS

The basic experimental apparatus for this study is shown in Figure 1 . A thin stainless steel cylindrical waveguide with an I.D. of 8.78 cm and a wall thickness of 0.05 cm is located in an evacuated chamber with base pressure $\lesssim 2 \times 10^{-6}$ torr. Linearly polarized microwave power at 2.45 GHz and densities up to 12 watts/cm^2 are incident from the left. The power is pulsed and relatively constant for about 4 msec.

The axial external magnetic field has a mirror ratio of 1.20 and distance between field maxima of 44 cm. Local electron cyclotron resonance occurs at about 1.5 cm before and after the field minimum.

The input microwave system is shown in Figure 2 . Rectangular S-band waveguide (3″ x 1.5″ O.D.) is used. The input rectangular guide ends at +22 cm (see Figure 1) where it radiates through a kovar vacuum seal window into the cylindrical guide. The space between the walls of the rectangular guide and the cylindrical guide is filled with two semicircular pieces of aluminum.

The linearly polarized microwave power in the cylindrical vacuum guide excites the dominant TE_{11} mode which is the only propagating mode at 2.45 GHz. This is equivalent to the sum of a right hand rotating circularly polarized mode (RHCP) and a left hand mode (LHCP). In vacuo the two modes propagate with the same velocity and sum to give the linearly polarized TE_{11} mode.

Plasma is produced by electron cyclotron resonance. The RHCP component of the incident wave is strongly coupled to the plasma electrons. The working gas is hydrogen in the 10^{-4} torr pressure range.

RF and Langmuir probes can be inserted from the chamber end at right. A Langmuir probe can also be lowered through the waveguide wall at center. A diamagnetic coil at center monitors plasma pressure. K-band microwave horns cut into the waveguide walls at center are used in an interferometer to monitor average plasma density.

Both the 20 db coupler shown in Figure 2 and the 70 db coupler (when reversed) can be used to measure reflected power. The 70 db coupler as shown in Figure 2 can monitor incident microwave power.

FIGURE CAPTIONS

Fig. 1. Schematic diagram of the experimental apparatus. The inner diameter of the cylindrical waveguide is 8.79 cm. The input rectangular waveguide ends at z=+ 22 cm.

Fig. 2. Schematic of the system which feeds microwave power into the cylindrical waveguide.

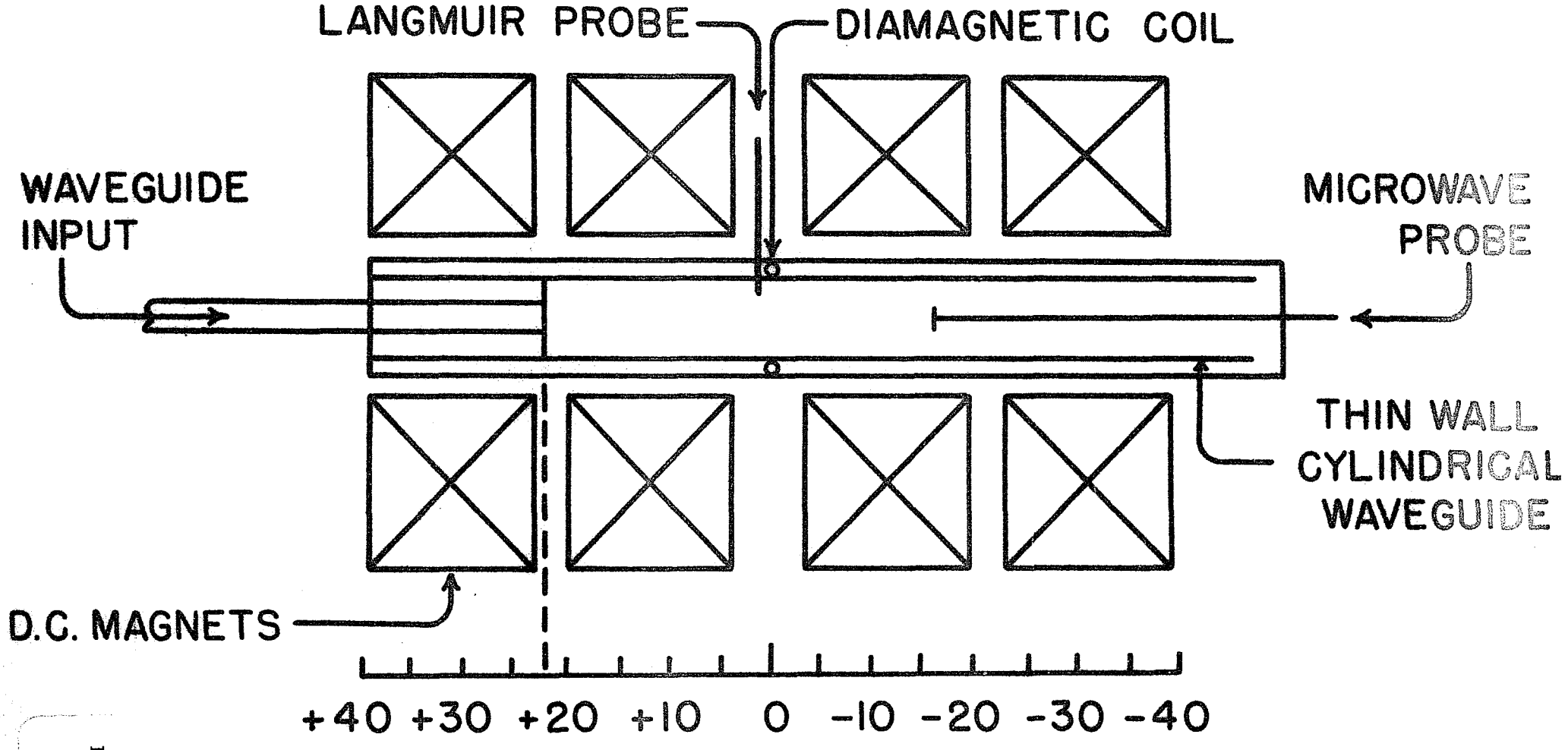
LANGMUIR PROBE
DIAMAGNETIC COIL
WAVEGUIDE INPUT
MICROWAVE PROBE
THIN WALL CYLINDRICAL WAVEGUIDE
D.C. MAGNETS
+40 +30 +20 +10 0 -10 -20 -30 -40
(CM)

Fig. 1

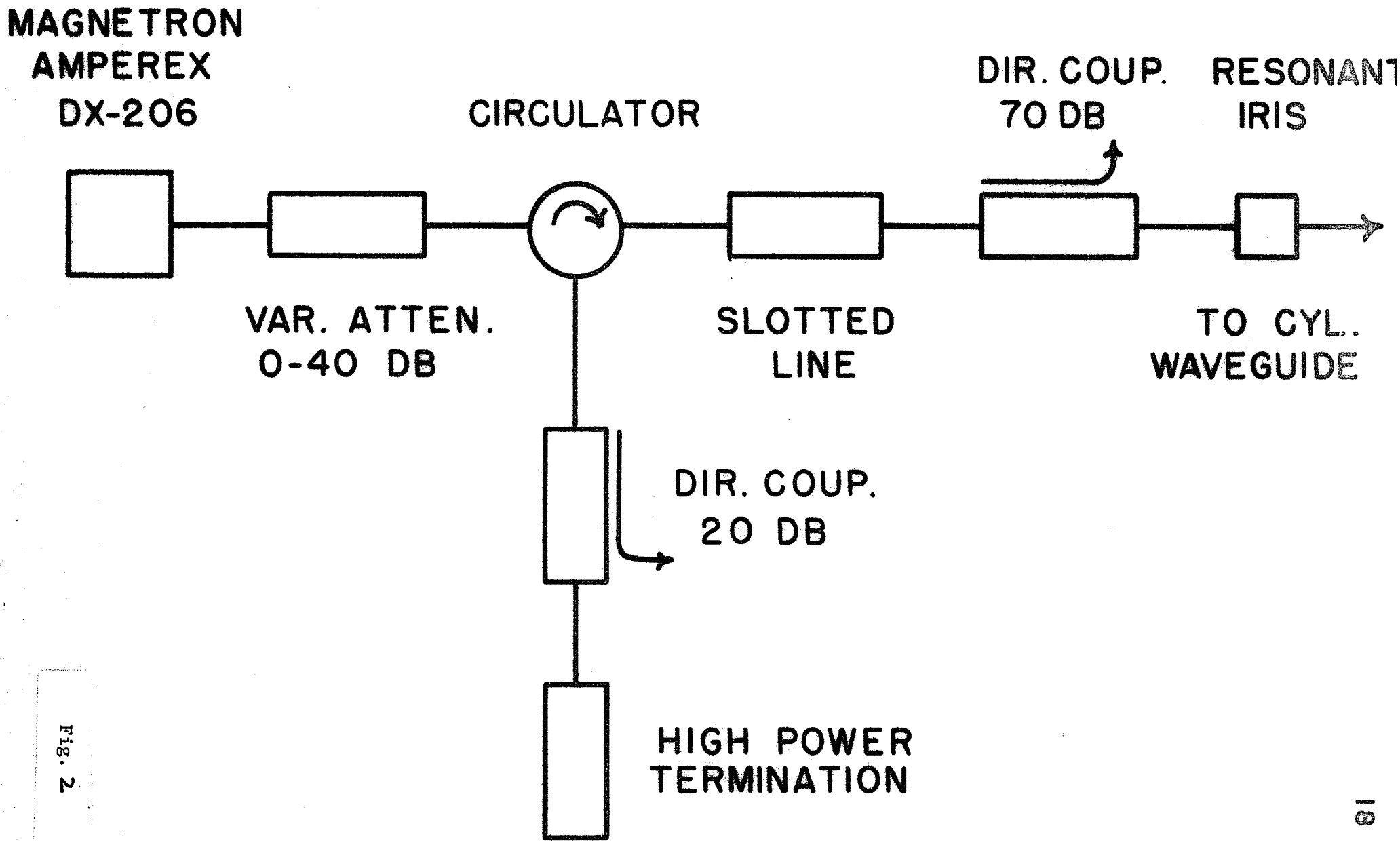
MAGNETRON
AMPEREX
DX-206
CIRCULATOR
DIR. COUP.
70 DB
RESONANT
IRIS
VAR. ATTEN.
0-40 DB
SLOTTED
LINE
TO CYL.
WAVEGUIDE
DIR. COUP.
20 DB
HIGH POWER
TERMINATION

Fig. 2

2. TYPICAL PARAMETERS

Details of the measurements of the various plasma parameters are discussed in appendix B. Typical values are to be noted here.

On the average the central plasma density n is $2 \times 10^{+11}$ /cc. This gives a plasma frequency of 4.02 GHz or $\omega_p^2/\omega^2 = 2.7$. The electron cyclotron frequency $|\omega_c|$ is no more than 20% higher than ω ($1.0 \leq |\omega_c|/\omega \leq 1.2$).

The electron temperature is about 8 ev. The ion temperature was not measured but was estimated to be 1/20 ev. Room temperature is 1/40 ev and through collisions with hot electrons the ions should acquire some energy. (See appendix C, page 118.) The resultant electron thermal speed is $1 \times 10^{+8}$ cm/sec and the ion thermal speed becomes $2 \times 10^{+5}$ cm/sec. The Debye length is 5×10^{-3} cm.

The ratio β of plasma pressure $nk_B T_e$ to static magnetic field pressure $B_o^2/8\pi$ is about 10^{-4} for $B_o = 875$ gauss. Because the plasma is fairly cold and has a very low β it should be stable to any magnetohydrodynamic instabilities.

A set of typical oscillograms is shown in Figure 3 . The upper trace is the integrated diamagnetic coil signal or perpendicular plasma pressure. The middle trace gives the crystal rectified RF probe signal or microwave power. The lower trace shows incident microwave power. The plasma pressure increases during breakdown of the hydrogen gas and then levels off. Microwave power is transmitted through the plasma for 1. msec and then ceases with a corresponding rise in plasma pressure. Reflected microwave power effectively goes to zero at this point so that both the RHCP and LHCP electromagnetic waves are being absorbed and thus heating the plasma ($p_\perp$ rises with n constant).

Figure 4 depicts the top and middle traces on an expanded time scale. Both traces are modulated at a frequency of about 75 KHz.

A number of parameters discussed elsewhere in the thesis are collected in Table I for comparison.

FIGURE CAPTIONS

Fig. 3. Typical oscillograms at a time scale of one msec per division. The integrated diamagnetic coil signal which is proportional to the perpendicular plasma pressure is shown on top. The RF dipole probe signal after microwave crystal rectification (the crystal output is proportional to power) is in the middle. The crystal rectified incident microwave power is on the bottom.

Fig. 4. The same oscillograms as in Fig. 3 but at a time scale of 0.1 msec per division.

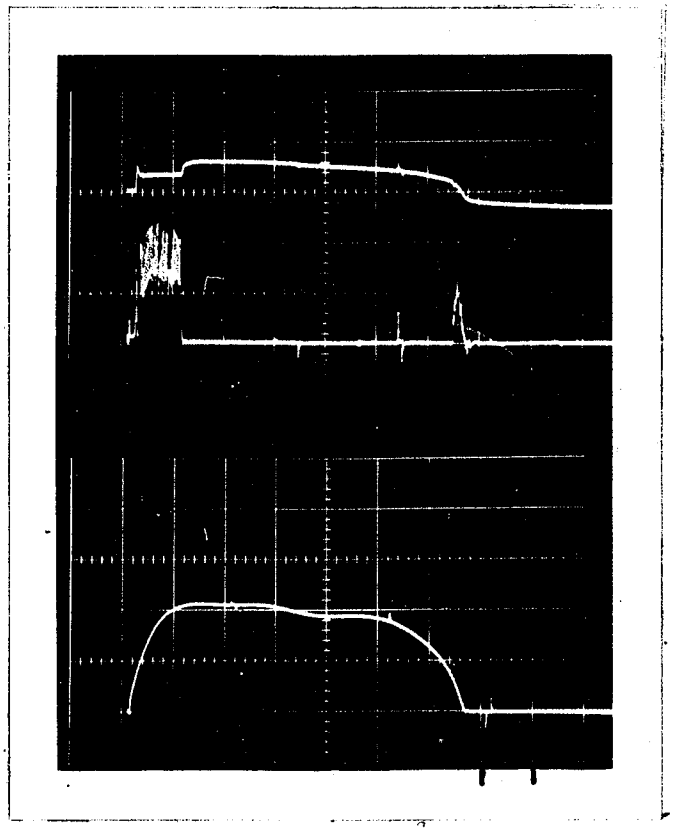

1.0 MSEC. / DIV.

FIG. 3

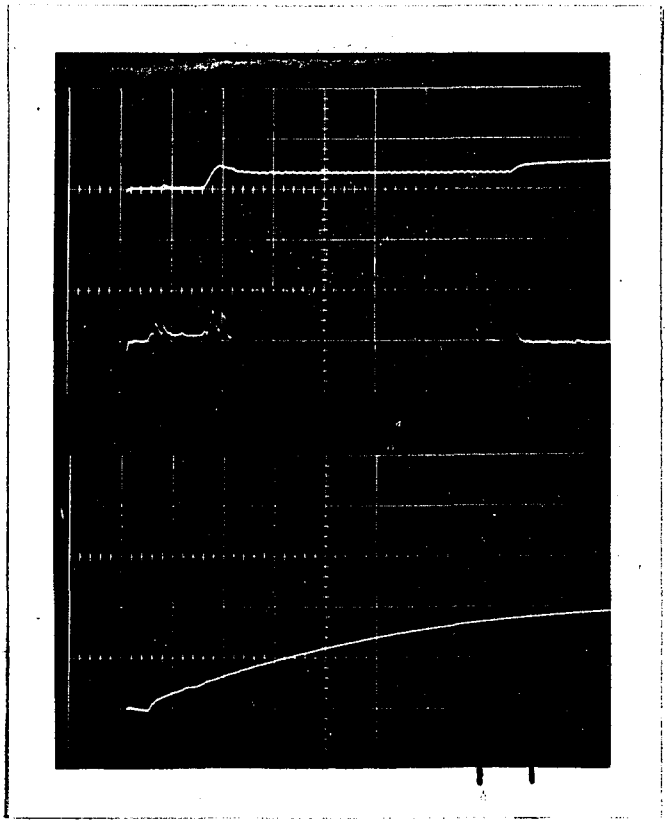

FIG. 4

TABLE I. TYPICAL PARAMETERS

FREQUENCIES	
Upper hybrid	4.7 GHz
Electron plasma	4.0 GHz
Electron cyclotron	2.45 GHz
Microwave input	2.45 GHz
Ion plasma	94 MHz
Lower hybrid	83 MHz
Ion-ion collisions	2×10^{7} sec.$^{-1}$
Ion cyclotron	1.32 MHz
Electron-neutral collisions	1×10^{6} sec.$^{-1}$
Electron-ion collisions	1×10^{6} sec.$^{-1}$
Ion acoustic (λ= 40 cm.)	69 kHz
Ion-neutral collisions	1×10^{4} sec.$^{-1}$
TIMES	
Classical electron diffusion time across guide radius	0.3 sec.
Experiment lifetime	5 msec.
Classical ion diffusion time across guide radius	1 msec.
Ion transit time between magnetic mirrors	0.1 msec.
Energy lifetime [a]	3 microsec.
LENGTHS	
Electron mean free path [b]	100 cm.
Plasma axial length [c]	22 cm.
Vacuum guide wavelength	20.9 cm.
Free space wavelength	12.2 cm.
Waveguide diameter	8.79 cm.
Axial density gradient [d]	6.4 cm.
Perp. density gradient [d]	2.6 cm.
Ion gyroradius	0.3 mm.
Electron gyroradius	0.1 mm.
Debye length	0.05 mm.

DENSITIES

Average electron (z=0)[e]	2×10^{11}/cc
Minimum electron (z=0)[f]	1.2×10^{11}/cc
Neutral hydrogen	1×10^{13}/cc
Unbounded left wave cutoff	1.5×10^{11}/cc
Bounded left wave cutoff	6.8×10^{10}/cc

a The right wave input power of 180 watts is set equal to the total plasma energy divided by the energy lifetime.

b The electron mean free path is for collisions with neutrals or ions.

c The plasma axial length is the distance over which $\omega_p^2/\omega^2 \gtrsim 1$.

d The density gradient scale lengths are calculated from the data of figures 5 and 8. The method of calculating the axial density gradient scale length L is shown below.

$$\frac{1}{L} \equiv \frac{\left|\frac{N_2 - N_1}{Z_2 - Z_1}\right|}{\left(\frac{N_2 + N_1}{2}\right)}$$

e The average density across the waveguide diameter as determined by Langmuir probe is about 2×10^{11}/cc. The average density as determined by microwave interferometer is closer to 3×10^{11}/cc. The average density as determined by diamagnetic coil using an electron temperature of 8 ev taken from the Langmuir probe data is about 3×10^{11}/cc.

f The minimum density at z=0 is determined by use of the Langmuir probe.

III. EXPERIMENTAL RESULTS

1. LOW FREQUENCY DENSITY MODULATIONS

As could be seen in the previous section the diamagnetic and RF probe signals were modulated at a frequency of about 75 KHz. This is explainable by the excitation of ion acoustic waves.[1] The frequency ω of such waves in an isothermal model is given as

$$\frac{1}{\omega^2} = \frac{1}{\omega_{pi}^2} + \frac{1}{k_z^2 K_B T_e / m_i} \tag{6}$$

For frequencies well below the ion plasma frequency ω_{pi} (here about 94 MHz) the frequency becomes

$$f = \frac{1}{\lambda}\sqrt{\frac{K_B T_e}{m_i}} \tag{7}$$

In an adiabatic model f must be multiplied by $\gamma^{1/2}$,[2] where γ is the ratio of the electron specific heats.

The inclusion of the static magnetic field and cylindrical waveguide boundary can be shown to have little effect on the dispersion relation for the frequencies and wavelengths of interest here.[3]

The wavelength was measured by an interferometric technique in which the diamagnetic modulations at z=0 were compared to the RF probe modulations at different axial positions. A 90^{o} shift($\lambda/4$) occurs for a shift of about 10 cm or $\lambda \approx 40$ cm.

With Te=8 ev, $m_i = 1.67 \times 10^{-24}$ gm for the proton, $\gamma = 1$, and $\lambda = 40$ cm, the calculated frequency is 69 KHz in reasonable agreement with the measured frequency of 75 KHz considering the large uncertainties in λ and γ.[4]

To further confirm that the modulations are due to density oscilla-

tions produced by ion acoustic waves, the working gas of hydrogen was replaced in turn by neon of atomic weight 20 and by argon of atomic weight 40. Neon yielded a frequency of 17.5 KHz or $1/\sqrt{18.3}$ that of hydrogen. Argon gave 6 kHz or $1/\sqrt{156}$ that of hydrogen. The frequency dependence on m_i^* was thus roughly that of ion acoustic waves. No account was taken here for any change in Te in comparing frequencies. The mechanism of plasma production is principally dependent on the electrons in ECR heating and not on the ions.

The ion acoustic waves cause both the electron and ion densities at a point in space to be slowly modulated in time. Thus the diamagnetic loop and the Langmuir probes whose signals are directly proportional to density are modulated. The RF probes and reflected power have their crystal rectified signals modulated as well through the effect of the electron density on the wavelength and reflection coefficient.

Typically the magnitude of these density modulations was about 20% although at one off axis radial position it was about 40% (as measured by Langmuir probe.) The resulting periodic density reductions are insufficient to allow the propagation of the left wave through the plasma where the density is on the average about three times the cutoff density.

2. PLASMA DENSITY PROFILES

On Figure 5 the axial density distribution is portrayed. This is taken from the ion saturation current Ii. The ion sat. current is proportional to density n times the square root of the electron temperature Te. Since Te varies only by about 30% in the perpendicular and axial directions and since $Ii \sim \sqrt{Te}$, the ion sat. current may be taken as indicative of the plasma density n. The average density at z=0 is about 2×10^{11}/cc. The relative density is of interest here. Density both before and after absorption of the left wave is shown superimposed on the static magnetic mirror field configuration. The fact that the density is highest after absorption is indicative of only a change in the perpendicular density profile, not the average density. The magnetic mirror confinement is quite evident with n peaking at the center of the machine where B_o is a minimum and falling off about 50% at the mirror points where B_o is a maximum.

The perpendicular density profiles were taken in the same way from the ion saturation current. Figure 6 shows a typical oscillogram of diamagnetic signal ($p_\perp$) on top and radial Langmuir probe signal on the bottom. The picture was taken twice to show the reproducibility. The relative density profiles at the times labeled a through e are plotted on Fig. 7. Initially the density is peaked on axis and falls off toward the waveguide walls. However several sudden transitions occur which change the density profile into one having a minimum on axis and maxima off axis.

The radial density profile at z=0 just before absorption is mirror imaged in Figure 8 . The same profile with the axial Langmuir probe is shown in Figure 9 . The two probes sampling the plasma in quite diffent ways are in good agreement.

The density profiles from z=-7.6 cm to z=-30.5 cm are shown in Figure 10 . The inner two maxima of Figure 8 have merged on the curve for z=-7.6 cm to form a low maximum on axis. By z=-15.3 cm this has disappeared. The maxima reduce to the minima on axis and the maxima move toward axis as the probe is moved out from the center of the machine. No profiles of the density could be taken in the "upstream" half of the machine because of interference with the plasma.

FIGURE CAPTIONS

Fig. 5. The axial density distribution in arbitrary units is shown both before and after absorption of the left wave along with the magnetic field configuration. The microwave power is incident from the left at z= +22 cm. and the left wave is cut off at about z= +11 cm.

Fig. 6. The integrated diamagnetic signal (perpendicular plasma pressure) and the ion saturation current (proportional to density) are shown on a time scale of 0.05 msec. per division. The pictures are shown twice to indicate the reproducibility.

Fig. 7. The ion saturation current (proportional to electron density) at times a through e on Figure 6 is plotted versus radial position r normalized by the guide radius a. The radial Langmuir probe is moved from radial point to radial point and a picture such as Fig. 6 is taken for each position.

Fig. 8. The density profile across the guide radius, as taken with the radial Langmuir probe at time d on Figure 6 is mirror imaged (the probe can only measure the density over one half of the guide diameter.)

Fig. 9. The axial Langmuir probe is used to map the relative electron density at time d on Figure 6 across the entire guide diameter and the profile thus obtained (at z=0) is in good agreement with Fig. 8.

Fig. 10. The relative density profiles at various axial positions and at the same time before absorption of the left wave as in figures 8 and 9 (time d on Figure 6.)

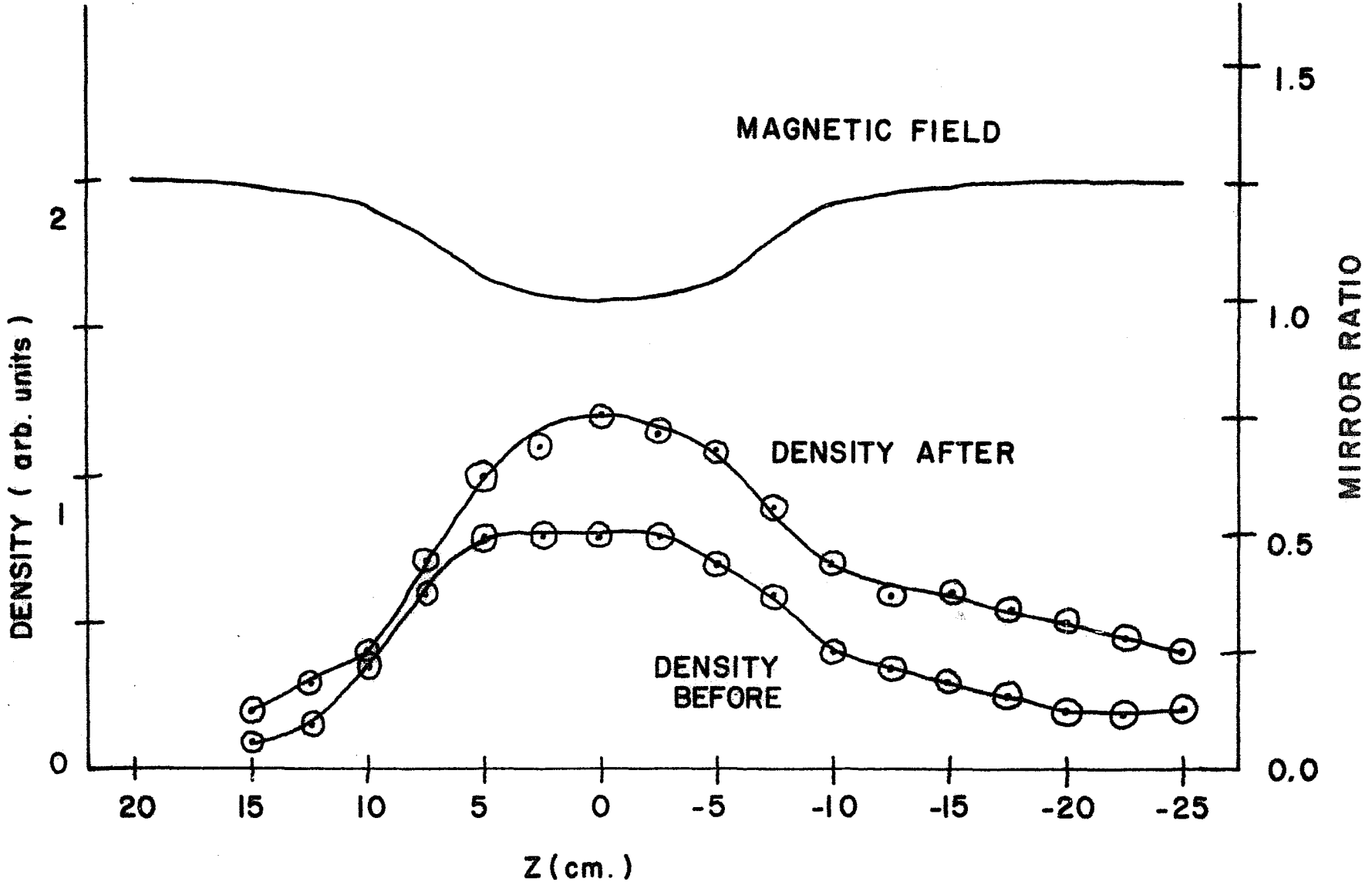
MAGNETIC FIELD
DENSITY AFTER
DENSITY
BEFORE
DENSITY (arb. units)
MIRROR RATIO
Z (cm.)
2
1
0
1.5
1.0
0.5
0.0
20
15
10
5
0
-5
-10
-15
-20
-25

FIG. 5

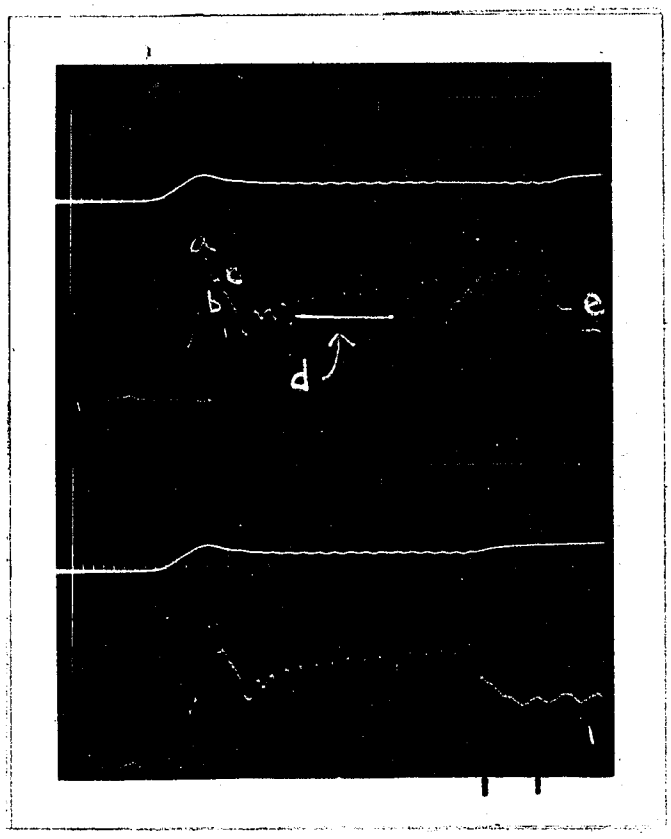

DIA.(PRESSURE)

ION SAT. CURRENT

0.05 MSEC. / DIV.

FIG. 6

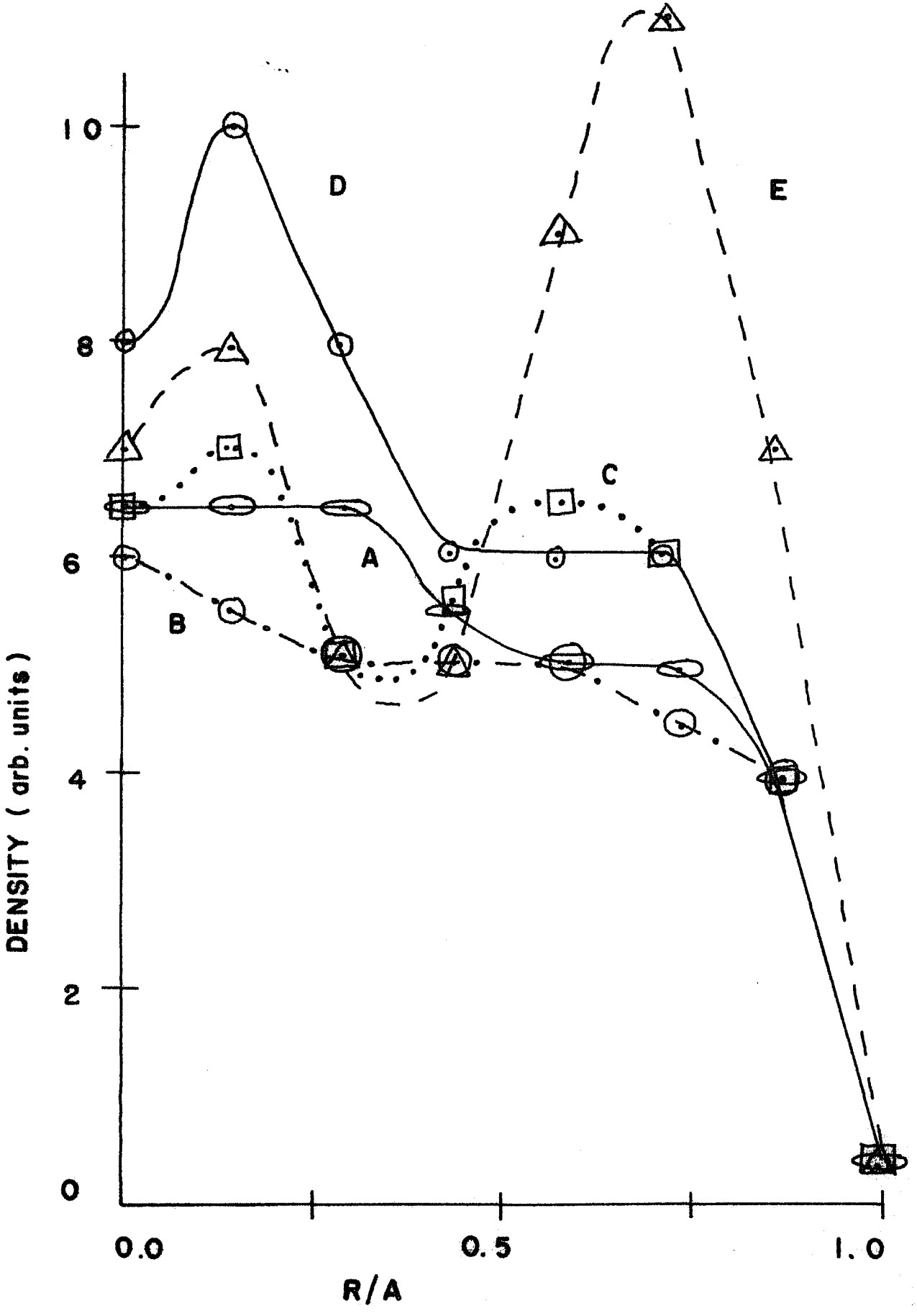

FIG. 7

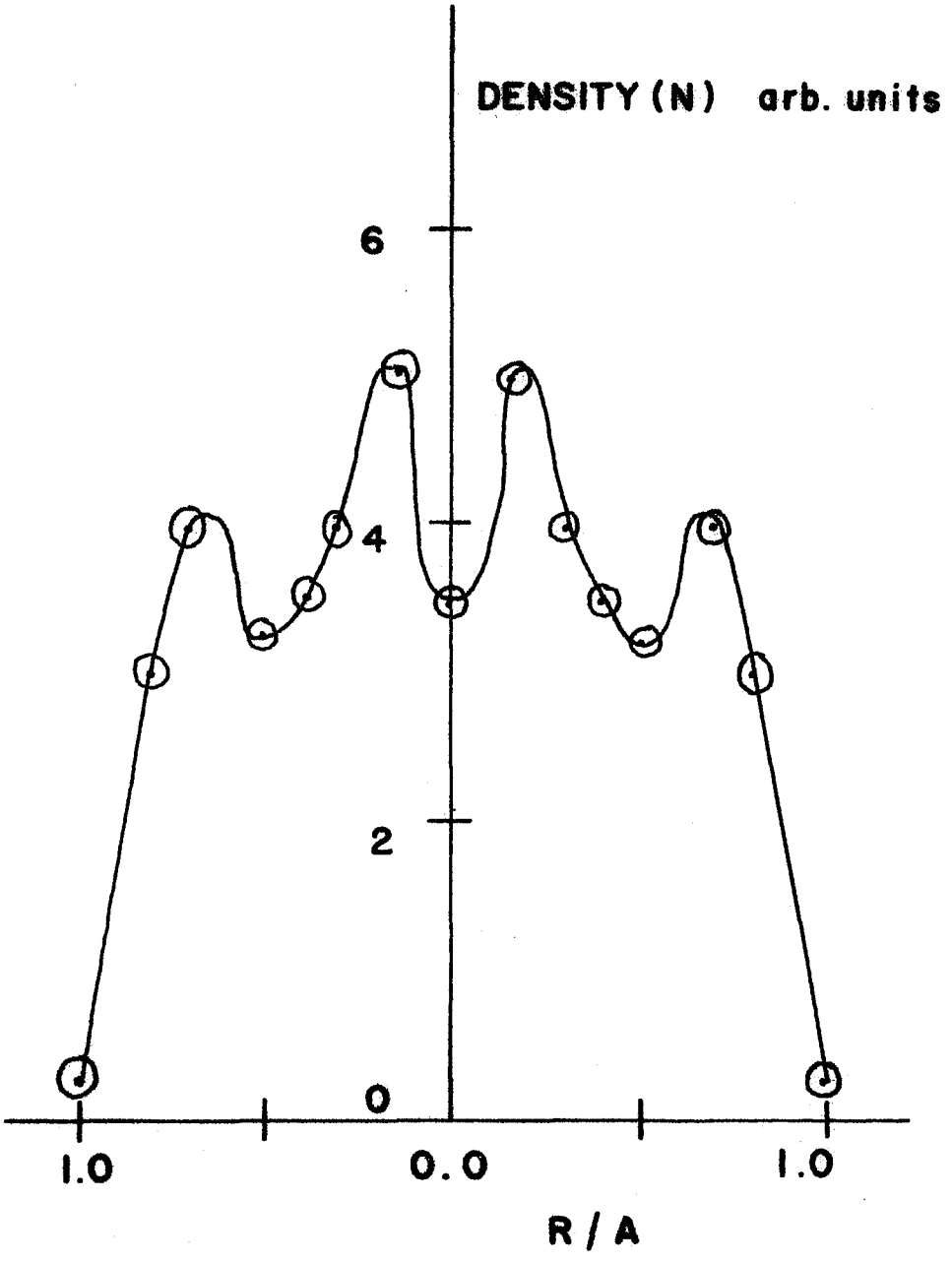

FIG. 8

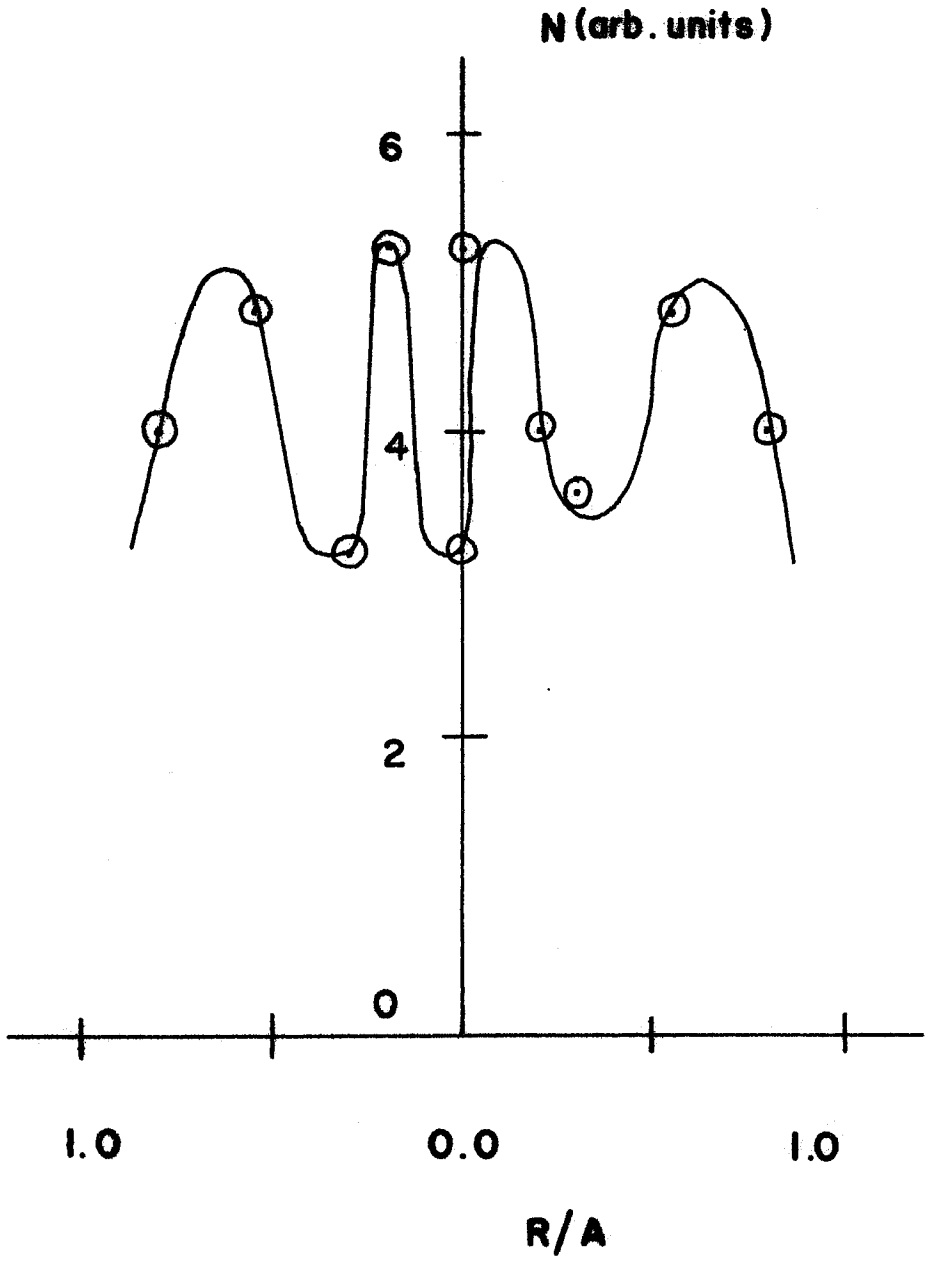

FIG. 9

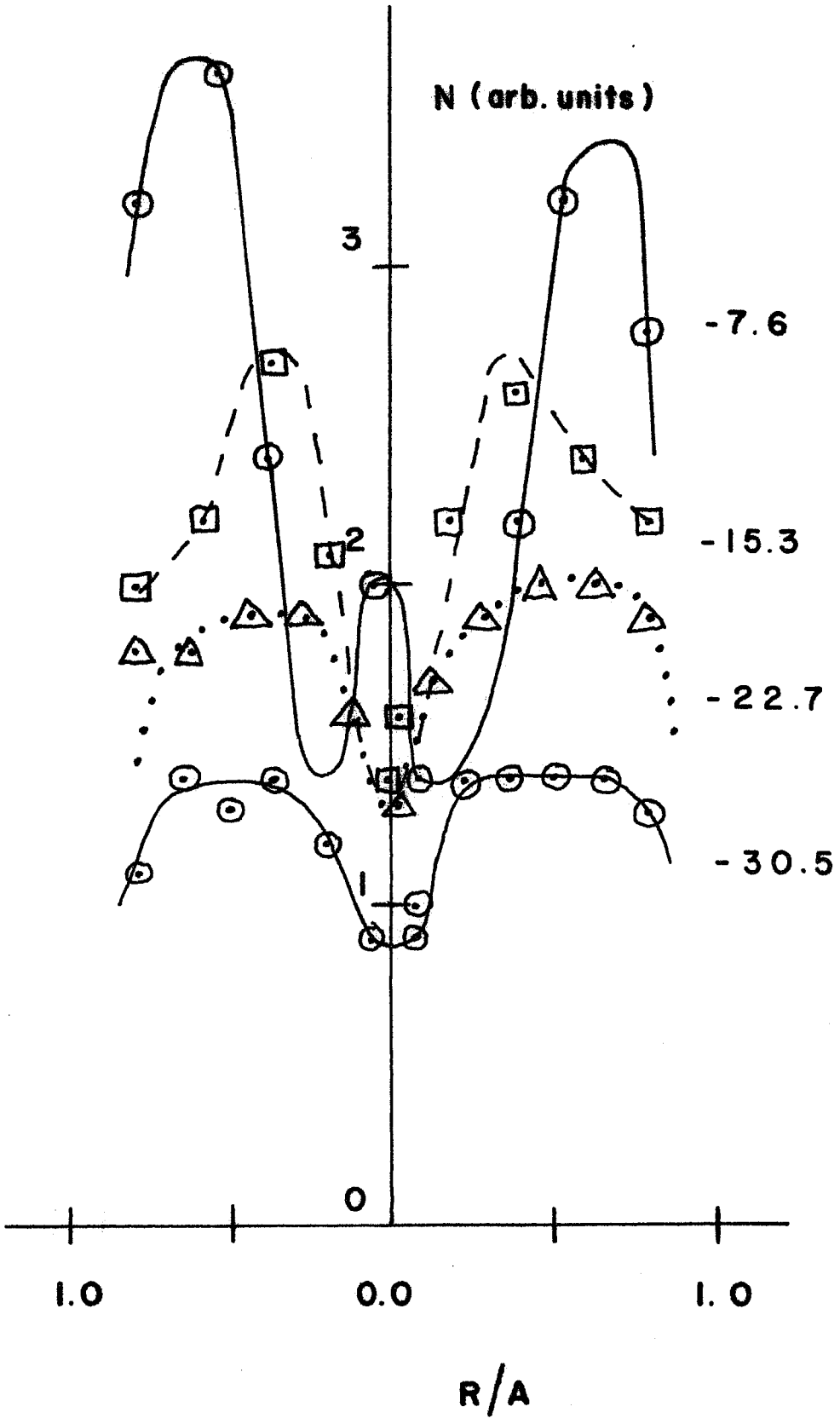

FIG. 10

The symmetry of the density profiles at z=-15.3 cm is shown in Figure 11 . Vertical and horizontal profiles are plotted and are in good agreement. The density here just before absorption of the left wave has a deep minimum on axis rising in all radial directions to the off axis maximum (an annular configuration).

To show that the density profile undergoes a transition off center as well, the axial probe was used at z=-15.3 cm to make profiles at the time of the diamagnetic signal peak and at a time just before absorption. (See Figure 12 .) The fact that the average density at the dia. peak time is lower than that just before absorption can be explained by the finite time ($\approx$ 0.1 msec) it takes for plasma formed in the center of the mirror machine (where cyclotron resonance occurs) to diffuse along the magnetic field out to z=-15.3 cm.

Density profiles at z=-15.3 cm were taken for several different input powers and neutral pressures. The results were similar to those already described.

We have observed an initially peaked on axis density falling off toward the waveguide walls to undergo a series of transitions into an annular configuration.

FIGURE CAPTIONS

Fig. 11. Vertical (boxes) and horizontal (circles) density profiles at z=-15.3 cm are shown to test the symmetry of the density distribution at time d on Figure 6.

Fig. 12. The transition from a peaked on axis to an annular density profile occurs at other axial positions besides z=0 as can be seen in the two profiles shown. The lower profile occurs at the time of the diamagnetic signal peak. The upper profile occurs at a later time just before absorption of the left wave. The profiles were taken at z=- 15.3 cm.

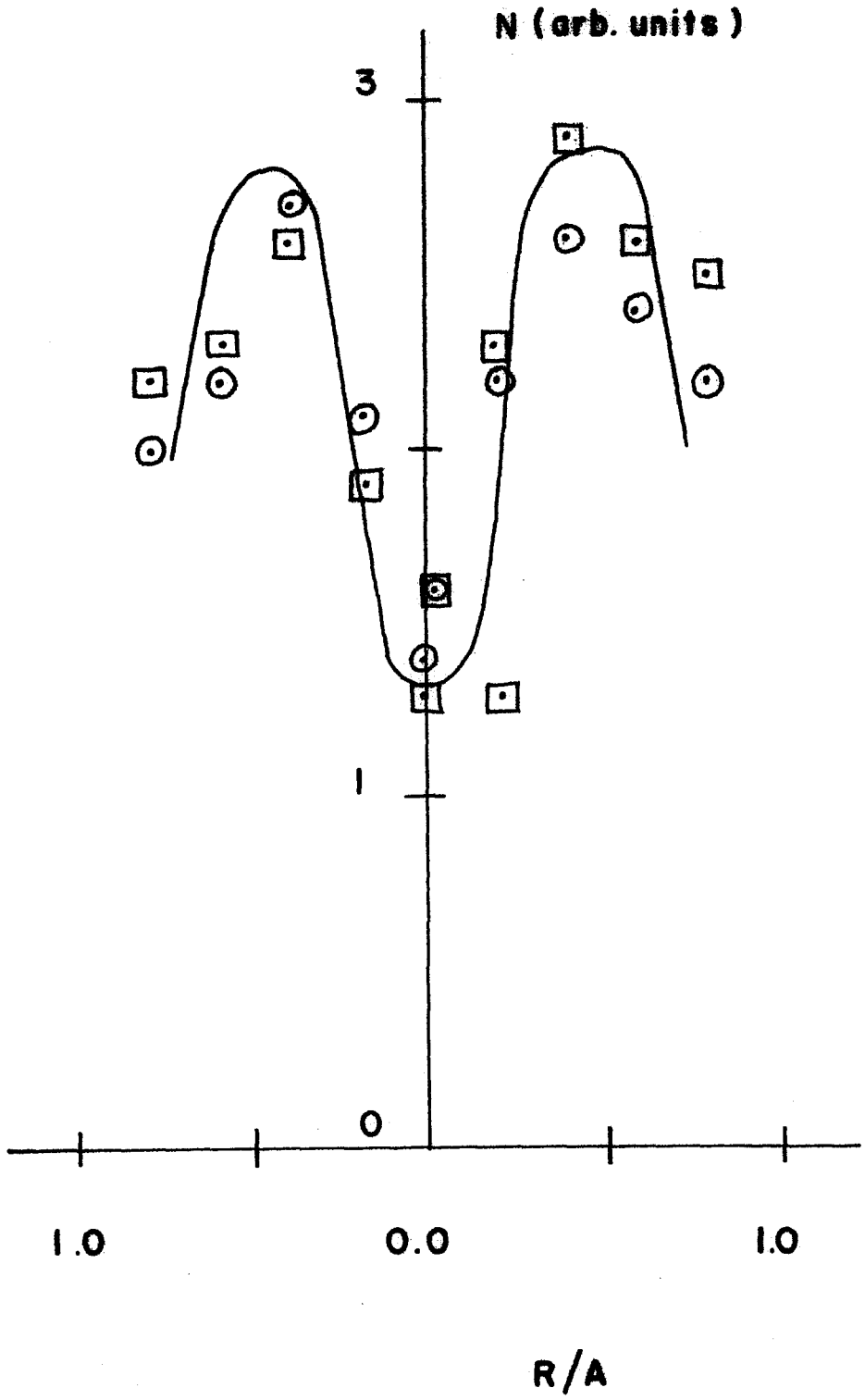

FIG. 11

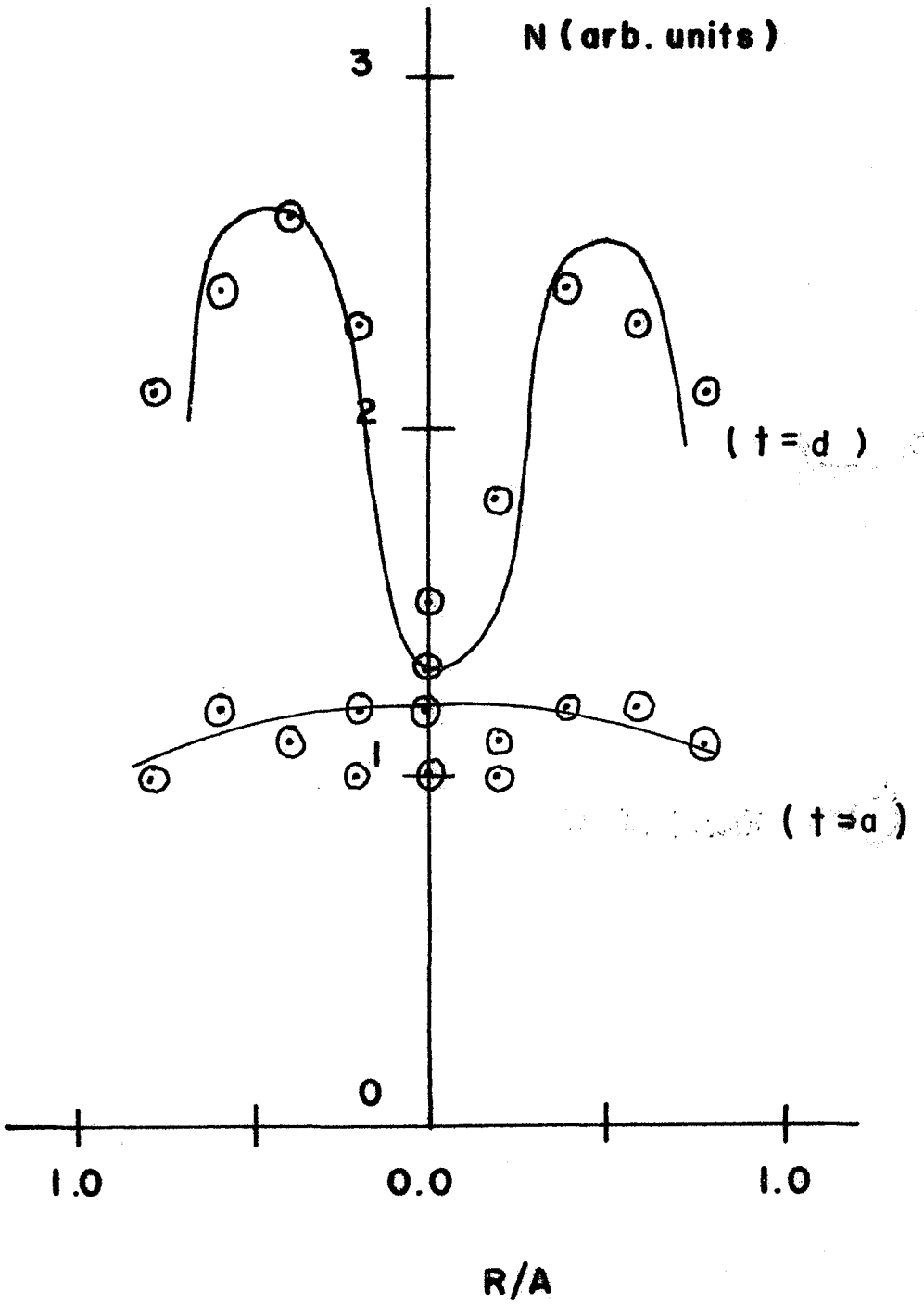

FIG. 12

3. ANOMALOUS TRANSMISSION AND ELECTROMAGNETIC PROFILES

The axial standing wave pattern was measured with the RF dipole probe. The crystal response representing power is shown in Figure 13 with the probe held vertical (V) and horizontal (H). The vertically polarized wave enters from the left and undergoes Faraday rotation with V⁄H at about z=+12.7 cm at a low power level. At about z=-16.5 cm the power rises again to a peak and then a series of minima and maxima (not shown) repeat in what is now essentially a vacuum guide.

A spiral antenna responding to only one CP was inserted to identify the wave transmitted through the plasma as being left handed. From the standing wave pattern in the vacuum region compared to the standing wave pattern in the guide with no plasma anywhere, the transmitted LHCP power can be estimated as about 25%.

From cold bounded theory the average plasma density of $2 \times 10^{+11}$ /cc is three times the cutoff density of the left wave. The wavenumber for the left wave is about $i\ 0.50\ cm^{-1}$ so that for a plasma of axial length 22 cm the power transmission should be effectively zero. (See appendix A-4.)

The second set of curves in Figure 13 shows the patterns after absorption. No transmission through the plasma occurs and both vertical and horizontal polarizations disappear by z=+4 cm. Effectively no reflected power exists after absorption so with neither transmission nor reflection both right and left waves are being absorbed. This will be discussed further in the next section.

The RF dipole was used to make horizontal profiles of the wave electric field at axial positions where the probe did not greatly interfere with the plasma. A typical oscillogram is shown in Figure 14 . The bottom trace is the crystal signal in millivolts (at z=-15.3 cm).

The rapid variations at the beginning of the trace are due to the initial breakdown of the hydrogen gas and the shifting of the standing wave pattern as the plasma density builds up. The peak marked a, however, occurs after the plasma density as seen on the diamagnetic signal trace has leveled off. This point a and the average of the ion acoustic modulated signal point b are plotted on Figures 15 and 16 as

FIGURE CAPTIONS

Fig. 13. The axial standing wave patterns are presented as taken with the dipole probe held vertically (V) and horizontally (H.) The upper curves occur before absorption and the lower curves after.

Fig. 14. The integrated diamagnetic signal and the rectified RF dipole signal are shown on a time scale of 0.1 msec per division.

Fig. 15. The electric field profiles at times a and b of Figure 14 are shown. The dipole probe was swept across the guide so as to couple to the theta component of the electric field E_θ at z=-15.3 cm.

Fig. 16. The same as Fig. 15 but the probe was swept to couple to the radial component of the electric field Er.

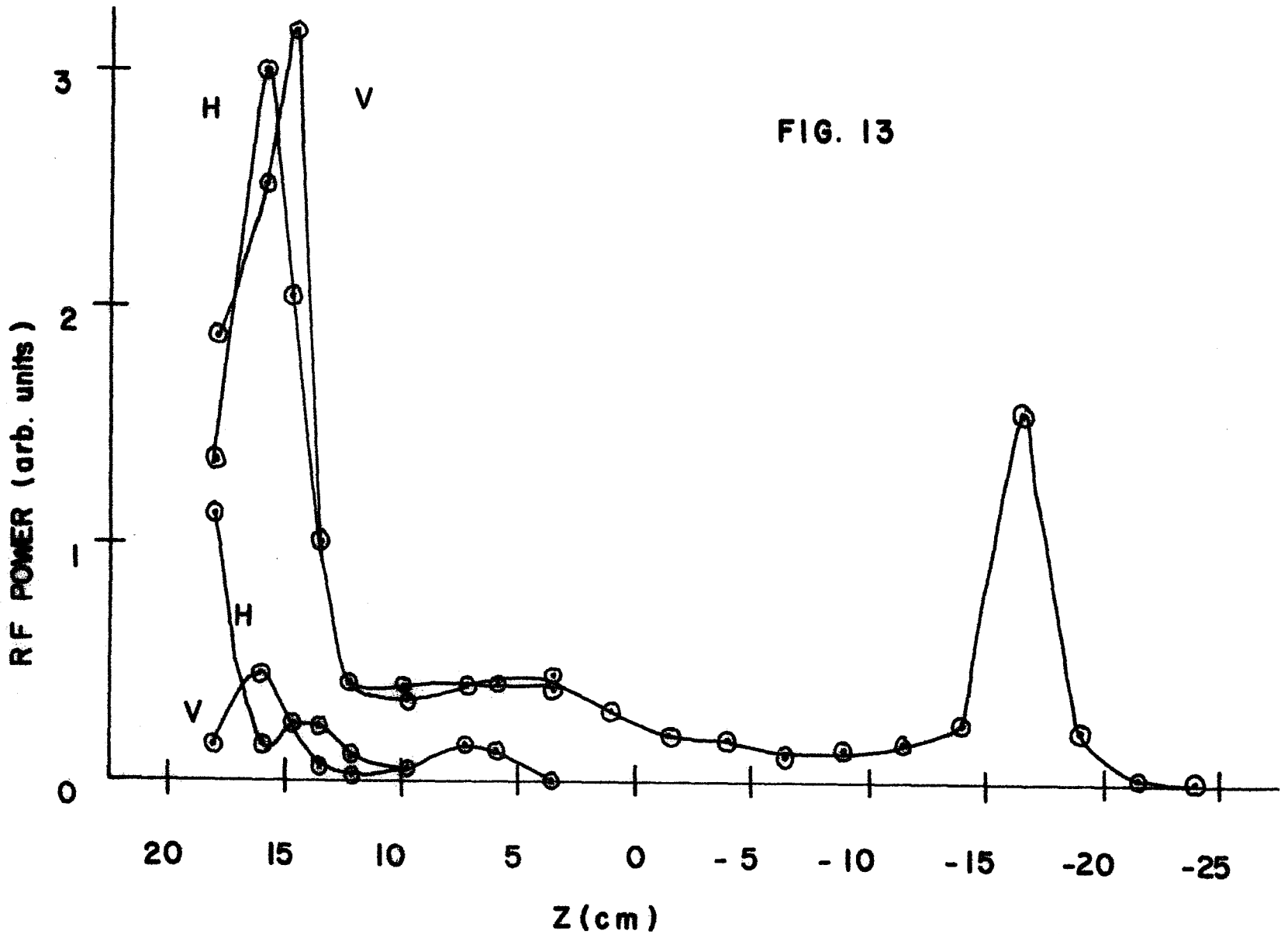

FIG. 13

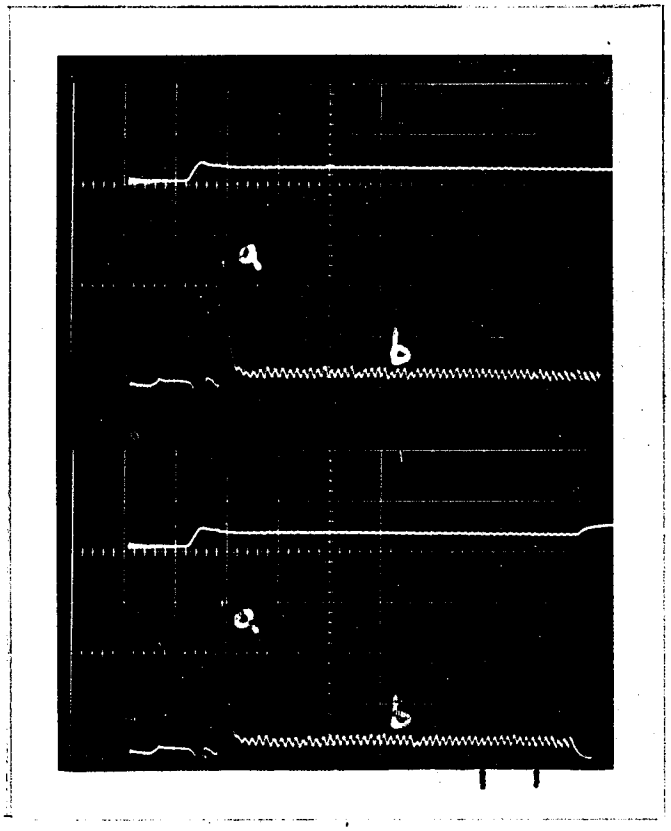

DIA.(PRESSURE)

RF POWER

0.1 MSEC. / DIV.

FIG. 14

FIG. 15

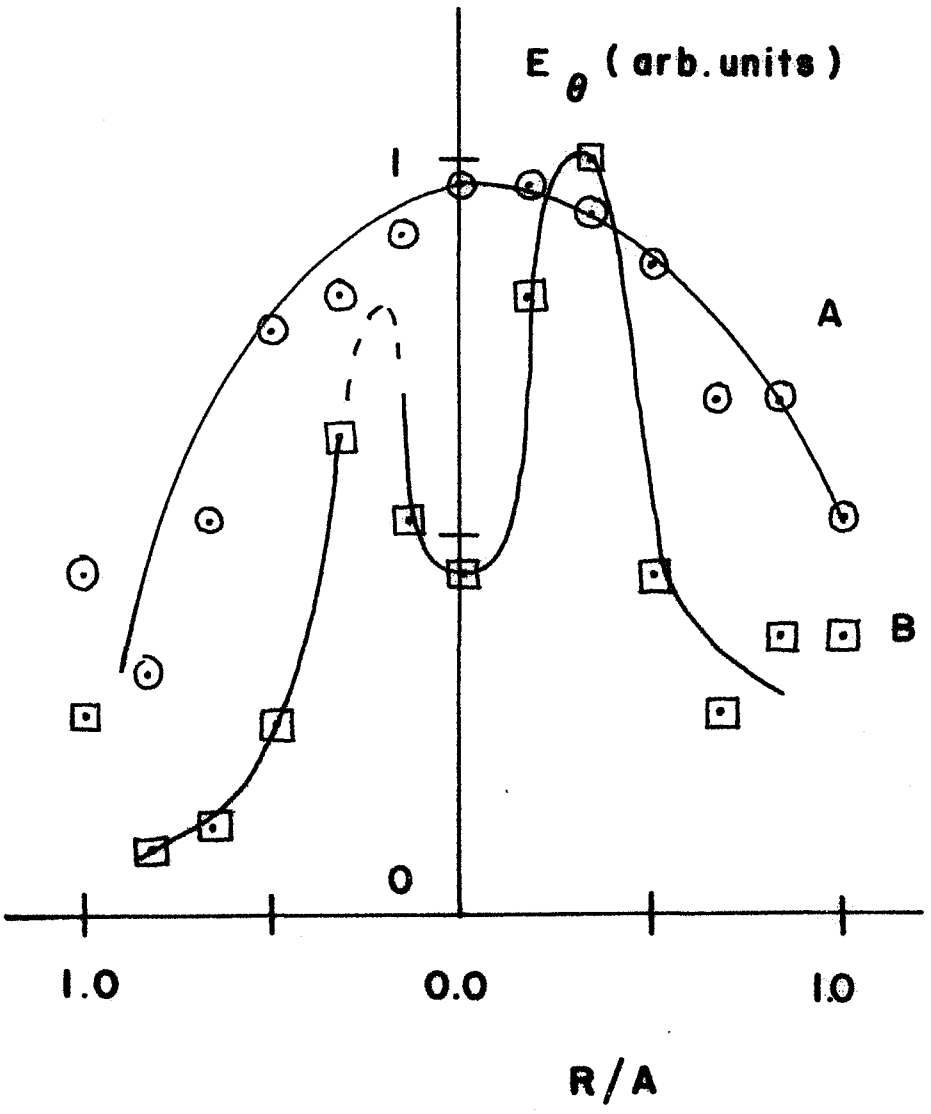

FIG. 16

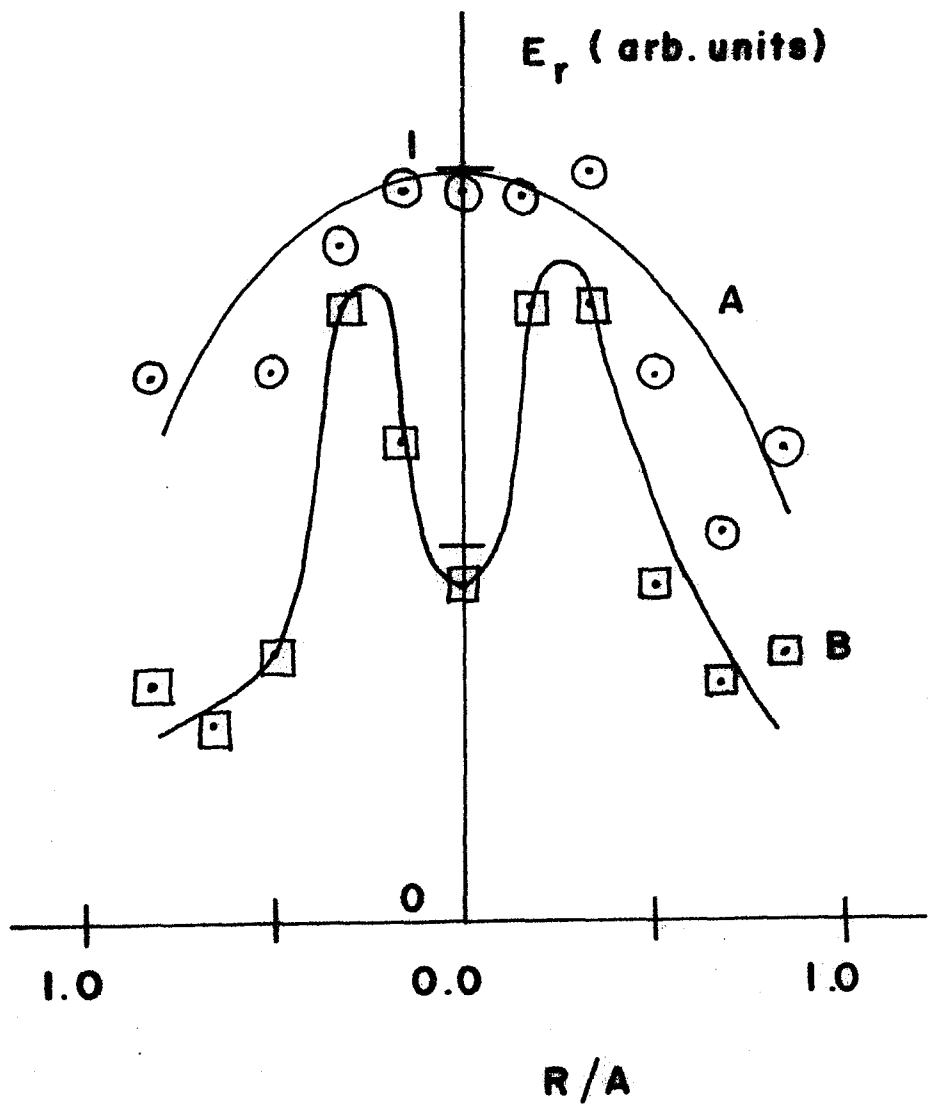

E_θ and E_r . The square root of the crystal response is taken as the electric field.

Like the density, the electric fields undergo a transition from peaked on axis falling off toward the waveguide walls to an annular configuration having a minimum on axis. In both cases $|E_\theta| \approx |E_r|$.

Profiles at z=-7.6 cm, -20.0 cm, and -25.4 cm are shown in Figures 17 , 18 , and 19 just before the absorption occurs. By the axial position of -25.4 cm the density is so low that the profiles are once again "normal".

Vertical profiles were taken at z=-15.3 cm to show the symmetry of the electric field. Figure 20 shows E_r for a vertical sweep just before absorption. (E_θ is similar.) Like the density profiles the electric field profiles have cylindrical symmetry.

Also, just as for the density, the electric field profiles showed little change with the neutral hydrogen pressure doubled from 2.5 to 5.0 x 10^{-4} torr or the input power halved from 400 watts to 200 watts. Decreasing the input power much further has the effect of stopping the production of plasma (no breakdown occurs.)

The density profiles at z=-7.6 cm, -15.3 cm, and -20.0 cm are superimposed on the E_θ profiles at the same axial positions just before absorption in Figures 21 , 22 , and 23 . The principal field maxima occur just inside the density maxima.

The wave magnetic field profile at z=-15,3 cm just before absorption was taken with the RF loop probe. The results are shown in Figures 24 and 25 . Like the wave electric field, the wave magnetic field has an annular configuration with $|H_r| \approx |H_\theta|$.

The fact that the electromagnetic fields in the "downstream" part of the mirror machine have their r and θ components of the same magnitude and have cylindrical symmetry indicates that this is a circularly polarized electromagnetic wave with m=+1. Because the standing wave pattern changes little between the mirror points (on axis) the wave can be said to have a long wavelength and a low wavenumber (near cutoff).

In the vacuum guide the RF dipole and loop probes can be calibrated for known field strengths. Using this calibration, the ratio $|E_\theta| / |H_r|$ is about 3 in the plasma at z=-15.3 cm. In gaussian units for a plane unbounded electromagnetic wave in vacuo this ratio is one. Thus the

wave in the plasma is indeed electromagnetic in nature.

We thus observe strong anomalous transmission of left handed microwave power through a nominally overdense plasma . The annular field profile measured is not predicted from cold bounded theory which uses a two density model for the observed annular density profile.

When the left wave incident power is reduced from about 180 watts to 90 watts, the percent transmitted power decreases from 25% to 5%. The plasma density does not change perceptibly with this decrease in the incident power, so the anomalous transmission does depend on the magnitude of the incident left wave power.

At neutral pressures below 1.6×10^{-4} torr and these power levels, the plasma formed after breakdown of the neutral hydrogen gas has a density of only about $2 \times 10^{+10}$/cc and is underdense. The left wave is then observed to fully penetrate the plasma, reflect off of the end of the chamber and form a standing wave pattern in the plasma that is little different from that of the vacuum waveguide.

At the typical neutral pressure of 2.5×10^{-4} torr and incident microwave power of 45 watts, the plasma is underdense with a density of about 4×10^{10} /cc. The measured wavenumber k_z in the plasma is 0.26 ± 0.04 cm^{-1} from the standing wave pattern as compared to the predicted theoretical k_z of 0.25 cm^{-1} from Fig. 37. The standing wave pattern in the plasma for this case is shown in Fig. 25 a. Thus the linear bounded theory for the left wave works provided the plasma is underdense and the wave is of low power.

FIGURE CAPTIONS

Fig. 17. Electric field profiles at z=-7.6 cm at time b of Figure 14.

Fig. 18. Electric field profiles at z=-20.0 cm at time b of Figure 14.

Fig. 19. Electric field profiles at z=-25.4 cm at time b of Figure 14.

Fig. 20. A vertical sweep by the dipole probe at z=-15.3 cm is shown to compare to Fig. 15 which shows a horizontal sweep (time b of Fig. 14.)

Fig. 21. The density n and the electric field E_θ profiles at z=-7.6 cm are superimposed (n at time d of Fig. 6 and E_θ at time b of Fig. 14.)

Fig. 22. The same as in Fig. 21 but at z=-15.3 cm

Fig. 23. The same as in Fig. 21 but at z=-20.0 cm

Fig. 24. The wave magnetic field Hr profile at z=-15.3 cm at time b of Figure 14 is shown. The loop RF probe was used.

Fig. 25. The same as Fig. 24 but H_θ is profiled

Fig. 25 a. The axial standing wave pattern with the dipole probe held vertically (V) and horizontally (H). The incident power is 45 watts. This can be compared to Fig. 13 for an incident power of 365 watts and the same neutral pressure of 2.5×10^{-4} torr.

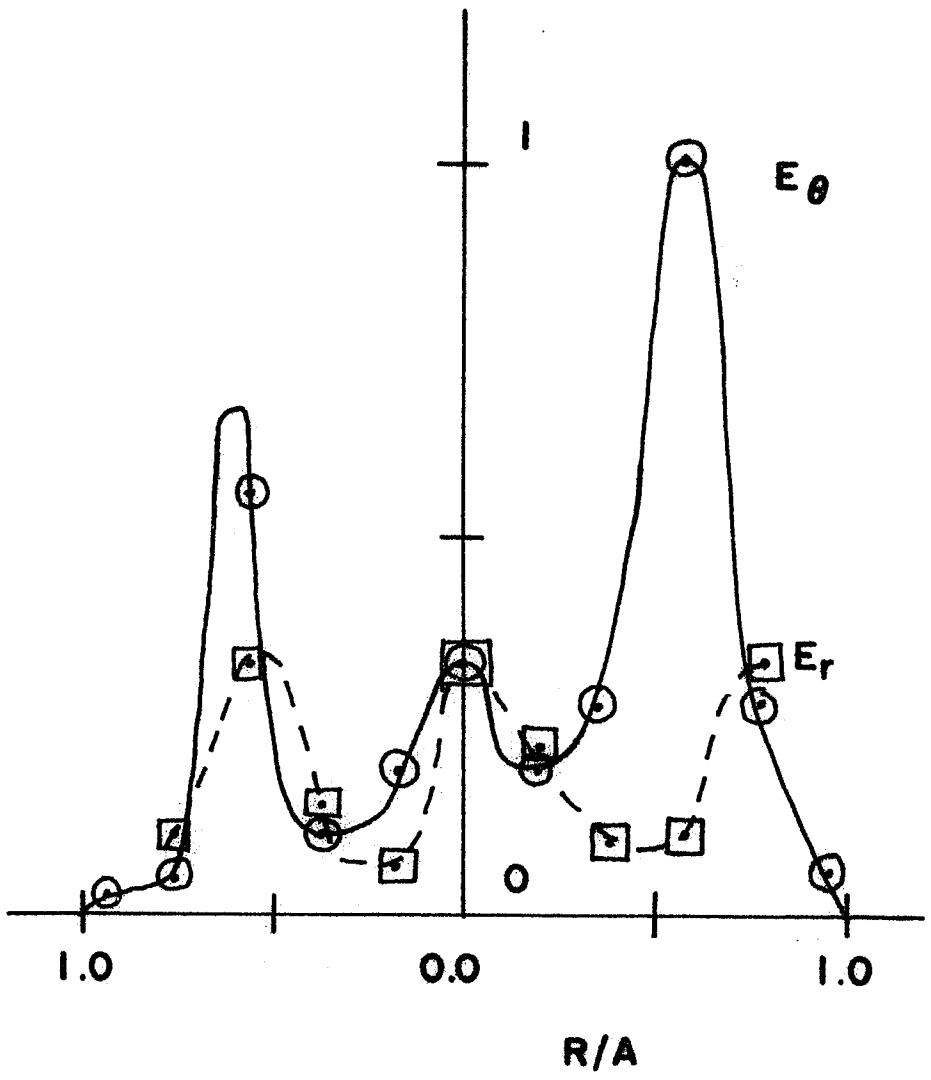

FIG. 17

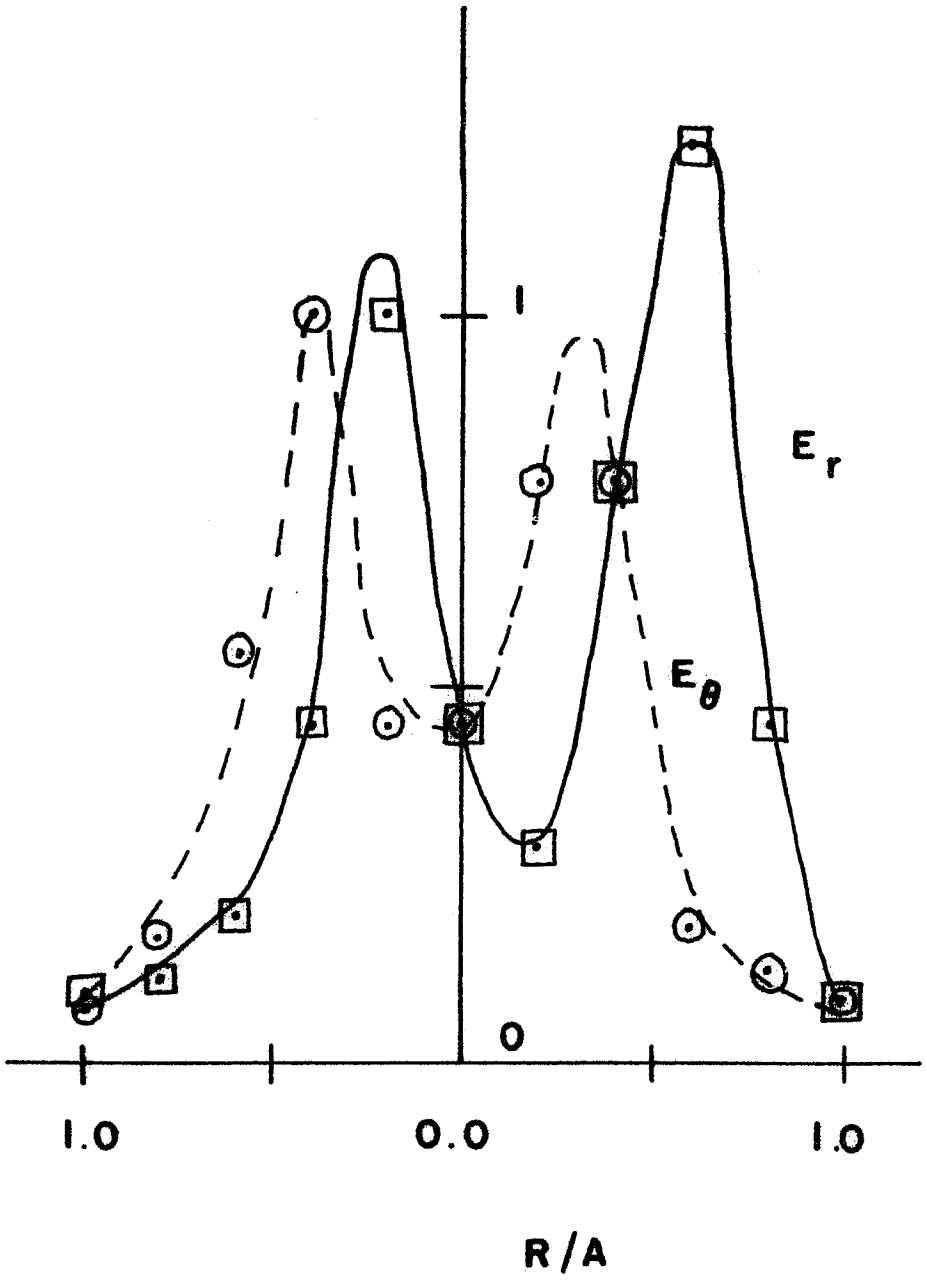

FIG. 18

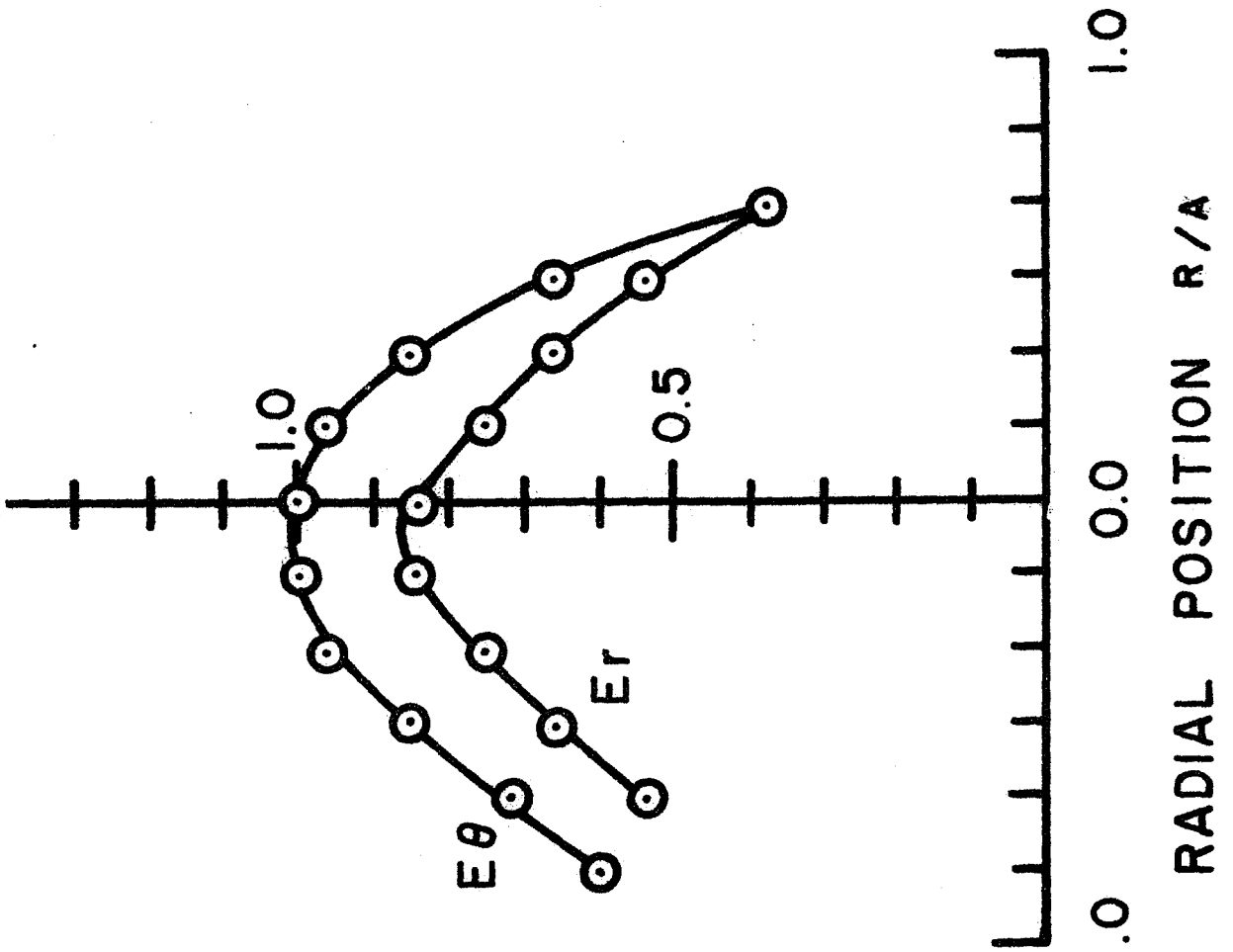

Fig. 19

FIG. 20

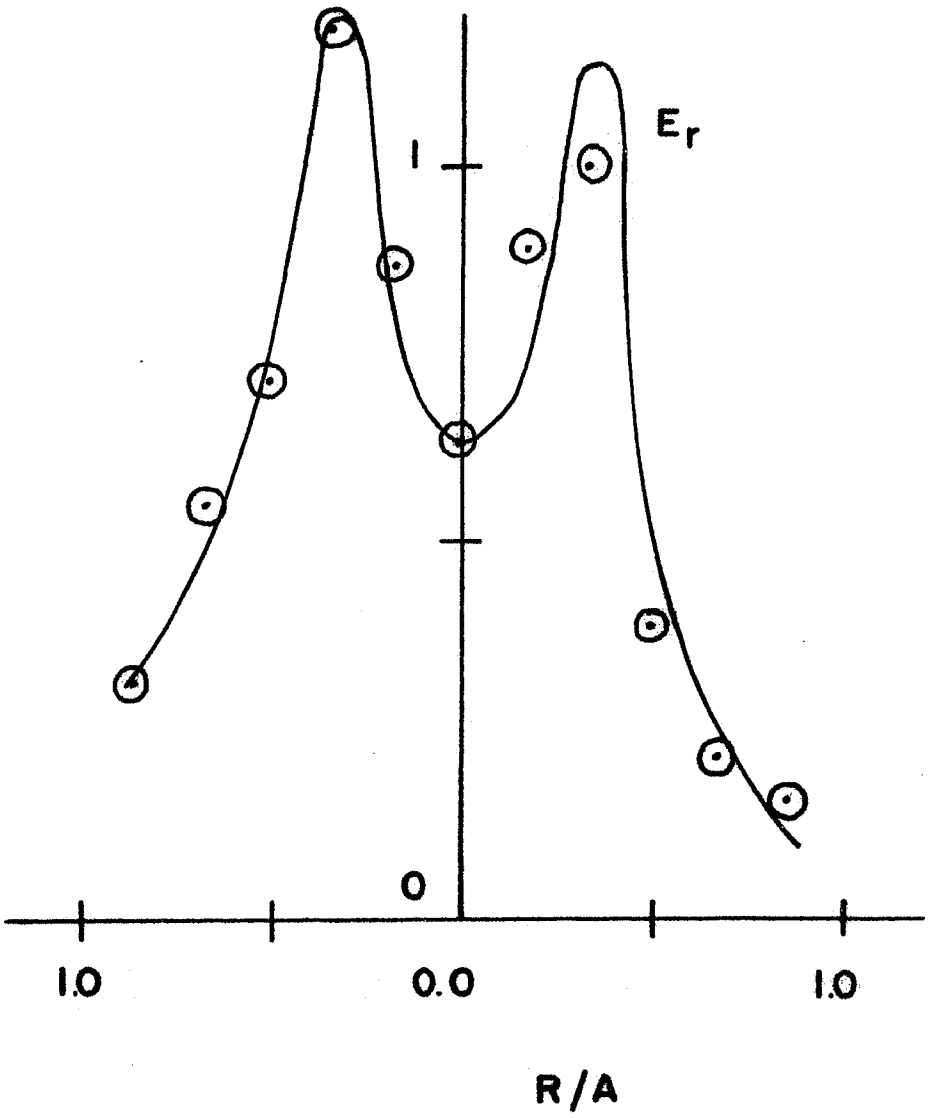

FIG. 21

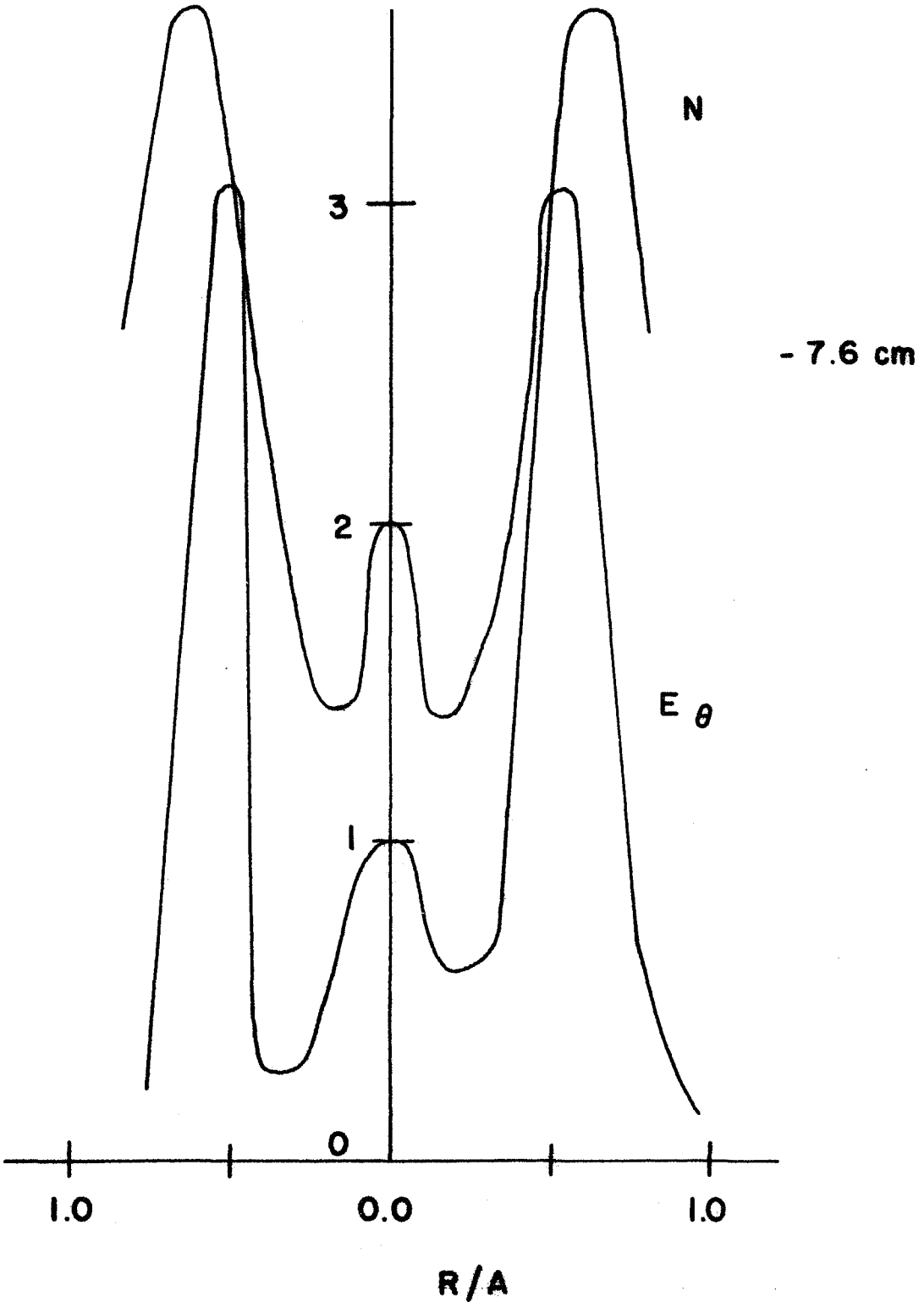

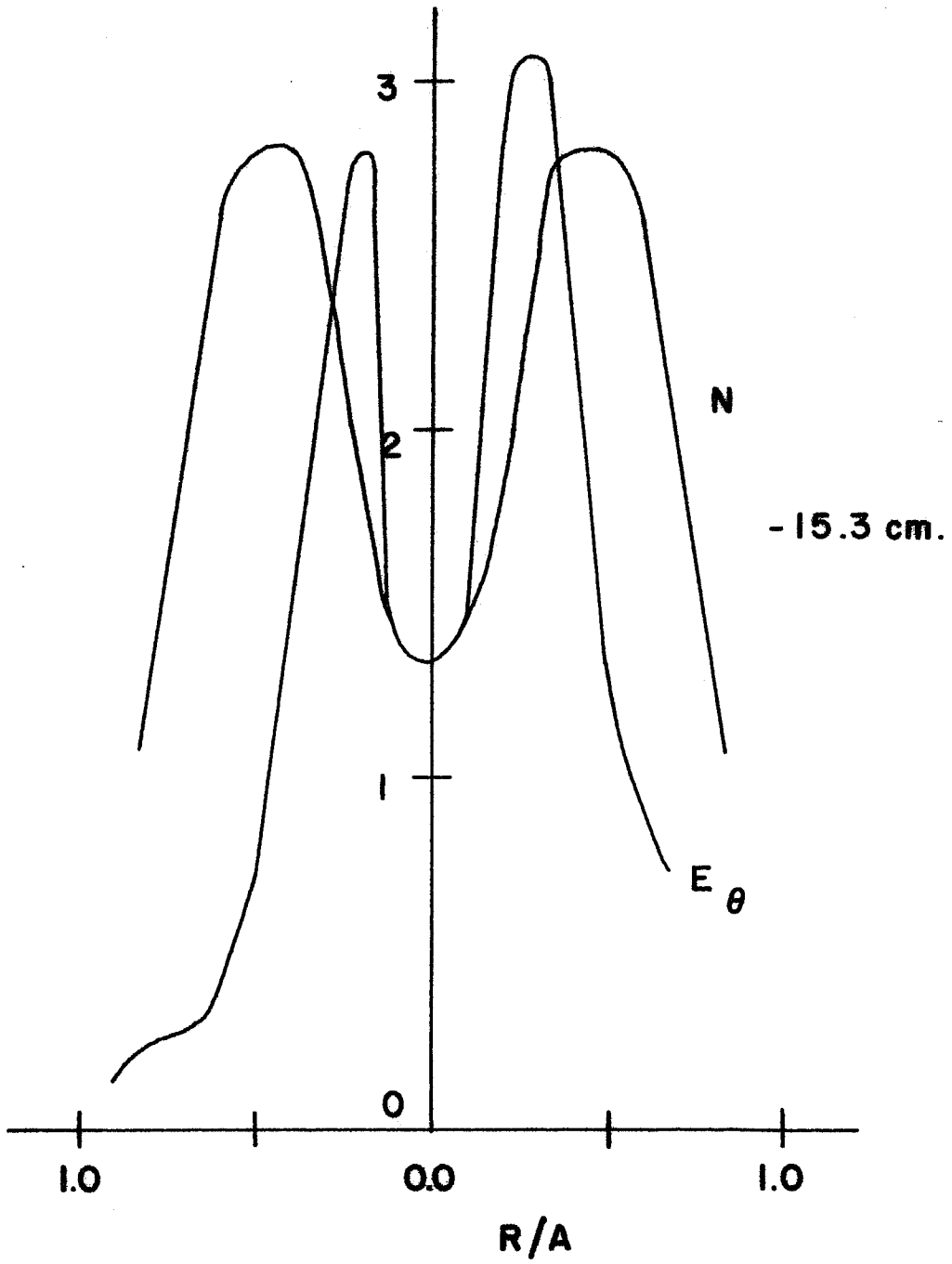

FIG. 22

FIG. 23

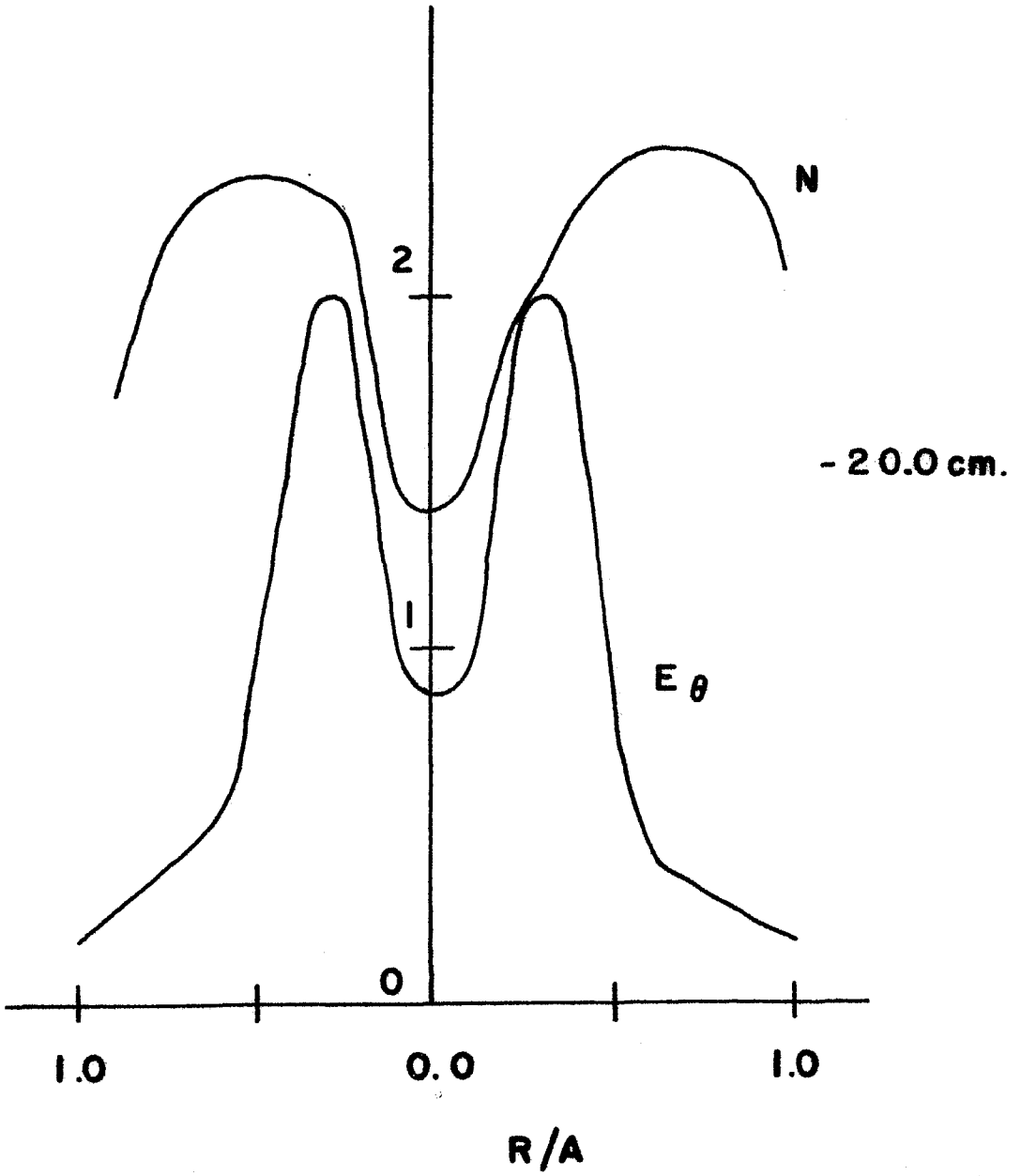

FIG. 24

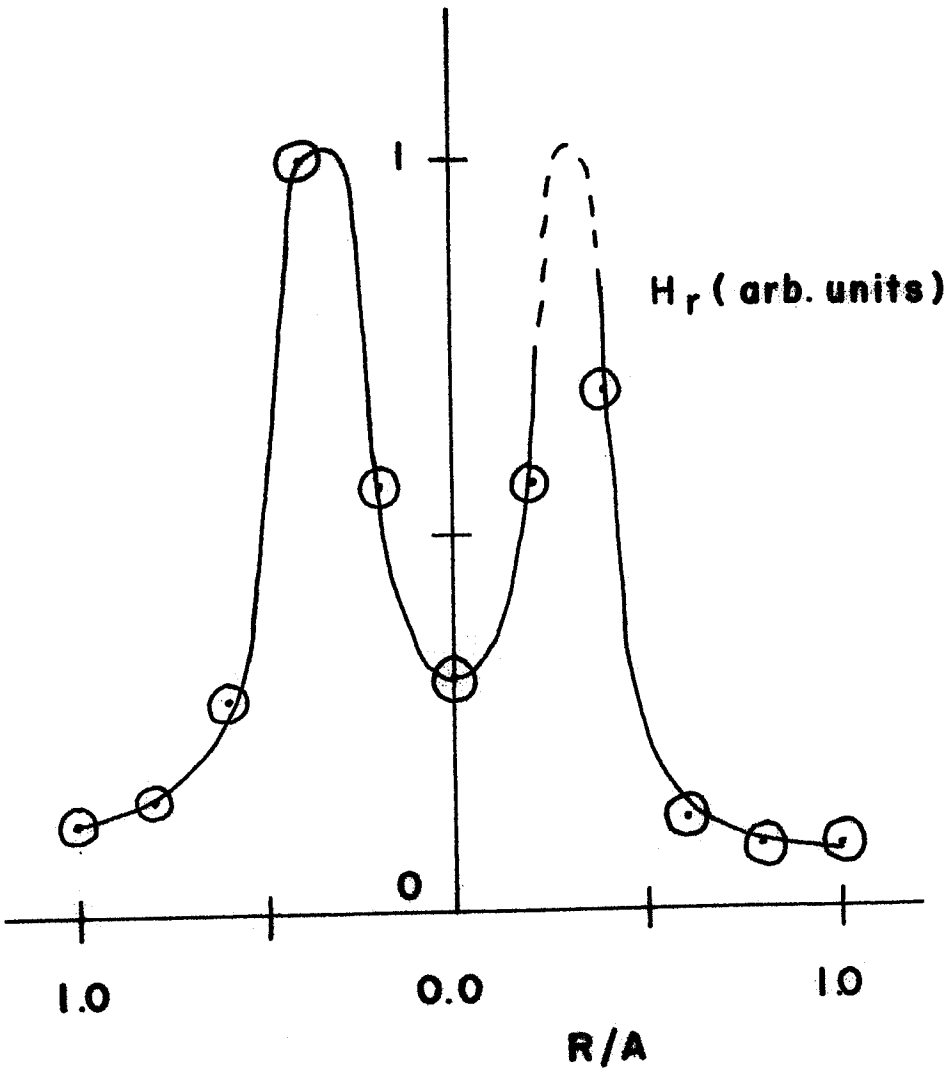

FIG. 25

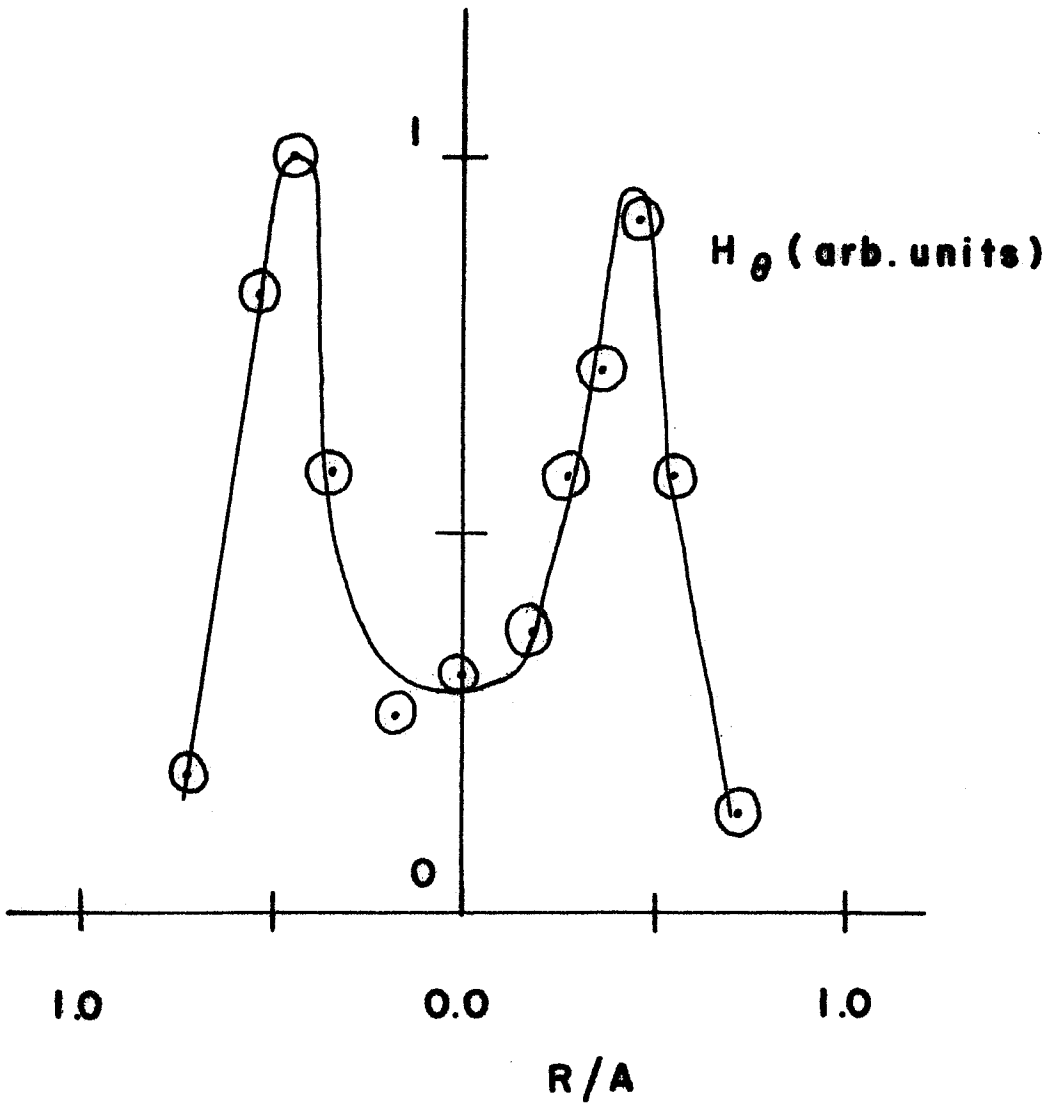

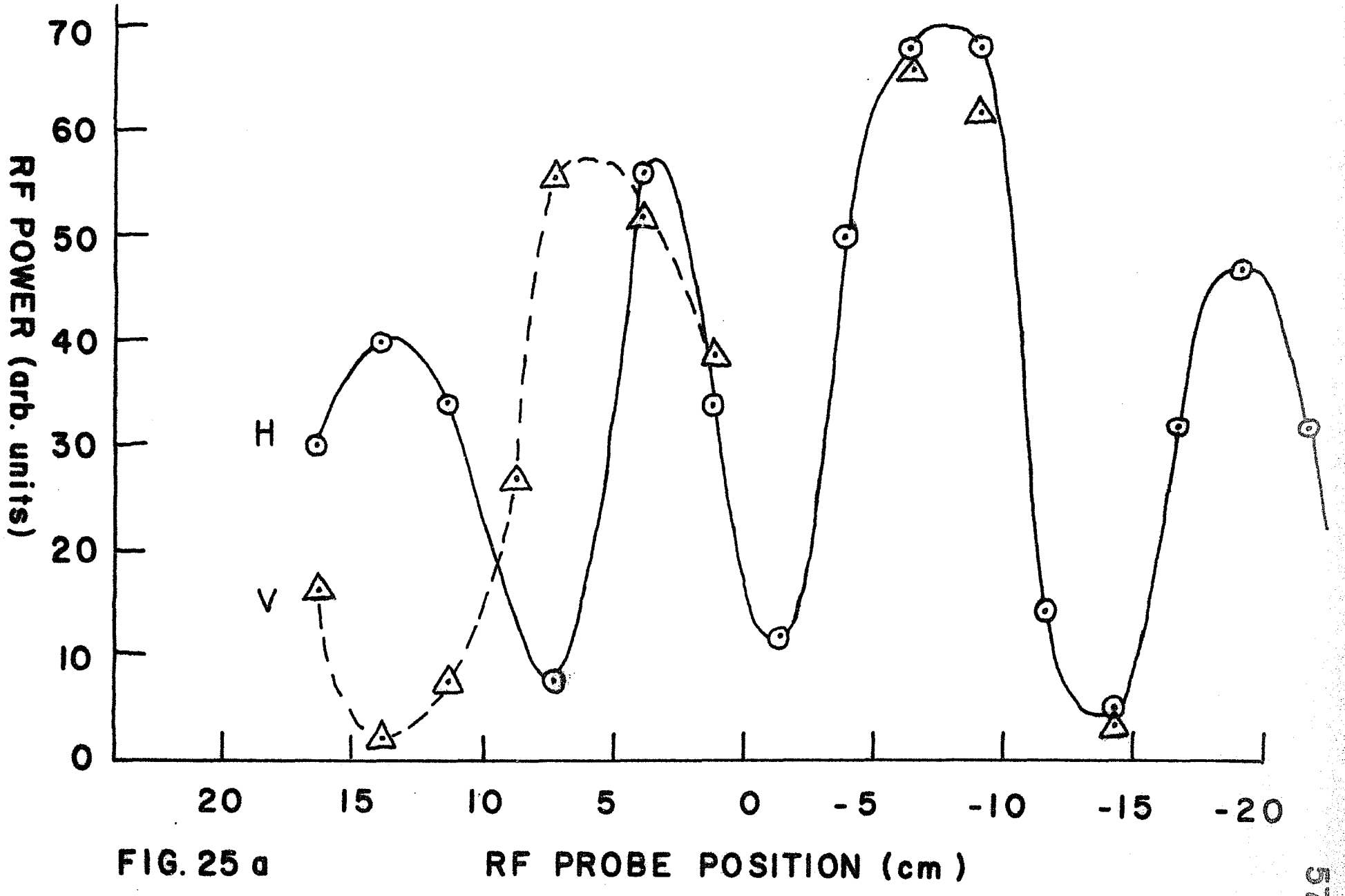
70
60
50
40
30
20
10
0
RF POWER (arb. units)
H
V
20
15
10
5
0
-5
-10
-15
-20
RF PROBE POSITION (cm)

FIG. 25 a

4. ANOMALOUS ABSORPTION

After a period of time of propagation through the plasma column the left wave is suddenly absorbed as can be seen in Figure 3 for the transmitted power.

The total transmitted power is now less than 0.01% and the total reflected power is less than 5%. The time for absorption to occur was found to decrease with increasing incident power as shown in Figure 26 . Note that over this range of incident power both the plasma density and temperature are only weakly dependent on incident power. A change of 50% in power produces only a 15% change in perpendicular plasma pressure.

Figure 27 shows percent reflected power both before and after absorption versus neutral pressure. Only in a narrow range from 2.0 to 3.5×10^{-4} torr does virtually complete absorption ever occur. Only in this pressure range does the strong anomalous transmission occur before absorption. At 5.0×10^{-4} torr there is no absorption and transmission is about 0.2% of the incident microwave power.

To better present the dependence of the absorption time τ on incident power and on neutral pressure as well, $1/\tau$ is plotted against power in Figure 28 (for fixed neutral pressure) and against neutral pressure in Figure 29 (for fixed power). Note that like the power, the neutral pressure has little effect on plasma pressure in this region of parameters.

The curve of $1/\tau$ versus P is linear. An extrapolation indicates a threshold power of 200 watts. Whether this is indeed a threshold cannot be determined because of the finite lifetime (5 msec) of the experiment.

The curve of $1/\tau$ versus neutral pressure has two linear regions. For low neutral pressures $1/\tau$ is independent of neutral pressure. Above 2.5×10^{-4} torr, $1/\tau$ decreases linearly with neutral pressure. Again an extrapolation which cannot be confirmed because of the finite lifetime of the experiment yields a threshold pressure of 3.65×10^{-4} torr, above which no absorption occurs.

There is evidence that indicates that the absorption of the left wave is due to an instability in which the left wave is converted into longitudinal waves which are then Landau damped, heating the plasma.

Figure 30 shows an oscillogram of the RF probe signal fed into a receiver tuned to 3.97 GHz. Upon absorption of the left wave low levels at this frequency and at 3.76, 3.88, and 4.08 GHz are excited. These frequencies are close to the predicted plasma frequency of 4.02 GHz for a density of $2 \times 10^{+11}$ /cc. Thus radiation near the electron plasma frequency is excited at the time of absorption.

FIGURE CAPTIONS

Fig. 26. The peak incident power in watts is plotted against the time to absorption of the left wave in milliseconds.

Fig. 27. Percent reflected power as a function of neutral pressure is plotted both before and after the absorption of the left wave. The incident microwave power is 365 watts. With a vacuum, the reflected power off of the end of the vacuum chamber is about 67%

Fig. 28. One over the time to absorption is plotted in $msec^{-1}$ versus incident power in watts for a fixed neutral pressure of 2.5×10^{-4} torr.

Fig. 29. One over the time to absorption is plotted in $msec^{-1}$ versus neutral pressure in 10^{-4} torr at a fixed incident power of 365 watts.

Fig. 30. The integrated diamagnetic signal and the unrectified dipole probe signal fed into a microwave receiver tuned to 3.97 GHz. The time scale is 0.2 msec per division and the video output of the receiver is shown on the lower trace. The picture is taken twice to show the reproducibilty.

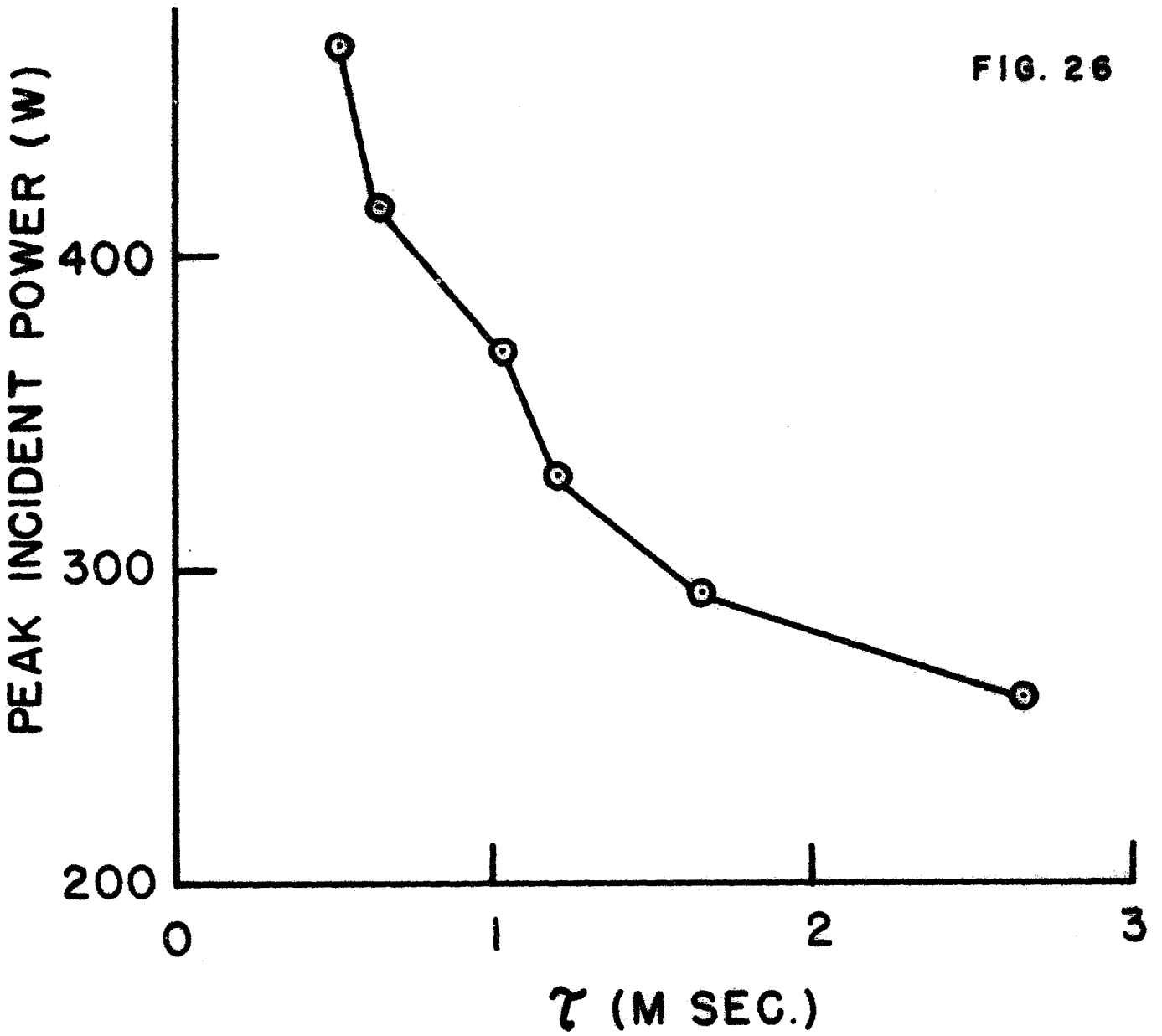

FIG. 26

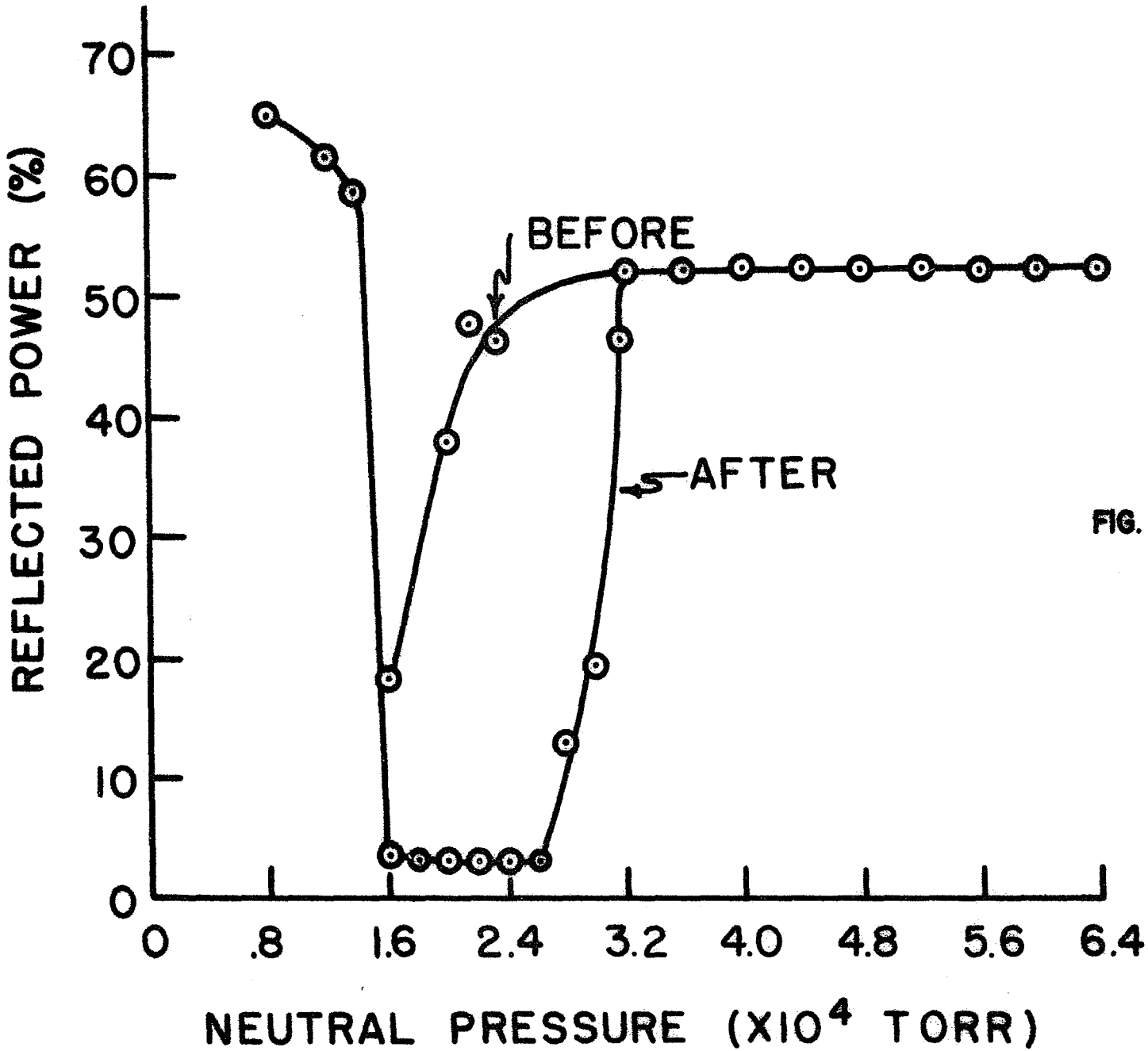
REFLECTED POWER (%)
70
60
50
40
30
20
10
0
BEFORE
AFTER
0
.8
1.6
2.4
3.2
4.0
4.8
5.6
6.4
NEUTRAL PRESSURE (X10⁴ TORR)

FIG. 27

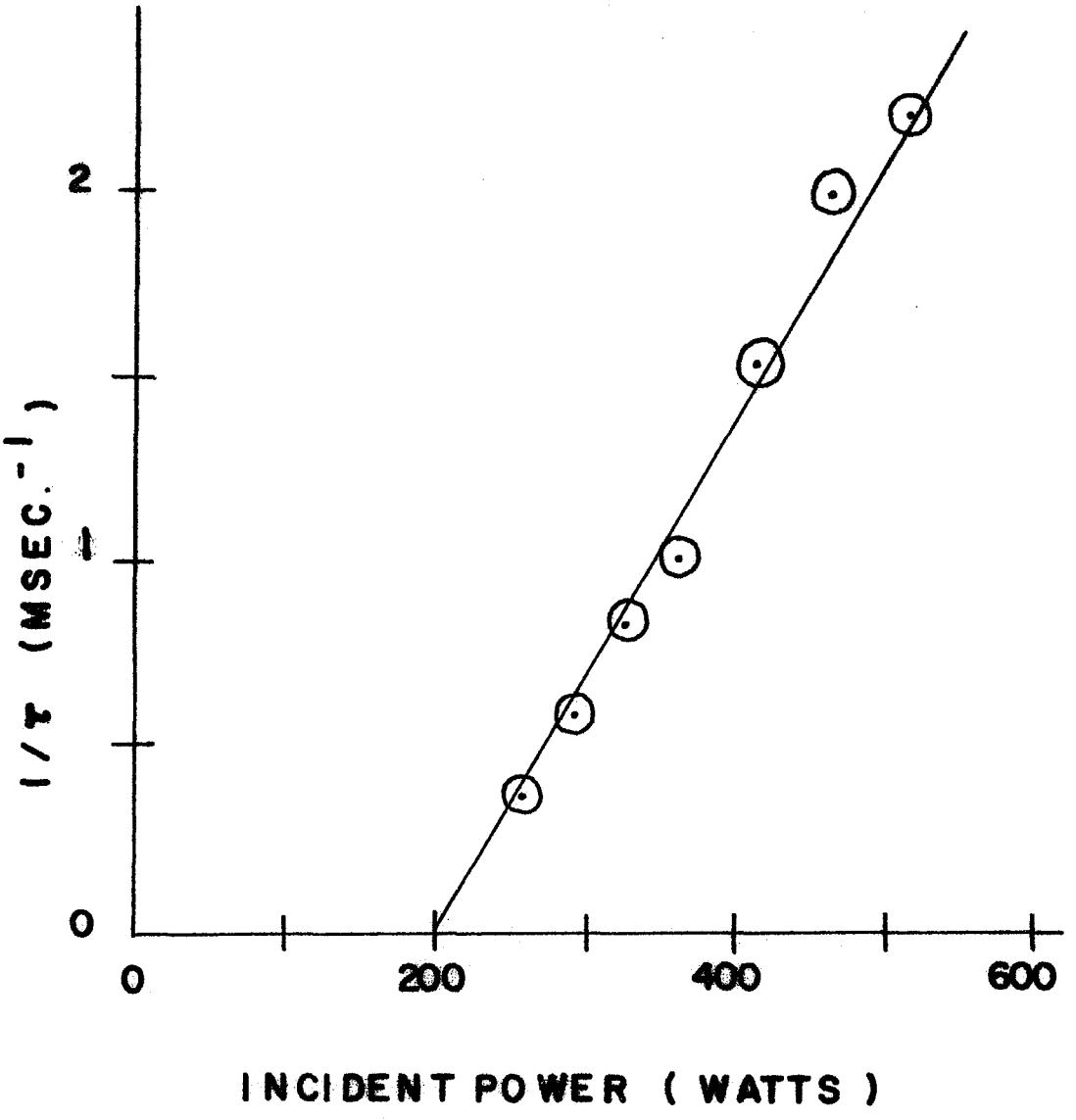

FIG. 28

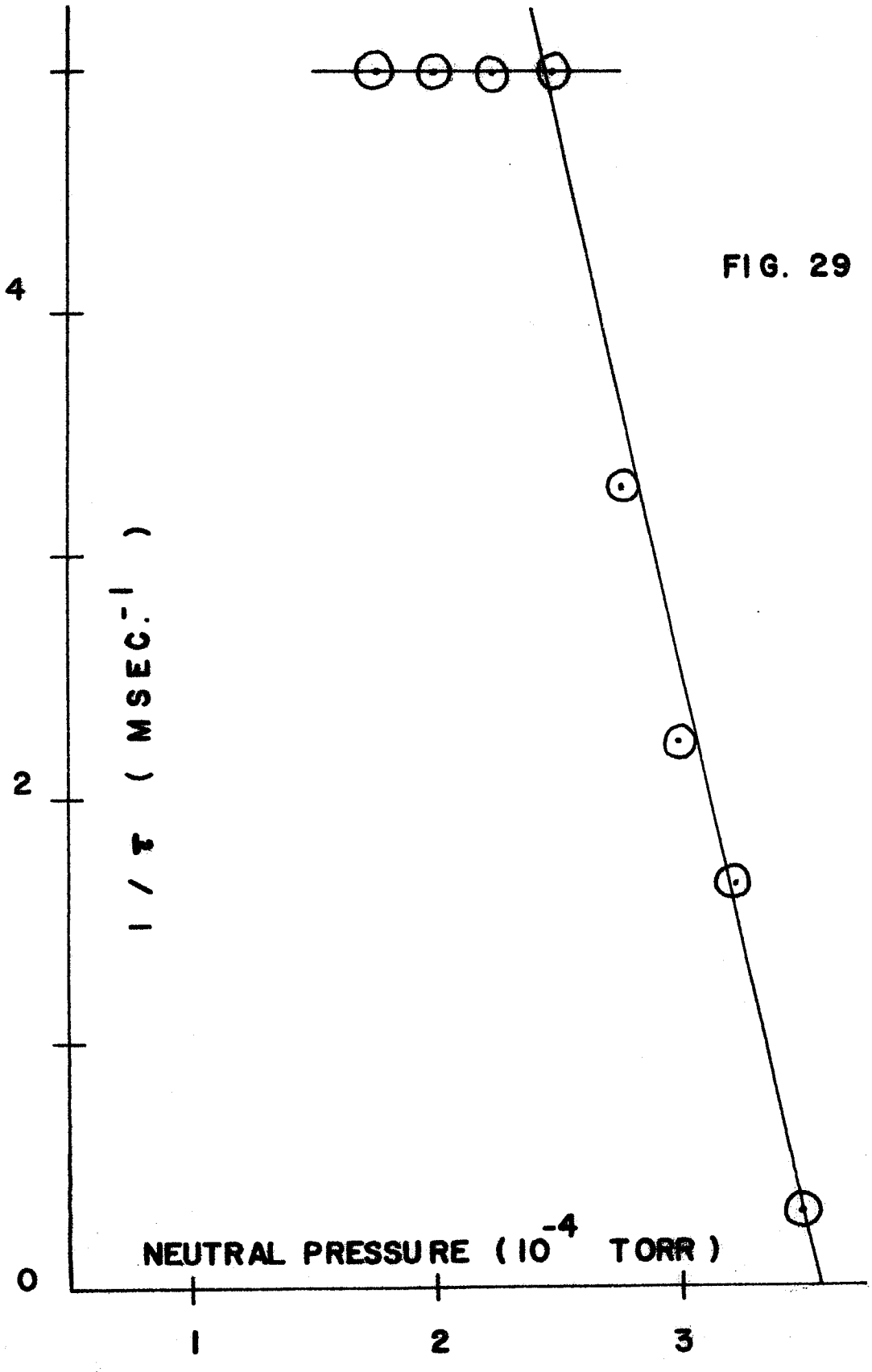

FIG. 29

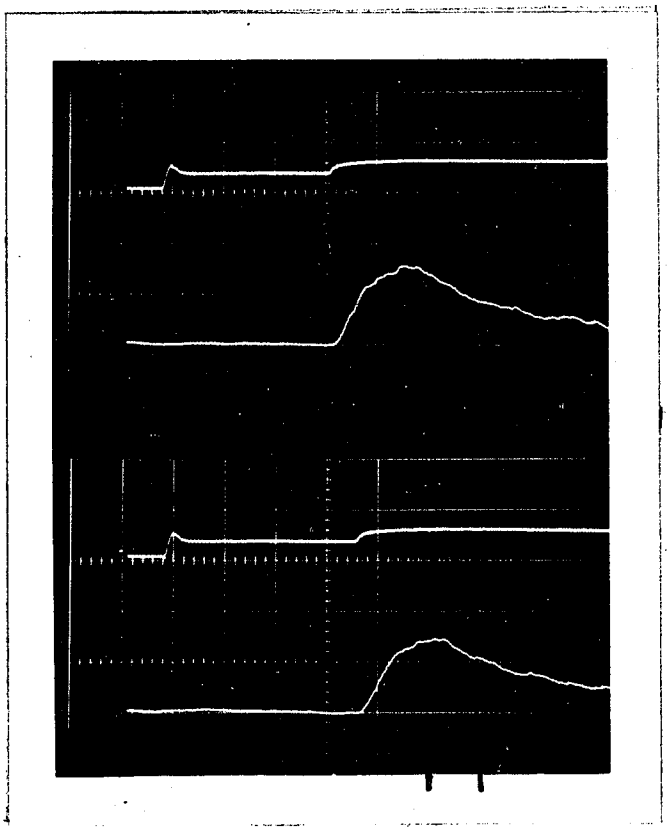

DIA.(PRESSURE)

RF AT 3.97 GHz

0.2 MSEC. / DIV.

FIG. 30

5. REFERENCES

1. T. Stix, The Theory of Plasma Waves, McGraw-Hill Book Co. (1962) pp. 22-25.

2. J.L. Shohet, Phys. Rev. 136, A 125 (1964).

3. L.A. Ferrari, A.W. McQuade, and R.J. La Haye, Physics of Fluids 17, 1785 (1974).

4. F.W. Sears, Thermodynamics, Addison-Wesley (1964) p. 247.

IV. CONCLUSIONS

Strong transmission of left wave power through a nominally overdense plasma is observed. For a certain set of experimental parameters about 25% of the left wave power is transmitted through the plasma while a linear theory predicts that less than 0.01% of the power should tunnel through.

The transition of both the perpendicular density and electromagnetic field profiles from peaked on axis to annular configurations indicates that the original non-propagating state is unstable. However, a simple two density model of the observed annular density profile cannot explain either the strong left wave transmission or the annular field profiles. The ponderomotive self-focusing mechanism may be in operation here but no theory now exists to calculate the threshold power for such self-focusing in a magnetized plasma. However, in an unmagnetized plasma near cutoff, the threshold power drops to about 2000 watts for the parameters of our experiment.[1] This is an order of magnitude too high for the mechanism to work here. Thermal self-focusing is not a viable explanation of the profile transitions when the electron mean free path is much longer than the axial length of the plasma.[2] The energy deposited by the wave in the plasma is then conducted out of the local "hot spot" region faster than the plasma pressure can build up and focus the wave. For the parameters of our experiment in an unmagnetized plasma, the threshold for thermal self-focusing[2] is about 140 watts per square cm, which is more than an order of magnitude too high for the mechanism to work unless an anomalously high collision frequency (and thus short electron mean free path) is in effect here to lower the threshold.

After a time τ of left wave propagation through the plasma, the plasma abruptly becomes opaque to both the left and right waves. Total reflected power drops to less than 5% of the incident microwave power and the electron temperature increases by up to 50% upon absorption of the left wave. Radiation near the electron plasma frequency is excited at the time of the left wave absorption, suggesting a mechanism in which the left wave is converted into electrostatic waves which then heat the the electrons via Landau damping. A parametric

decay of the left wave at 2.45 GHz into such electrostatic waves near the electron plasma frequency at 4.0 GHz is not a viable explanation of the effect as the frequency selection rule is not satisfied.

An effect in which an electromagnetic wave can penetrate into a nominally overdense magnetized plasma and transfer its energy to the plasma with a subsequent increase in the electron temperature has been observed. No satisfactory theoretical explanation of the effect exists at this time. Further experiments with an independently produced plasma and a solely left handed incident wave should lead to a better understanding of the mechanism behind the effect.

1. REFERENCES

1. P. Kaw, G. Schmidt and T. Wilcox, Physics of Fluids 16, 1522 (1974).

2. F.W. Perkins and E.J. Valeo, Phys. Rev. Letters 32, 1234 (1974).

APPENDIX A - THE LINEAR THEORY OF ELECTROMAGNETIC WAVE PROPAGATION IN A MAGNETIZED PLASMA

1. THE COLD UNBOUNDED PLASMA

Consider a fully ionized hydrogen plasma of density n electrons per cc, of infinite extent, and with an external static magnetic field $\vec{B}_o$ applied in the z-direction. An electromagnetic wave propagating in such a medium will exert forces on the charged particles and therebye induce oscillating charge and current densities. As a result the magnetized plasma will act like a dielectric medium.

The cold plasma approximation is to neglect the thermal motion of the charges. The force due to the wave magnetic field is neglected as being of order v/c of the force due to the wave electric field, where v is the particle speed and c is the speed of light.

Assuming a wave electric field of the form

$$\vec{E} = \vec{E}_o \exp(i\vec{k}\cdot\vec{r} - i\omega t) \tag{8}$$

where $\vec{k}$ is the wavenumber and ω the radial frequency, one computes the current densities through the use of Newton's second law.

These current densities can be expressed in terms of a conductivity tensor $\vec{\vec{\sigma}}$.

$$\vec{j} = \vec{\vec{\sigma}}\cdot\vec{E} \tag{9}$$

The more usual way of expressing the response of the plasma is by defining an effective dielectric tensor for the medium.

$$\vec{\vec{K}} \equiv \vec{\vec{1}} + \frac{4\pi i}{\omega}\vec{\vec{\sigma}} \tag{10}$$

where

$$\vec{\vec{K}} = \begin{pmatrix} K_{xx} & K_{xy} & 0 \\ -K_{xy} & K_{xx} & 0 \\ 0 & 0 & K_{zz} \end{pmatrix} \tag{11}$$

$$K_{xx} = (K_R + K_L)/2 \tag{12}$$

$$K_{xy} = i(K_R - K_L)/2 \tag{13}$$

$$K_{zz} = K_p \tag{14}$$

and

$$K_R = 1 + \frac{\omega_p^2/\omega^2}{\frac{|\omega_c|}{\omega} - 1} \tag{15}$$

$$K_L = 1 - \frac{\omega_p^2/\omega^2}{\frac{|\omega_c|}{\omega} + 1} \tag{16}$$

$$K_p = 1 - \omega_p^2/\omega^2 \tag{17}$$

Here zz designates the direction of the static magnetic field and $|\omega_c| = eB_o/mc$ is the electron cyclotron frequency. ω_p is the plasma frequency,

$$\omega_p = \left(\frac{4\pi N e^2}{m_e} \right)^{1/2} \tag{18}$$

Frequencies well above the ion cyclotron and ion plasma frequency are of interest here so the ion motion can be neglected. The ions are too massive to respond to very high frequency fields.

As can be seen from the form of the dielectric tensor the plasma is anisotropic. The response of the plasma to the wave depends on the orientation of the wave to the static magnetic field.

The plasma is also dispersive. Different frequencies ω will have different phase velocities ω/k.

In general the plasma is also dissipative. The inclusion of warm plasma or collisional effects can act to damp the waves. Collisions disrupt the electron motion induced by the wave and can absorb energy out of the wave as a result. In this experiment the collision frequency ν for electrons with either ions or neutrals is about 10^{+6} sec^{-1} ($\nu/\omega \approx 10^{-4}$.) Thus the wave induces about 10,000 oscillations in the electrons before a collision can disrupt the motion. Collisional damping should be negligible as a result and will be considered so here. The damping due to thermal motion will be considered in the next section.

Placing the dielectric tensor in Maxwell's equations leads to an equation for the waves.[1]

$$\vec{K} \times (\vec{K} \times \vec{E}) + \frac{\omega^2}{c^2} \vec{\vec{K}} \cdot \vec{E} = 0 \tag{19}$$

For propagating waves along $\vec{B}_o$ there are only two modes. One is right hand circularly polarized (RHCP), rotates in the same sense as the electrons about $\vec{B}_o$ and resonates at the electron cyclotron fre-

quency:

$$\frac{c^2 K_z^2}{\omega^2} = K_R = 1 + \frac{\omega_p^2/\omega^2}{\frac{|\omega_c|}{\omega} - 1} \tag{20}$$

When $\omega = |\omega_c|$, the electrons are acted upon by a static electric field. For the cold plasma in this limit $k_z \to \infty$, $\lambda \to 0$, $\omega/k_z \to 0$, and $v_g \equiv d\omega / dk_z \to 0$. This is seen in Figure 31 for typical experimental values (f=2.45 GHz, $B_o \approx 875$ gauss, n=2 x 10^{+11} /cc.)

The second mode of propagation along $\vec{B}_o$ is left hand circularly polarized (LHCP), rotates in the same sense as the ions, and would resonate at the ion cyclotron frequency (which is far below the frequen- of interest here):

$$\frac{c^2 K_z^2}{\omega^2} = K_L = 1 - \frac{\omega_p^2/\omega^2}{\frac{|\omega_c|}{\omega} + 1} \tag{21}$$

If the right hand side of the above dispersion relation is negative, as it is for this experiment, k_z^2 is negative, so k_z is imaginary. The wave would have the form

$$\exp\left(-|K_z|z - i\omega t\right) \tag{22}$$

and would be attenuated. This is an evanescent mode where no energy can be propagated (Re time averaged Poynting vector is zero). Such a mode is cutoff and the plasma is said to be overdense. When the right hand side goes through zero, is cutoff, the wave should be reflected back into the propagating region where $k_z^2 > 0$.

FIGURE CAPTION

Fig. 31. The wavenumber k_z, the phase velocity normalized by the speed of light v_{ph}/c, and the group velocity normalized by the speed of light v_g/c for the right wave at a density of $2 \times 10^{+11}$ /cc and frequency of 2.45 GHz are plotted against the ratio of electron cyclotron frequency $|\omega_c|$ to wave frequency ω.

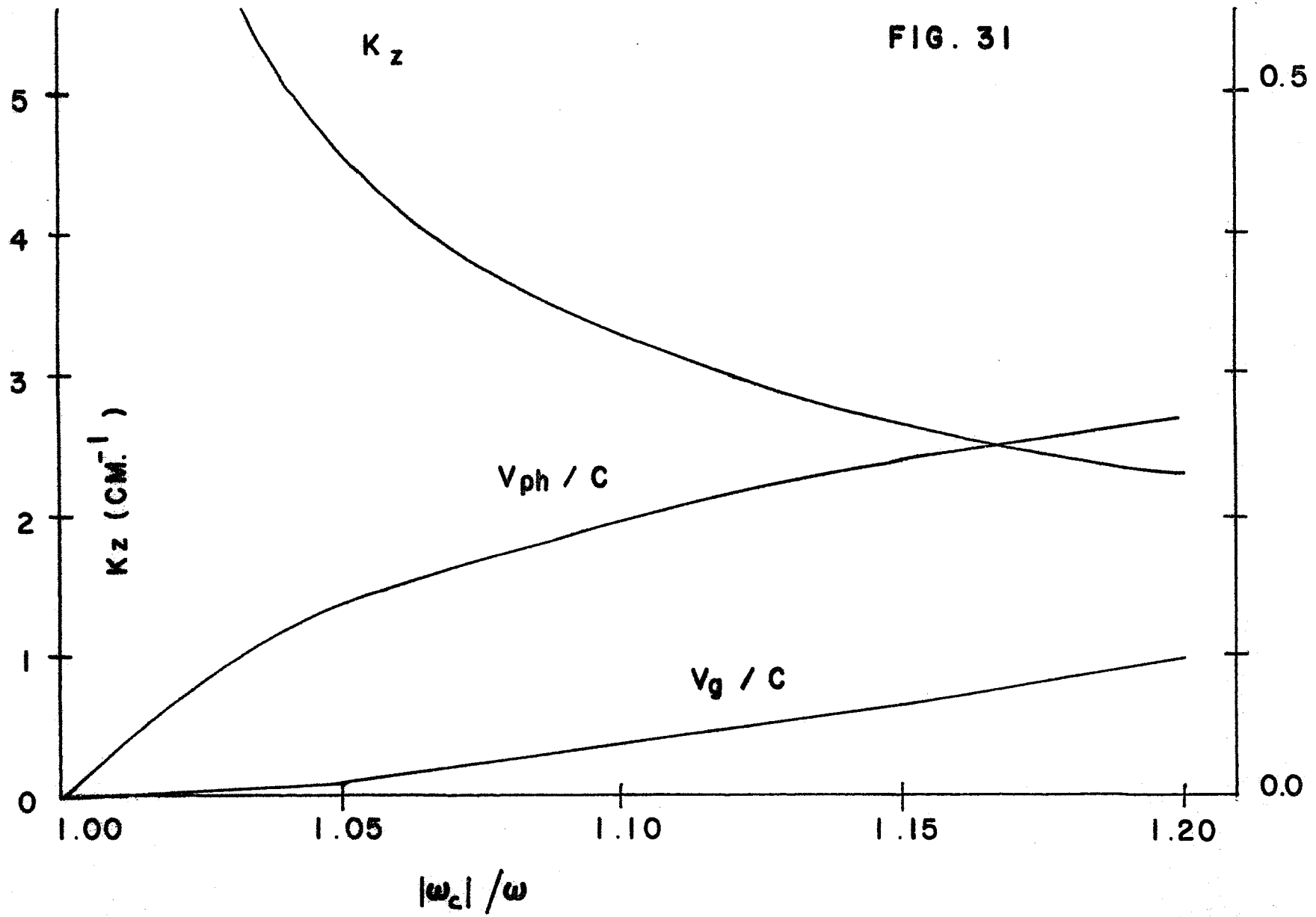
FIG. 31
K_z
V_{ph} / C
V_g / C
K_z ($CM.^{-1}$)
$|\omega_c|$ /ω
0
1
2
3
4
5
0.0
0.5
1.00
1.05
1.10
1.15
1.20

2. THE WARM PLASMA

At or near a resonance the cold plasma theory breaks down. For the cold RHCP mode when $\omega - |\omega_c| = 0$, k_z diverges. For finite electric field the Maxwell's equation

$$\nabla \times \vec{E} = -\frac{1}{c} \frac{\partial \vec{B}}{\partial t} \tag{23}$$

then requires the wave electric field $\vec{E}$ to become parallel to $\vec{k}$ so that the magnetic induction remains finite. Furthermore the phase velocity goes to zero and the linearizing assumptions used in Newton's second law to compute the current densities no longer hold.

By including the effects of thermal motion, a warm plasma, the propagation at or near a resonance can be correctly described. If the electrons have thermal motion v_z along B_{o_z} then the electron is resonant only when the Doppler shifted frequency equals the cyclotron frequency.

$$\omega \pm K_z V_z = |\omega_c| \tag{24}$$

If the electrons have a distribution of thermal velocities then only a few electrons meeting the above condition can be resonant. For a Maxwellian distribution

$$\overline{V}_z \approx \sqrt{\frac{K_B T_e}{m_e}} \tag{25}$$

and cold plasma theory should hold provided

$$|\omega \pm |\omega_c|| \gg |K_z \overline{V}_z| \tag{26}$$

For 8 ev electrons the right mode more than about 5% from resonance and the left mode for all parameters of interest here should obey cold plasma theory.

The right wave very near to resonance requires a statistical treatment. Let $f(\vec{v}, \vec{r}, t)$ be the distribution function for the electrons. This is the probability of finding the electron in the phase space interval $\vec{v}$ to $\vec{v} + d\vec{v}$, $\vec{r}$ to $\vec{r} + d\vec{r}$, and t to t + dt. Without the wave f is equal to some zero order distribution f_o such as a Maxwellian.

$$f_o = \left(\frac{m_e}{2\pi K_B T_e}\right)^{3/2} \exp\left(-\frac{mv^2}{2K_B T_e}\right) \tag{27}$$

The wave is assumed to make a small perturbation $|f_1| \ll |f_o|$ on the zero order distribution. f_1 is found by solving to first order in f_1 and $\vec{E}_1$ the Vlasov equation for the electrons.[2]

$$\frac{\partial f}{\partial t} + \vec{v} \cdot \frac{\partial f}{\partial \vec{r}} - \frac{e}{m_e}\left(\vec{E}_1 + \frac{\vec{v} \times \vec{B}_1}{c} + \frac{\vec{v} \times \vec{B}_o}{c}\right) \cdot \frac{\partial f}{\partial \vec{v}} = 0 \tag{28}$$

The resultant charge and current densities are given from the appropriate integrals of f_1.

$$\rho = -N_o e \int f_1 \, d\vec{v} \tag{29}$$

$$\vec{j} = -N_o e \int \vec{v} f_1 \, d\vec{v} \tag{30}$$

These integrals then give the thermally corrected dielectric constant for the RHCP mode. To perform the integrals a suitable zero order distribution function f_o must be chosen.

The most general f_o of interest here is a bi-Maxwellian ($T_\perp \neq T_{//}$) with a mirror loss cone effect.[3] In a mirror machine electrons with

$|v_z| > v_\perp (R-1)^{1/2}$ (where R is the mirror ratio) are moving fast enough to escape the machine, a loss cone.[4] The normalized f_o becomes

$$f_o = 0 \quad , \qquad v_\perp < |v_z| / (R-1)^{1/2}$$

$$f_o = \frac{1}{N \pi^{3/2} \alpha_\perp^2 \alpha_z} \exp\left(- \left(\frac{v_\perp}{\alpha_\perp}\right)^2 - \left(\frac{v_z}{\alpha_z}\right)^2 \right) ,$$

$$v_\perp > |v_z| / (R-1)^{1/2} \tag{31}$$

$$N \equiv \left(\frac{(R-1)\,\Theta}{(R-1)\,\Theta + 1} \right)^{1/2} \tag{32}$$

$$\Theta \equiv \left(\alpha_\perp / \alpha_z \right)^2 \tag{33}$$

$$\alpha_z \equiv \left(\frac{2 K_B T_{e\parallel}}{m_e} \right)^{1/2} \tag{34}$$

$$\alpha_\perp \equiv \left(\frac{2 K_B T_{e\perp}}{m_e} \right)^{1/2} \tag{35}$$

Using the above f_o leads to the thermally corrected dispersion relation for the right wave. $Z(\phi)$ is known as the plasma dispersion function.[5]

$$\frac{c^2 k_z^2}{\omega^2} = 1 + \frac{\omega_p^2}{\omega^2}\left[\frac{\omega}{k_z \alpha_z N} Z(\phi) + (\theta - 1)\left(1 + \phi Z(\phi)\right) + \frac{1}{R-1}\left(\frac{1}{2} + \phi^2\left(1 + \phi Z(\phi)\right)\right)\right] \quad (36)$$

$$\phi \equiv \frac{\omega - |\omega_c|}{k_z \alpha_z N} \quad (37)$$

$$Z(\phi) \equiv \frac{1}{\sqrt{\pi}} \int_{-\infty}^{+\infty} \frac{e^{-t^2}}{(t - \phi)}\, dt \quad (38)$$

The dispersion relation has been evaluated numerically for typical experimental parameters. The power flow into the mirror machine is calculated by integrating the Im k_z thus obtained over z.

$$P = P_o \exp\left(-2 \int_{z_o}^{z} I_m K_z(z)\, dz\right) \quad (39)$$

Figure 32 shows the real and imaginary parts of k_z for the typical mirror ratio of 1.20 and a mirror ratio of 1000 (no loss cone in effect). Allowing for a loss cone has qualitatively little effect on k_z for these conditions.

The cold plasma theory is in excellent agreement with the warm plasma result until about 6% from resonance. Then Re k_z goes to a finite maximum rather than infinity and Im k_z appears. This Im k_z diminishes the wave amplitude (electron cyclotron damping.)[6]

Figure 33 shows the normalized power flow into the mirror machine.

FIGURE CAPTIONS

Fig. 32. The real and imaginary parts of the wavenumber for the right wave with the conditions of Fig. 31 and the addition of thermal effects are plotted. Computations are shown for Te = 8 ev, $Te_{\perp} = Te_{//}$, and mirror ratios R of 1.2 and 1000.

Fig. 33. The computed percent transmitted right wave power is plotted as a function of axial position. The power damping is computed from the imaginary part of the wavenumber in Fig. 32 and the axial magnetic field profile of Fig. 5.

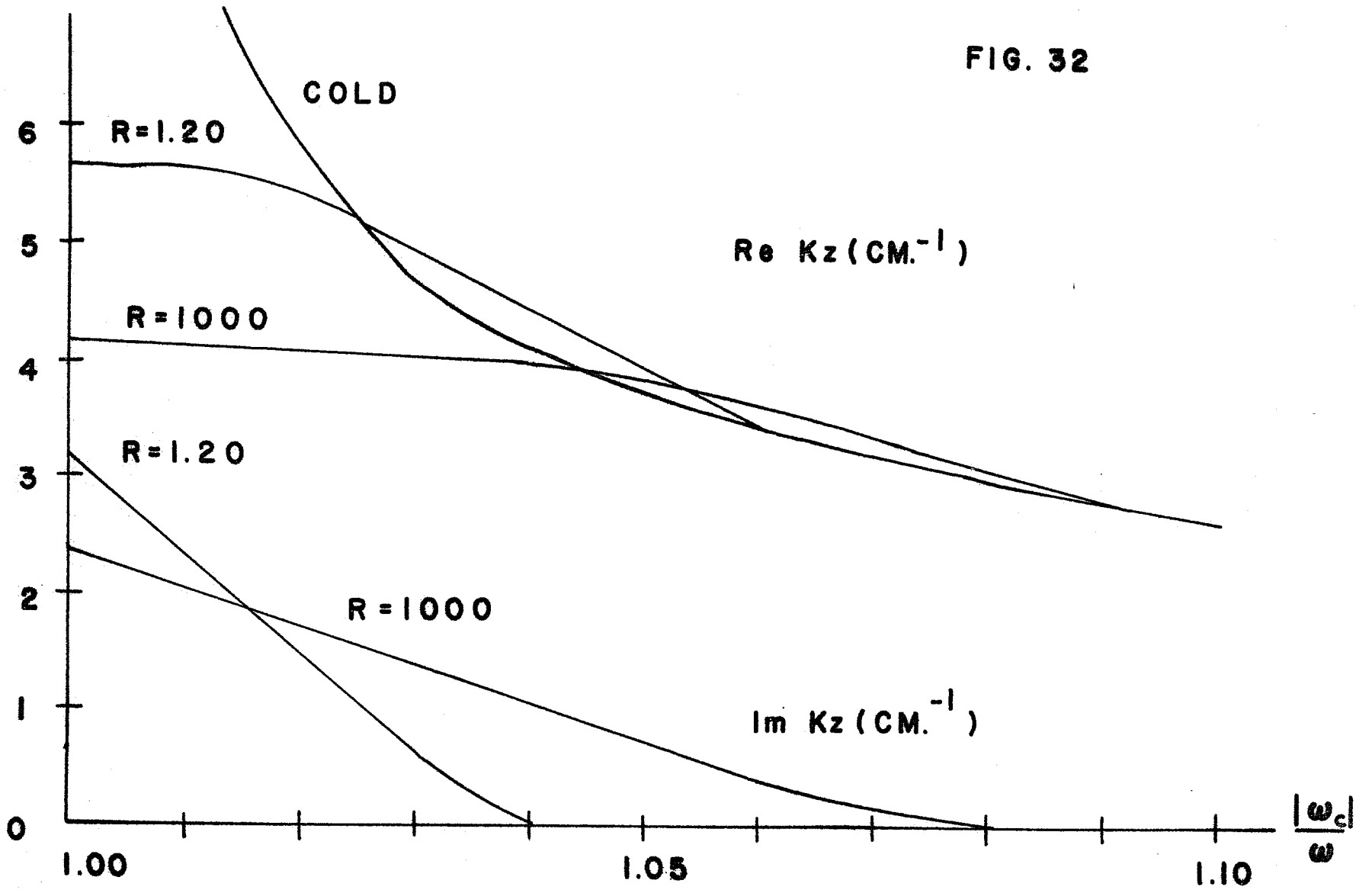
FIG. 32
COLD
R=1.20
R=1000
R=1.20
R=1000
Re Kz (CM.-1)
Im Kz (CM.-1)
6
5
4
3
2
1
0
1.00
1.05
1.10
|ωc|/ω

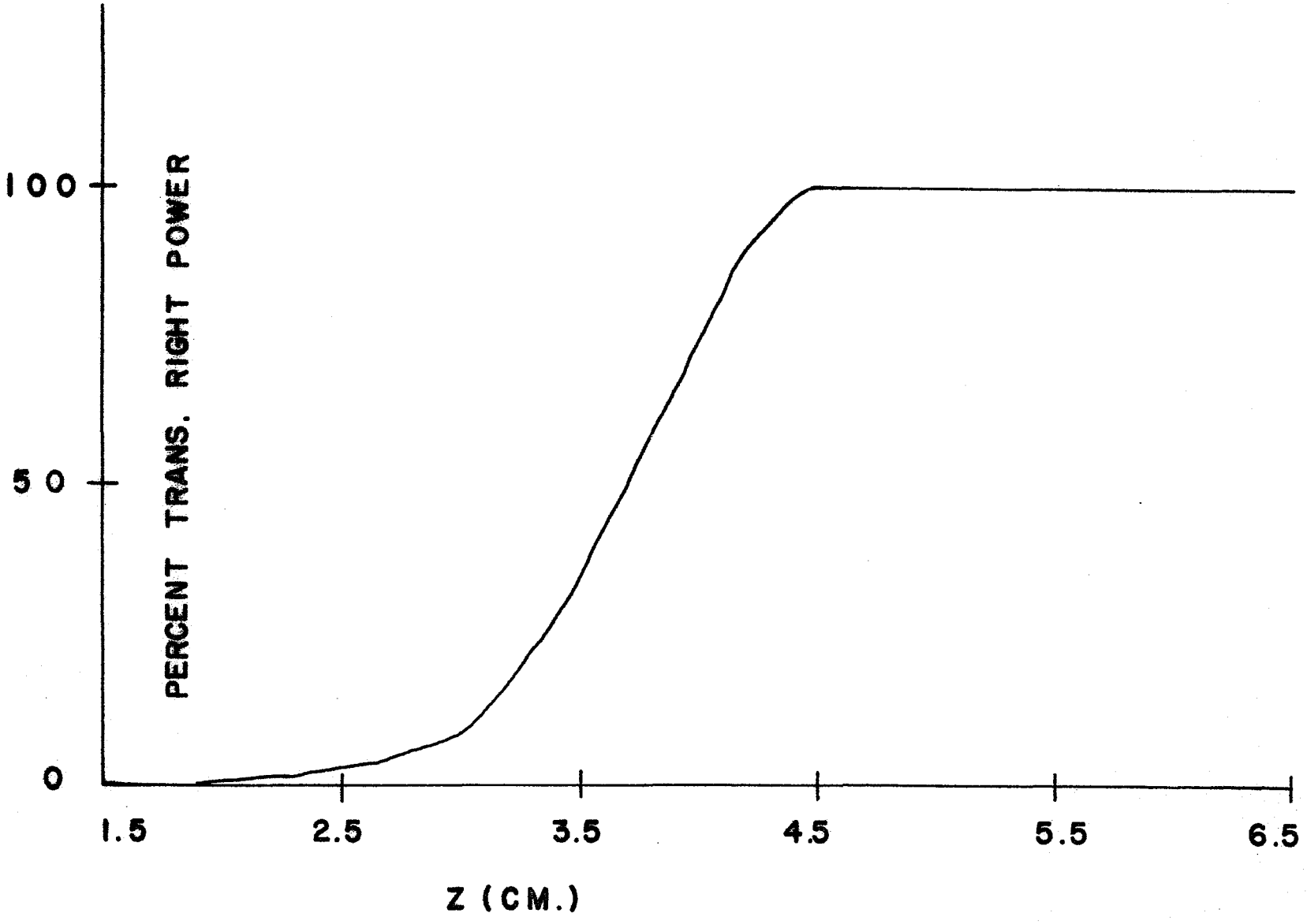

FIG. 33

$|\omega_c|/\omega = 1.20$ at z=+22 cm where the wave enters the machine. The magnetic field steadily decreases until $|\omega_c|/\omega = 1.00$ at z=+1.5 cm. Note that all of the right wave power is absorbed before the wave reaches the true resonance region at z=+1.5 cm. This is done by resonant electrons satisfying [2,7]

$$\omega + k_z v_z - |\omega_c| = 0 \tag{40}$$

With a mirror geometry for the magnetic field, linear instabilities can arise in which the electromagnetic waves considered here can be amplified instead of being damped.[4,8,9] A loss cone in velocity space caused by the leakage of axially fast electrons out of the finite ratio mirrors or an anisotropic temperature distribution in which the perpendicular electron temperature $T_{e\perp}$ is much greater than the parallel electron temperature $T_{e\parallel}$ can arise. With a mirror ratio R of 1.20 and $T_{e\perp}/T_{e\parallel} \gtrsim 5$, such an instability can be computed to exist for the right wave where $|\omega_c|/\omega \approx 1.05$. However, as the wave propagates deeper into the mirror machine where $|\omega_c|/\omega \approx 1.00$, the amplification changes to damping and effectively no right wave power is calculated to be transmitted through the machine.

The analysis of equations (31) to (38) was also applied to the left wave but no significant change from cold plasma theory could be computed.

3. THE COLD PLASMA IN A CYLINDRICAL WAVEGUIDE

In any laboratory experiment the plasma of interest cannot be infinite in extent but must be bounded. Since waveguides are convenient devices for transmitting radio frequency waves, the properties of a magnetized plasma contained in a perfectly conducting cylindrical waveguide are of interest here.

The waveguide is to be of radius a. The static magnetic field is in the axial direction. To begin both the static magnetic field and the plasma density are considered to be uniform.

The problem in enclosing the plasma in a conducting waveguide is that boundary conditions are placed on the fields. At the walls (r=a) $Ez=0=E_\theta$. It is no longer possible for there to be no variation in the fields in the direction perpendicular to the static magnetic field. The dispersion relation for both the right and left modes will depend on the boundaries.

To solve for the dispersion relation, the z, t dependence is again taken as exp $(ik_z z - i\omega t)$ but the fields are allowed to have a radial dependence g(r) which is to be determined and an azimuthal dependence exp $(-im\theta)$. Placing the cold plasma dielectric tensor in Maxwell's eqns. leads to a series of equations for the fields which can be factored into a dispersion relation relating k_z , ω , and the perpendicular wave numbers p. In general two values of p are needed.[10]

$$p^4 - \left[-k_z^2\left(\frac{K_{zz}}{K_{xx}}+1\right)+\frac{\omega^2}{c^2}\left(K_{zz}+\frac{K_R K_L}{K_{xx}}\right)\right]p^2$$

$$+\frac{K_{zz}}{K_{xx}}\left(-k_z^2+\frac{\omega^2}{c^2}K_R\right)\left(-k_z^2+\frac{\omega^2}{c^2}K_L\right)=0 \qquad (41)$$

The boundary conditions that Ez and E_θ go to zero at r=a lead to a boundary value equation which when solved along with the dispersion relation give the complete solution for the propagation.[11]

$$g_2 J_M'(\rho_1 a)\, J_M(\rho_2 a) - g_1 J_M'(\rho_2 a)\, J_M(\rho_1 a)$$

$$= i M \frac{\omega^2}{c^2} K_{xy} \frac{(\rho_2^2 - \rho_1^2)}{a}\, J_M(\rho_1 a)\, J_M(\rho_2 a) \qquad (42)$$

where
$$g_{1,2} = \left(\frac{\omega^2}{c^2} K_{xy}\right)^2 - \left(\frac{\omega^2}{c^2} K_{xx} - k_z^2\right)^2$$

$$- \rho_{1,2}^2 \left(\frac{\omega^2}{c^2} K_{xx} - k_z^2\right) \qquad (43)$$

If $k_z^2 = 0$ as for a cutoff, the dispersion relation reduces to

$$\rho_1^2 = \frac{\omega^2}{c^2} K_{xx} \qquad (44)$$

the ordinary mode across $\vec{B}_o$ which is used in microwave interferometers, and

$$\rho_2^2 = \frac{\omega^2}{c^2} \frac{K_R K_L}{K_{xx}} \qquad (45)$$

the extraordinary mode across $\vec{B}_o$. Two values of p^2 are needed in general, one for $\vec{E}$ along the magnetic field and one for $\vec{E}$ perpendicular to the magnetic field.

Near a resonance $k_z^2 \to \infty$ and the dispersion relation can be reduced to

$$p^4 + K_z^2 p^2 + 0 = 0 \tag{46}$$

This has solutions for p of 0 and ik_z .

These approximate results for the values of p^2 near cutoffs (LHCP) and resonances (RHCP) can be used to check the exact solutions.

All of the fields are of the form $\exp(ik_z z - i\omega t - im\theta)$ where m is an integer. A mode m is RHCP for negative m and LHCP for positive m in the sense that the whole field pattern either rotates in a CW sense (m neg.) or a CCW sense (m pos.). At fixed z

$$\frac{d\theta}{dt} = -\frac{\omega}{m} \tag{47}$$

A solution for typical parameters and m=-1 (a right mode) is shown in Figure 34 . There is little effect on k_z due to the boundaries. This is because as k_z approaches a resonance the RHCP mode's wavelength goes to a minimum and the ratio of wavelength to guide radius becomes small. If the boundaries are many wavelengths away from the center of the guide, then one would expect them to have little effect on the parallel propagation.[13]

Now consider a left mode near ECR for the right mode with m=+1. The effect of the cylindrical conducting boundary can best be shown by plots of cutoff frequency versus electron density. For the unbounded case any frequency below 2.45 GHz will be cutoff for densities above 1.5 x 10^{+11} /cc. For the vacuum waveguide any frequency below 2.00 GHz will be cutoff. Putting a magnetized plasma inside the waveguide has the effect of raising the cutoff frequency. Putting a cylindrical conducting boundary around the magnetoplasma has the effect of lowering the cutoff density. The bounded and unbounded cutoff values are shown in Figure 35 .

For the density of 2 x 10^{+11} /cc and frequency of 2.45 GHz used in this experiment the m=+1 left mode is cutoff, does not propagate, is evanescent. An electric field profile for this evanescent mode is shown in Figure 36 .

Figure 37 shows a plot of k_z^2 versus density. At densities above $6.8 \times 10^{+10}$ /cc the left wave is cutoff. As the density is reduced below this cutoff density the wave can propagate. In the vacuum guide only the dominant TE_{11} mode can propagate.

Figure 38 shows a typical electric field profile for an m=+1 mode with density $1 \times 10^{+10}$ /cc that is below cutoff. The profiles are not very different in appearance from vacuum profiles (except for the Ez.)

In conclusion, the addition of cylindrical conducting boundaries on a left mode in a magnetized plasma has the effect of raising the band of frequencies for which the mode does not propagate. For the operating conditions of this experiment the plasma is overdense to the LHCP wave and the wave should be reflected by the plasma where $k_z^2=0$. This region should be close to the first mirror point and little if any power should be transmitted through the plasma past the second mirror point.

FIGURE CAPTIONS

Fig. 34. The bounded and unbounded axial wavenumbers are compared for the right handed wave. $|p_1|$ and $|p_2|$ are the computed perpendicular wavenumbers. The conducting cylindrical waveguide has a radius of 4.39 cm.

Fig. 35. The cutoff frequency in GHz is plotted against density in units of 10^{11}/cc. The left curve includes the effect of a cylindrical conducting guide of radius 4.39 cm. The electron cyclotron frequency used in these calculations is 1.10 times the incident microwave frequency of 2.45 GHz.

Fig. 36. The computed electric field profiles are plotted versus normalized radial position r/a for the m=+1 left wave at conditions typical of this experiment ($n=2 \times 10^{11}$/cc and $|\omega_c|/\omega = 1.10$.)

Fig. 37. The bounded left wave (m=+1) wavenumber squared in cm^{-2} is plotted versus density in units of 10^{11}/cc ($|\omega_c|/\omega = 1.10$, a=4.39 cm.) The wavenumber goes through zero (the wave is cut off) at a density of 6.8×10^{10}/cc.

Fig. 38. The same as Fig. 36 but a density of 1×10^{10}/cc for which the left wave can propagate is used.

FIG. 34

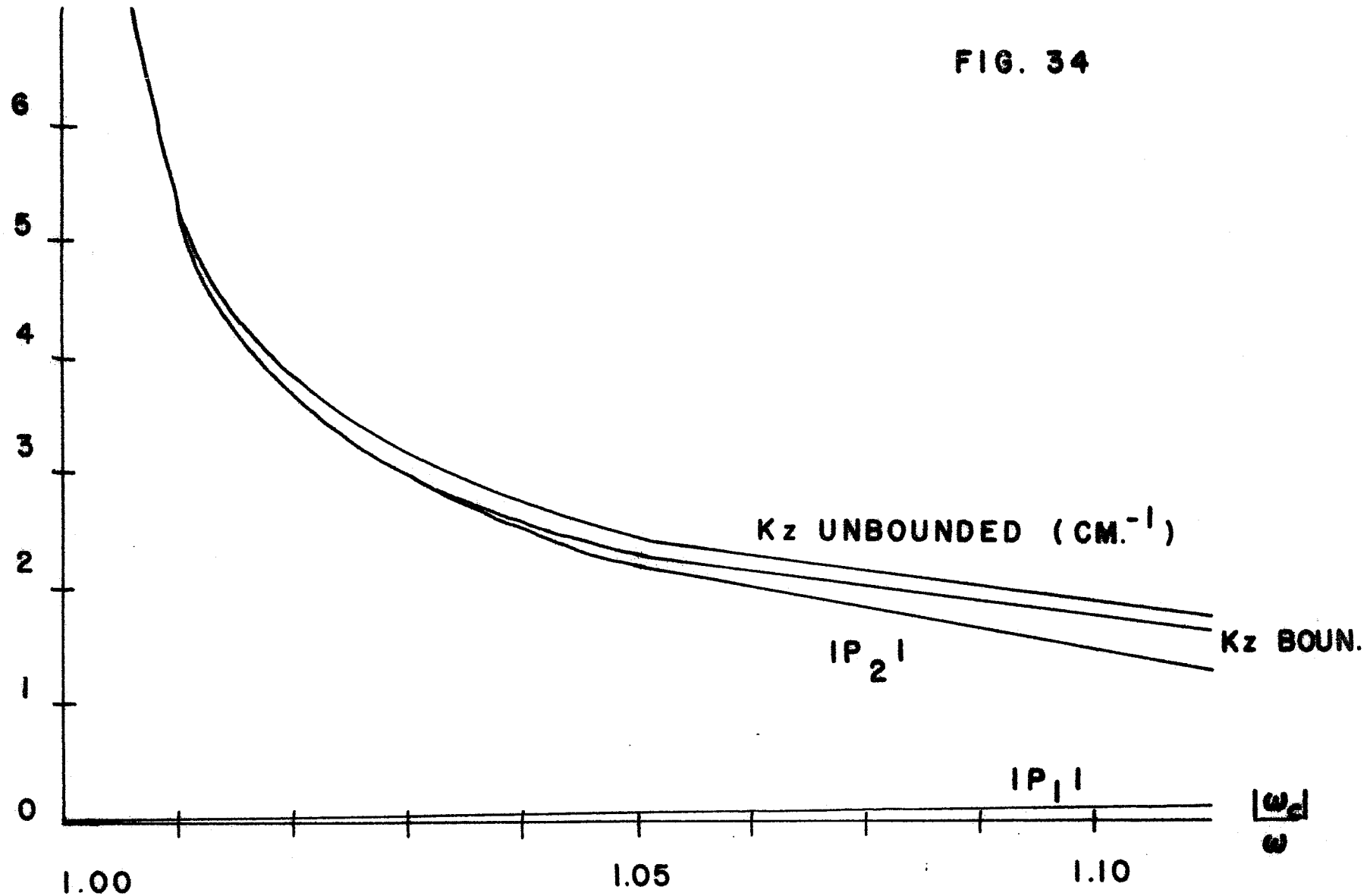
6
5
4
3
2
1
0
Kz UNBOUNDED (CM.$^{-1}$)
Kz BOUN.
$|P_2|$
$|P_1|$
$\frac{|\omega_c|}{\omega}$
1.00
1.05
1.10

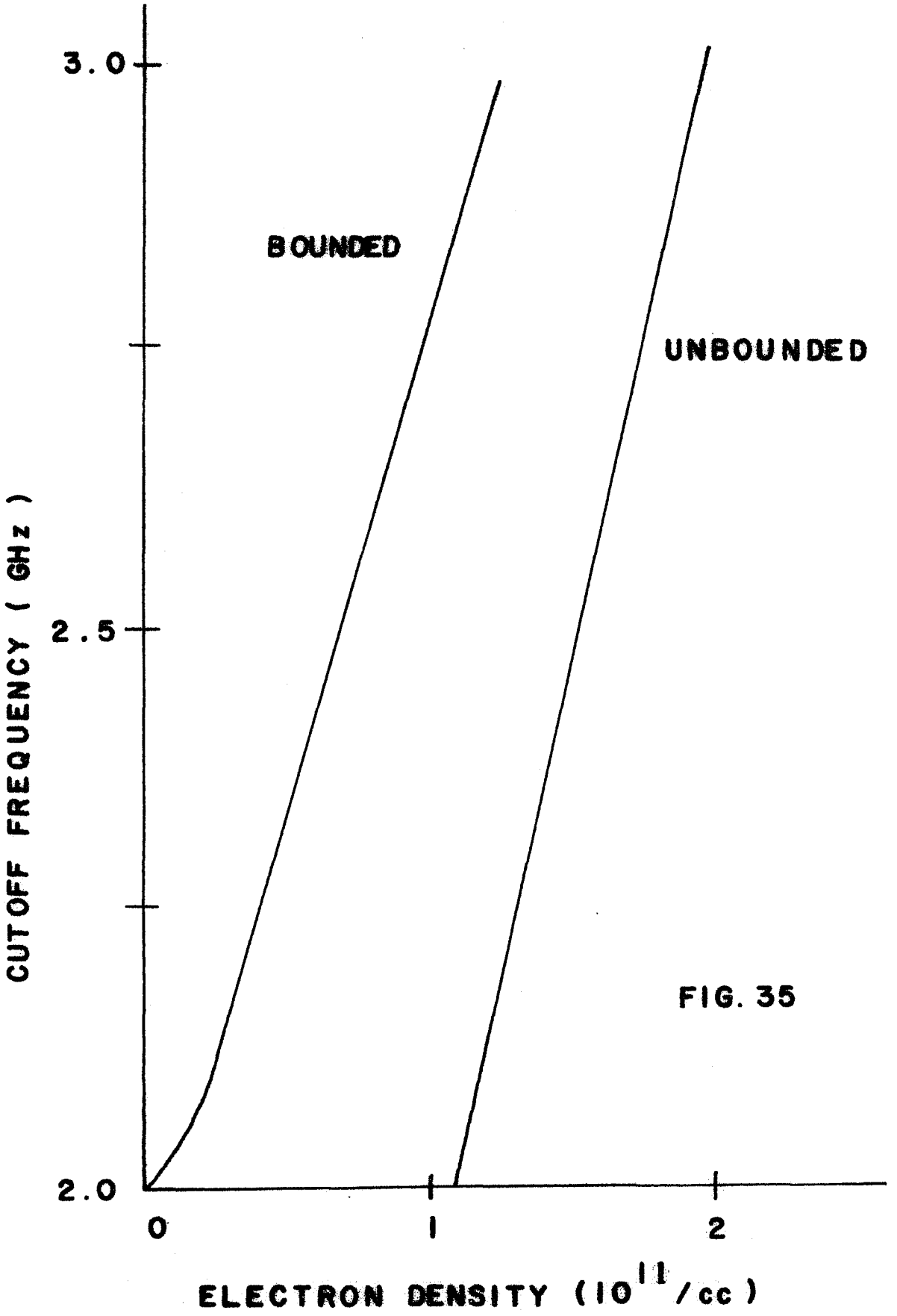
3.0
2.5
2.0
BOUNDED
UNBOUNDED
CUTOFF FREQUENCY (GHz)
0
1
2
ELECTRON DENSITY (10^{11}/cc)

FIG. 35

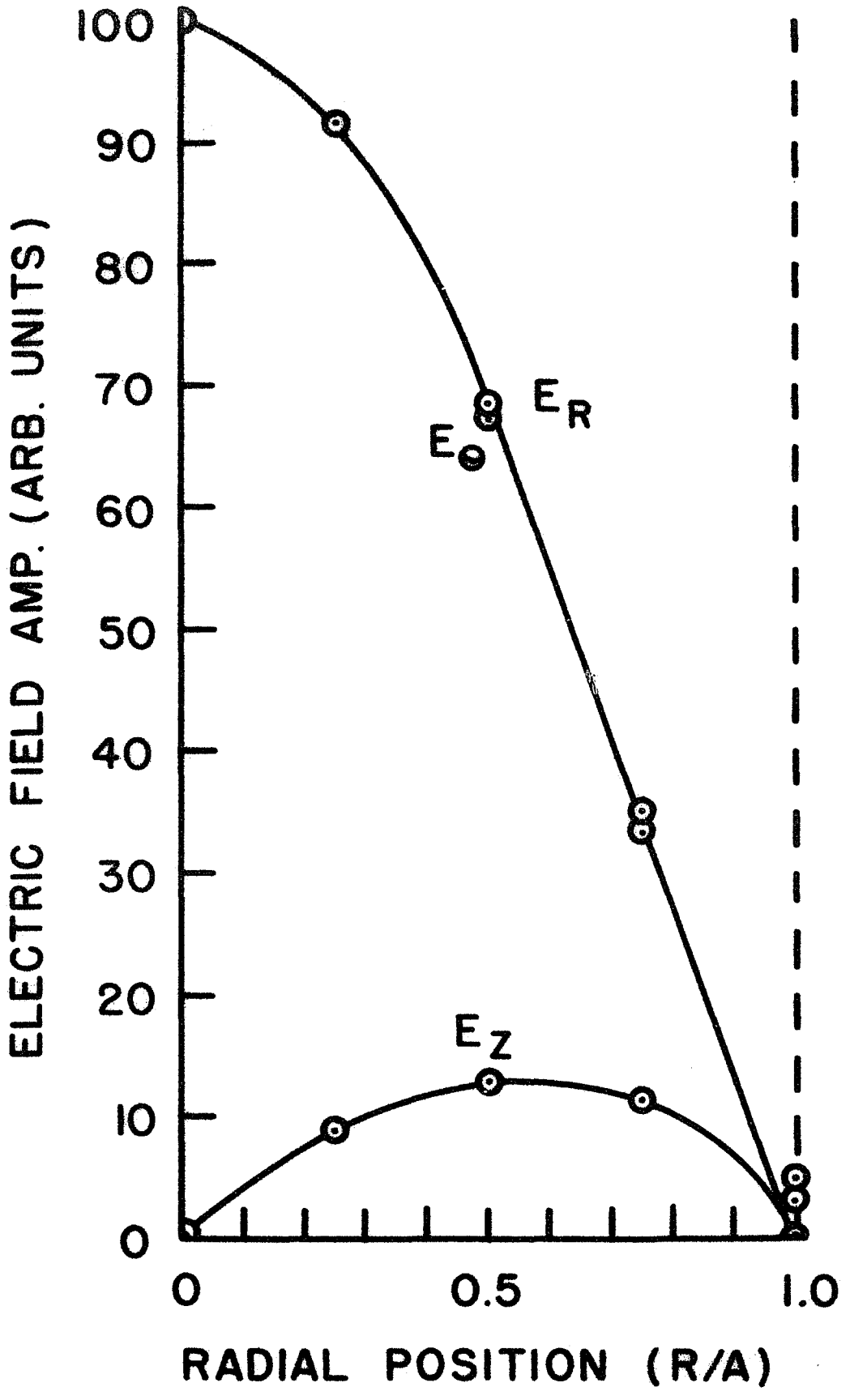
100
90
80
70
60
50
40
30
20
10
0
ELECTRIC FIELD AMP. (ARB. UNITS)
E_R
E_θ
E_Z
0
0.5
1.0
RADIAL POSITION (R/A)

FIG. 36

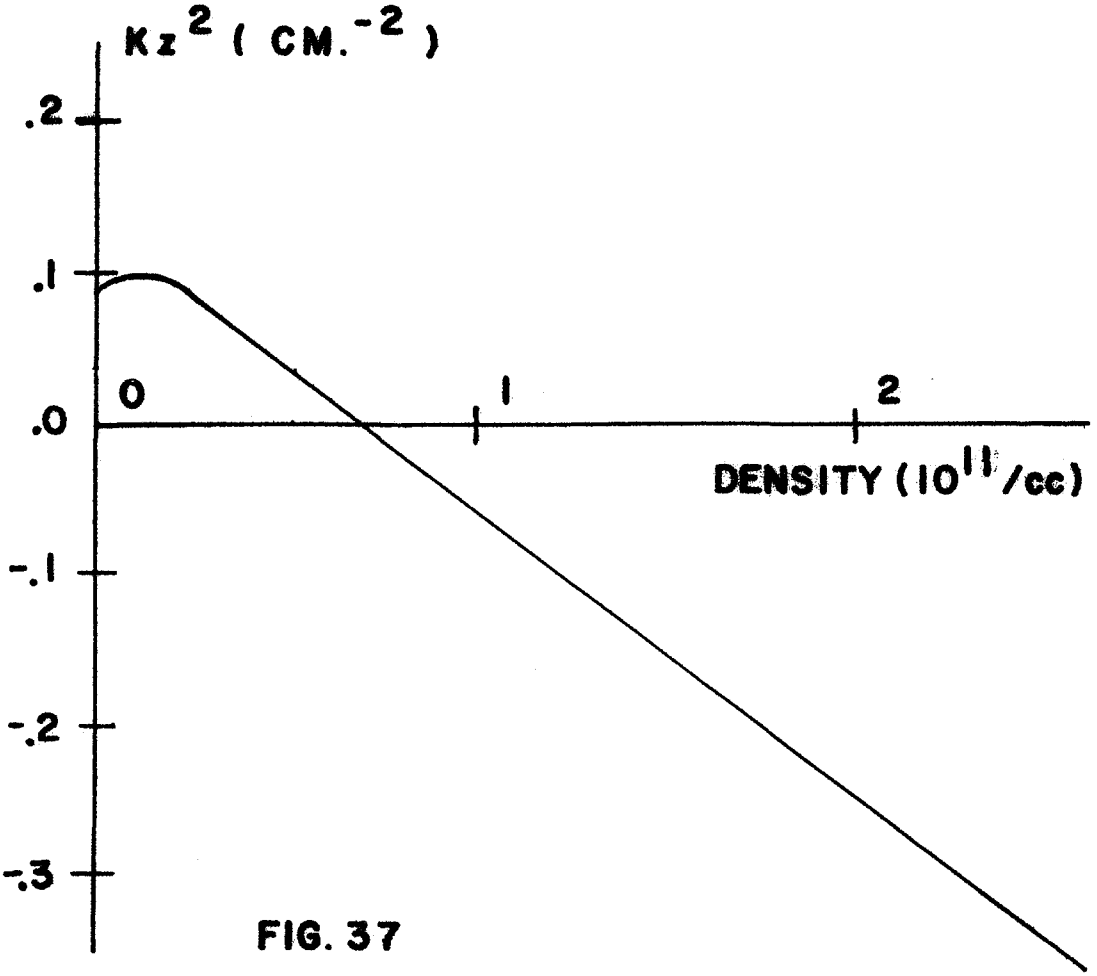

FIG. 37

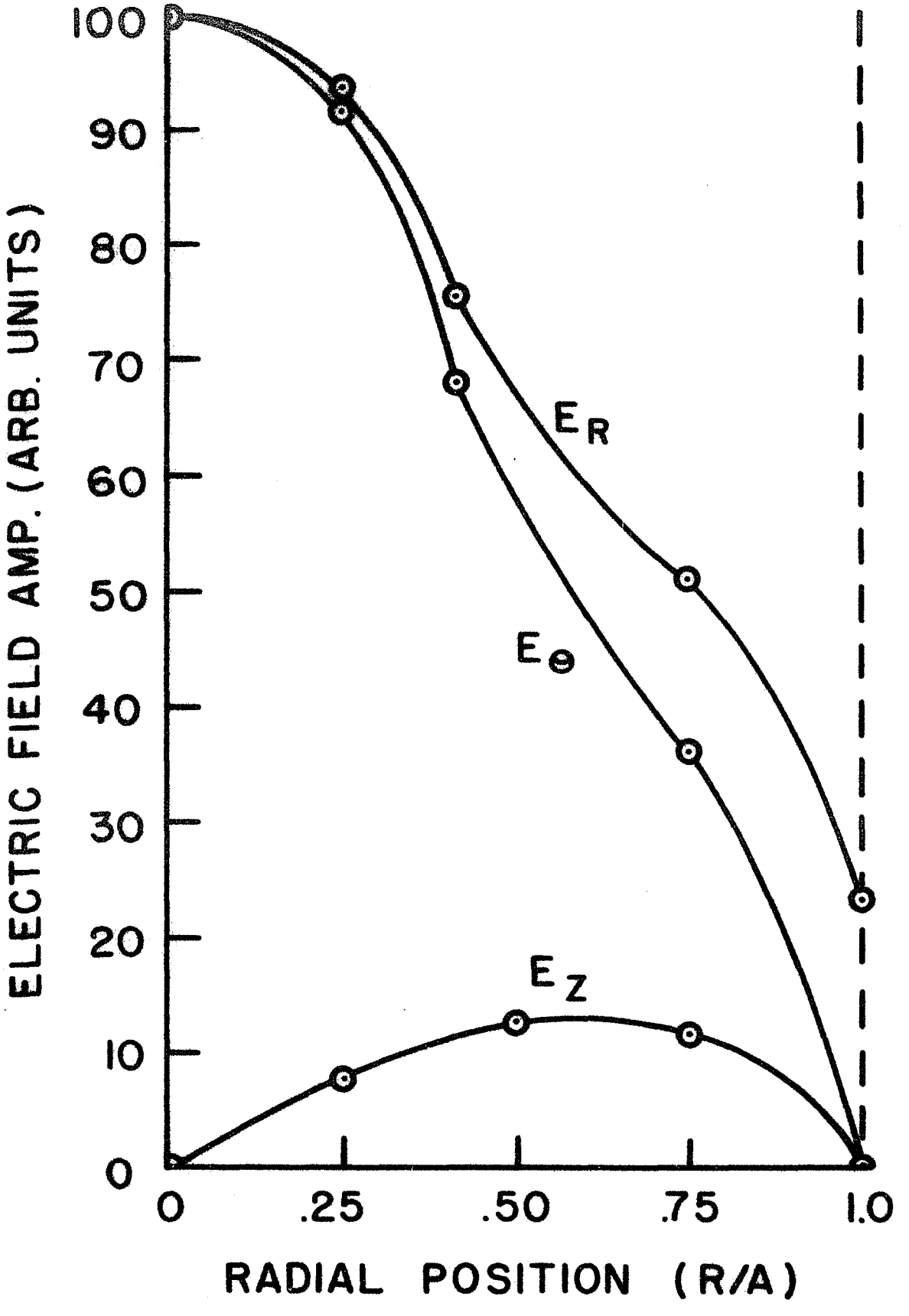
100
90
80
70
60
50
40
30
20
10
0
ELECTRIC FIELD AMP. (ARB. UNITS)
E_R
E_Θ
E_Z
0
.25
.50
.75
1.0
RADIAL POSITION (R/A)

FIG. 38

4. THE EFFECTS OF MAGNETIC FIELD AND DENSITY GRADIENTS

The calculations for the propagation of electromagnetic wave modes in a magnetized , plasma filled waveguide were based on the static magnetic field and the density being uniform. This is certainly not so. The magnetic field is in a mirror configuration. The plasma density has an axial variation of about 50% in 10 cm and has a perpendicular gradient as well.

The effects of the axial gradients can be tested by the WKB method.[14] If the plasma is at least several wavelengths long and

$$Q \equiv \left| \frac{1}{K_z^2(z)} \frac{d K_z(z)}{d z} \right| \ll 1 \qquad (48)$$

then the WKB approximation can be used. This is not valid for the left wave as the distance of 11 cm over which the density rises from zero to cutoff is less than the wavelength of about 22 cm. If the distance over which the plasma parameters change significantly is much longer than a wavelength, then the local values of the parameters determine the local wavelength.

For this experiment $Q \lesssim 0.02$ for the right hand circularly polarized wave in the plasma column. The wavelength for the right mode is so short ($\lambda \approx 1$ cm) that the wave propagates several wavelengths before n or B_{0z} can change appreciably. The WKB validity for the left mode is not as good because it is near cutoff. In fact, at the cutoff point, $k_z^2 \to 0$ and the WKB solutions break down. The WKB method then predicts complete reflection with the possibility of weak evanescent tunneling. However, for a plasma column of length 20 cm and density greater than $1 \times 10^{+11}$ /cc, the power tunneling factor $\exp(-2|k_z|z)$ would be less than 10^{-4}.

For the densities of this experiment no microwave power should be transmitted through the plasma region because of the strong cyclotron damping of the right wave and the plasma being overdense to the left wave which should be completely reflected. This is provided that there are no perpendicular density gradients.

The effect of a perpendicular density gradient is approximated by allowing the plasma to have two densities. From r = 0 to r = a the plasma density is to be n_1. From r = a to r = b (the waveguide wall) the plasma density is to be n_2. The form of the fields is known in each region. For $0 \leq r \leq a$, the z and Θ components of the electric field $\vec{E}$ and magnetic field $\vec{H}$ are given as[15]

$$E_z = A\, J_1(p_1 r) + B\, J_1(p_2 r)$$

$$E_\Theta = A\left[i \ell_2 \frac{J_1(p_1 r)}{r} + L_2 p_1 J_1'(p_1 r)\right] + B\left[i \ell_1 \frac{J_1(p_2 r)}{r} + L_1 p_2 J_1'(p_2 r)\right]$$

$$H_z = A\, h_1 J_1(p_1 r) + B\, h_2 J_1(p_2 r)$$

$$H_\Theta = A\left[i y_2 \frac{J_1(p_1 r)}{r} + Y_2 p_1 J_1'(p_1 r)\right] + B\left[i y_1 \frac{J_1(p_2 r)}{r} + Y_1 p_2 J_1'(p_2 r)\right]$$

where A and B are unknown constants to be determined,

$$i \equiv \sqrt{-1}$$

$$i \ell_{1,2} \equiv \left(\frac{p_{1,2}^2}{D} \frac{w^2}{c^2} K_{xx} - 1\right)(K_{xy}/i)$$

$$L_{1,2} \equiv \left(\frac{p_{1,2}^2}{D} \left(-K_z^2 + \frac{w^2}{c^2} K_{xx}\right) - 1\right) K_{xx}$$

$$i\,y_{1,2} \equiv \left(1 - \frac{\rho_{1,2}^2}{D}\left(-K_z^2 + \frac{w^2}{c^2}K_{xx}\right)\right)$$

$$Y_{1,2} \equiv -\frac{\rho_{1,2}^2}{D}\,\frac{w^2}{c^2}\,(K_{xy}/i)$$

$$D \equiv \left(-K_z^2 + \frac{w^2}{c^2}K_R\right)\left(-K_z^2 + \frac{w^2}{c^2}K_L\right)$$

$$h_{1,2} \equiv \frac{(K_{xy}/i)\,K_{zz}/K_{xx}}{-K_z^2 + \frac{w^2}{c^2}\,\frac{K_R K_L}{K_{xx}} - \rho_{1,2}^2}$$

and J_1 is the first order Bessel function of the first kind. The primes represent derivatives with respect to the arguments.

For $a \leq r \leq b$ the fields are given by[15]

$$E_z = C\,J_1(\rho_3 r) + D(\rho_4 r) + E\,Y_1(\rho_3 r) + F\,Y_1(\rho_4 r)$$

$$E_\theta = C\left[i\ell_4\,\frac{J_1(\rho_3 r)}{r} + L_4\rho_3\,J_1'(\rho_3 r)\right]$$
$$+ D\left[i\ell_3\,\frac{J_1(\rho_4 r)}{r} + L_3\rho_4\,J_1'(\rho_4 r)\right]$$
$$+ E\left[i\ell_4\,\frac{Y_1(\rho_3 r)}{r} + L_4\rho_3\,Y_1'(\rho_3 r)\right]$$
$$+ F\left[i\ell_3\,\frac{Y_1(\rho_4 r)}{r} + L_3\rho_4\,Y_1'(\rho_4 r)\right]$$

$$H_z = C\, h_3\, J_1(\rho_3 r) + D\, h_4\, J_1(\rho_4 r)$$
$$+ E\, h_3\, Y_1(\rho_3 r) + F\, h_4\, Y_1(\rho_4 r)$$
$$H_\theta = C\left[i y_4 \frac{J_1(\rho_3 r)}{r} + Y_4 \rho_3 J_1'(\rho_3 r)\right]$$
$$+ D\left[i y_3 \frac{J_1(\rho_4 r)}{r} + Y_3 \rho_4 J_1'(\rho_4 r)\right]$$
$$+ E\left[i y_4 \frac{Y_1(\rho_3 r)}{r} + Y_4 \rho_3 Y_1'(\rho_3 r)\right]$$
$$+ F\left[i y_3 \frac{Y_1(\rho_4 r)}{r} + Y_3 \rho_4 Y_1'(\rho_4 r)\right]$$

where C through F are additional unknown constants, Y_1 is the first order Bessel function of the second kind, and ℓ_3, ℓ_4 etc. are similarly defined as ℓ_1, ℓ_2 etc.

To express the fields in a two density plasma, six unknown constants are thus required. However, there are two boundary conditions. The tangential electric field must vanish at the wall of the perfectly conducting waveguide and the tangential electric and magnetic fields must be continuous at the boundary between the two regions of different density. The boundary conditions give six algebraic equations relating the six unknown constants A through F. A trial axial wavenumber k_z is used to calculate the trial perpendicular wavenumbers p from equation (41.) The determinant of the matrix X relating the six unknowns must vanish upon the use of the correct k_z. The repeated trials were performed on the Queens College Sigma 7 computer. The elements of the matrix X whose determinant must vanish for the correct solution are

$$X_{11} = J_1(p_1 a)$$

$$X_{21} = h_1 J_1(p_1 a)$$

$$X_{31} = i \ell_2 J_1(p_1 a)/a + L_2 p_1 J_1'(p_1 a)$$

$$X_{41} = i \gamma_2 J_1(p_1 a)/a + \Upsilon_2 p_1 J_1'(p_1 a)$$

$$X_{51} = 0$$

$$X_{61} = 0$$

$$X_{12} = J_1(p_2 a)$$

$$X_{22} = h_2 J_1(p_2 a)$$

$$X_{32} = i \ell_1 J_1(p_2 a)/a + L_1 p_2 J_1'(p_2 a)$$

$$X_{42} = i \gamma_1 J_1(p_2 a)/a + \Upsilon_1 p_2 J_1'(p_2 a)$$

$$X_{52} = 0$$

$$X_{62} = 0$$

$$X_{13} = -J_1(p_3 a)$$

$$X_{23} = -h_3 J_1(p_3 a)$$

$$X_{33} = -i \ell_4 J_1(p_3 a)/a - L_4 p_3 J_1'(p_3 a)$$

$$X_{43} = -i \gamma_4 J_1(p_3 a)/a - \Upsilon_4 p_3 J_1'(p_3 a)$$

$$X_{53} = J_1(p_3 b)$$

$$X_{63} = i \ell_4 J_1(p_3 b)/b + L_4 p_3 J_1'(p_3 b)$$

$$X_{14} = -J_1(p_4 a)$$

$$X_{24} = -h_4 J_1(p_4 a)$$

$$X_{34} = -i \ell_3 J_1(p_4 a)/a - L_3 p_4 J_1'(p_4 a)$$

$$X_{44} = -i\eta_3 J_1(p_4 a)/a - Y_3 p_4 J_1'(p_4 a)$$

$$X_{54} = J_1(p_4 b)$$

$$X_{64} = i\ell_3 J_1(p_4 b)/b + L_3 p_4 J_1'(p_4 b)$$

$$X_{15} = -Y_1(p_3 a)$$

$$X_{25} = -h_3 Y_1(p_3 a)$$

$$X_{35} = -i\ell_4 Y_1(p_3 a)/a - L_4 p_3 Y_1'(p_3 a)$$

$$X_{45} = -i\eta_4 Y_1(p_3 a)/a - Y_4 p_3 Y_1'(p_3 a)$$

$$X_{55} = Y_1(p_3 b)$$

$$X_{65} = i\ell_4 Y_1(p_3 b)/b + L_4 p_3 Y_1'(p_3 b)$$

$$X_{16} = -Y_1(p_4 a)$$

$$X_{26} = -h_4 Y_1(p_4 a)$$

$$X_{36} = -i\ell_3 Y_1(p_4 a)/a - L_3 p_4 Y_1'(p_4 a)$$

$$X_{46} = -i\eta_3 Y_1(p_4 a)/a - Y_3 p_4 Y_1'(p_4 a)$$

$$X_{56} = Y_1(p_4 b)$$

$$X_{66} = i\ell_3 Y_1(p_4 b)/b + L_3 p_4 Y_1'(p_4 b)$$

Provision is made in the computer program to express the derivatives of the Bessel functions in terms of the Bessel functions themselves. For example $xJ_1'(x)=J_1(x)-xJ_2(x)$. Provisions are also made to use the appropriate modified Bessel functions when the arguments are imaginary; any or all of the perpendicular wavenumbers p may for certain conditions become purely imaginary.

The results of the calculations are shown in Figure 39. For $n_1 = n_2$ and b/a=2 the uniform result is reproduced. During the initial phase of the experiment $n_1 > n_2$. The density falls off as one goes off axis. Here b/a=2 is taken as typical and n_1 is fixed at 2×10^{11}/cc. Reducing the outer density to zero still does not allow propagation to occur. The loading of plasma on axis prevents propagation.

During the second phase of the experiment $n_1 < n_2$. Again b/a=2 is taken as typical. n_2 is fixed at 2×10^{11}/cc. As the inner density n_1 is reduced to zero, the wave eventually can propagate but only for n_1 less than 1.2×10^{10}/cc. Field profiles for this case are not appreciably different than those of the uniform density case.

Letting the size of the inner lower density region vary is shown in Figure 40 for n_1=5 and 7×10^{10}/cc. For propagating wave solutions the inner density must be below 7 and occupy a large region of the waveguide cross section.

In conclusion, the two density model for the observed perpendicular density gradients explains neither the transmission nor the field profiles observed here.

FIGURE CAPTIONS

Fig. 39. The wavenumber squared for the left wave is again plotted versus electron density with the additional effect of an inner density n_1 from r=0 to r=a and an outer density n_2 from r=a to r=b (the waveguide radius.) The three curves are for $n_1 = n_2$, $n_1 = 2 \times 10^{+11}$ /cc and n_2 varied, and for $n_2 = 2 \times 10^{+11}$ /cc and n_1 varied.

Fig. 40. The same as Fig. 39 but with $n_2 = 2 \times 10^{+11}$ /cc and a/b varied.

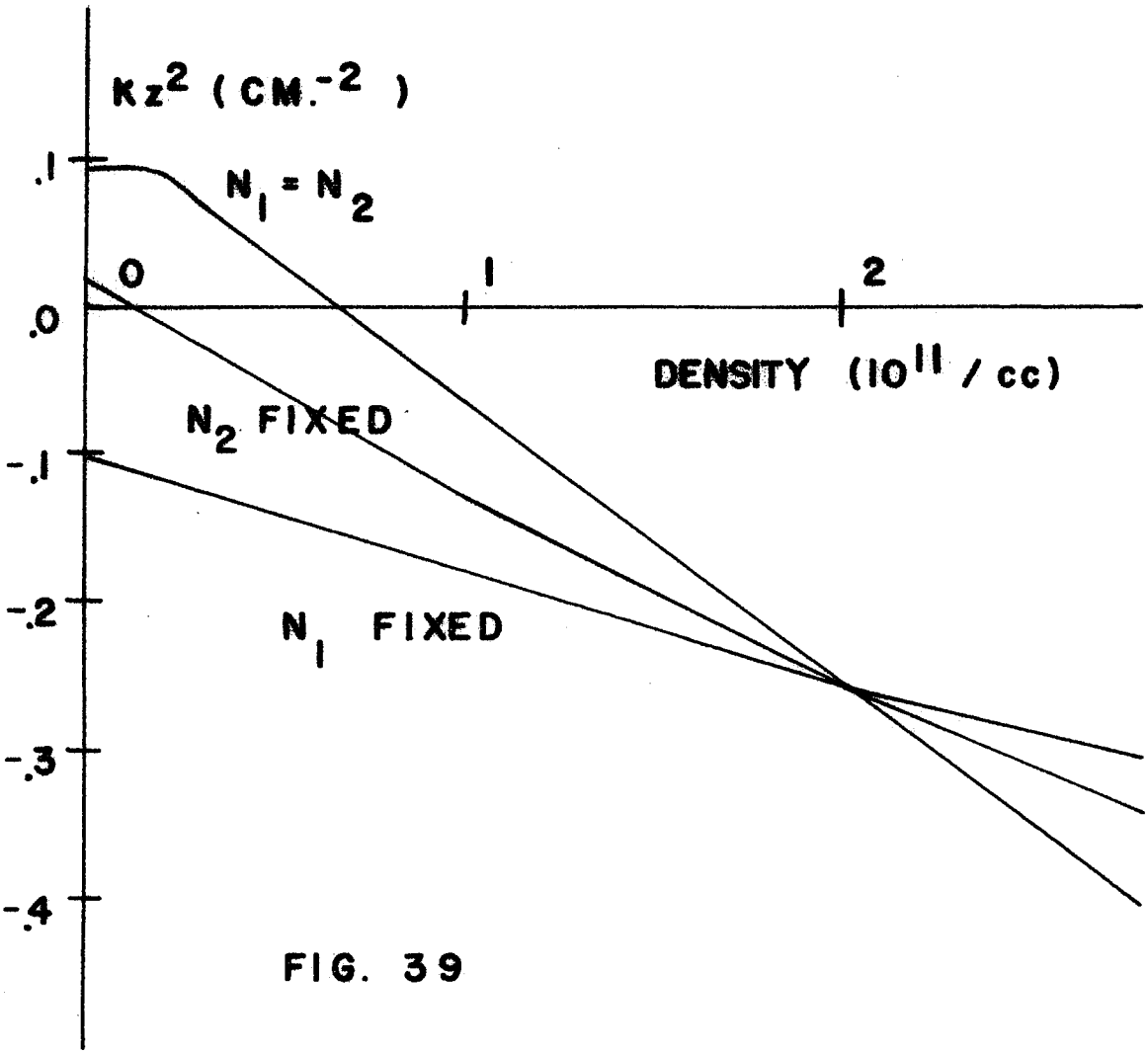

FIG. 39

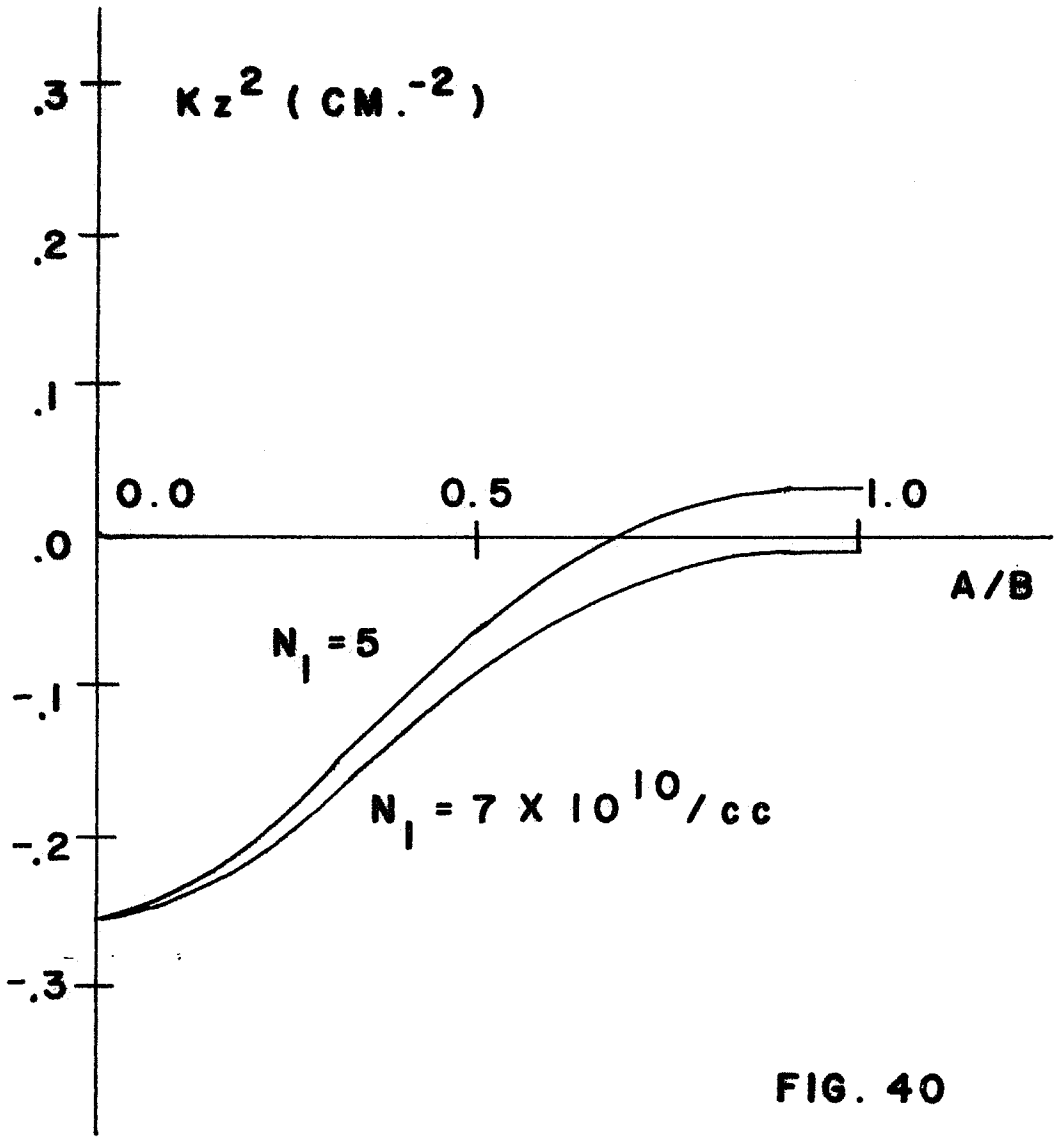

FIG. 40

5. REFERENCES

1. T. Stix, The Theory of Plasma Waves, McGraw-Hill Book Co. (1962) pp. 9-12.

2. G. Schmidt, The Physics of High Temperature Plasmas, Academic Press (1966) pp. 57-68, 237-244.

3. N.A. Krall and A.W. Trivelpiece, Principles of Plasma Physics, McGraw-Hill Book Co. (1973) pp. 22-23.

4. J.E. Scharer, Physics of Fluids 10, 652 (1967).

5. B.D. Fried and S.D. Conte, The Plasma Dispersion Function, Academic Press (1961).

6. B.D. McVey and J.E. Scharer, Physics of Fluids 17, 142 (1974).

7. A. Iiyoshi et al, Physics of Fluids 10, 749 (1967).

8. G. Schmidt, pp. 244-248.

9. J. Marsh, Physics of Fluids 15, 647 (1972).

10. W.P. Allis et al, Waves in Anisotropic Plasmas, M.I.T. Press (1962) pp. 132-178, 226-228.

11. G. Kent and E. Mendelovicz, Plasma Science PS-2, 35 (1973).

13. D.G. Swanson, Physics of Fluids 10, 428 (1967).

14. L.I. Schiff, Quantum Mechanics, McGraw-Hill Book Co. (1968) pp. 268-279.

15. W.P. Allis et al, pp. 236-240.

APPENDIX B - DIAGNOSTICS

1. MICROWAVE INTERFEROMETER

The average plasma density n along a given path length can be obtained from the phase shift induced by the plasma in the ordinary mode when the plasma density builds up.

Two k-band microwave horns ($f \approx 20$ GHz) are inserted in opposite faces of the cylindrical waveguide at the center of the mirror machine. A k-band signal is split up. One part of amplitude A is sent directly into a magic tee. The second part of amplitude B is transmitted between the two horns across the initially vacuous waveguide. A and B are added in one arm of the magic tee and are subtracted in the second. If Θ is the phase difference between A and B then the powers in the two arms are given by $A^2 + B^2 + 2AB\cos\Theta$ and $A^2 + B^2 - 2AB\cos\Theta$. Initially A and B are adjusted to be equal in amplitude and Θ is adjusted to be zero.

The ordinary mode across the static magnetic field has its electric field vector along the field, induces electron motion along $\vec{B}_o$, and thus to first order is unaffected by the field. The dispersion relation is given by

$$\frac{c^2 p^2}{\omega^2} = 1 - \frac{\omega_p^2}{\omega^2} \tag{49}$$

where p is the wavenumber. If $\omega_p^2 \ll \omega^2$ (here $f_p \approx 4$ GHz and $f \approx 20$ GHz) then the index of refraction becomes

$$\frac{cp}{\omega} \approx 1 - \frac{1}{2}\frac{\omega_p^2}{\omega^2} \tag{50}$$

The plasma increases the wavelength slightly when it builds up. This induces a phase shift $\Delta\Theta$ in the transmitted signal across the waveguide which in turn changes the power levels in the two arms of the magic tee.

The average density for a path length of 2a (a is the waveguide radius) can be written as[2]

$$\overline{N}_{1/cc} = \frac{118.4\ f_{cps}\ \Delta\theta_{RADIANS}}{2a_{cm.}} \qquad (51)$$

By monitoring the power levels in the two branches of the magic tee as well as the transmitted power by itself, the phase shift induced by the plasma at different times can be measured and from this the average plasma density.

Frequencies of 19.775 GHz and 22.000 GHz are used for comparison. The average density before and after absorption was calculated for typical experimental conditions. At 19.775 GHz the density before was found to be $(2.6 \pm 0.5) \times 10^{+11}$ /cc and the density after was $(3.3 \pm 0.2) \times 10^{+11}$ /cc. At 22.000 GHz the density before was found to be $(2.2 \pm 0.8) \times 10^{+11}$ /cc and the density after was $(2.9 \pm 1.0) \times 10^{+11}$ /cc.

The results were very reproducible and the uncertainties indicated are due to the reading errors in the oscilloscope traces (maximum branch of the magic tee, minimum branch, and transmitted signal.)

In all cases the average electron density was found to be greater than $2 \times 10^{+11}$ /cc. This represents an ionization of only a few percent of the available neutral hydrogen atoms. The mean average electron density from five different frequency trials is $(2.7 \pm 0.3) \times 10^{11}$/cc before absorption and $(3.0 \pm 0.4) \times 10^{11}$/cc after absorption. The uncertainties indicated are the mean deviations of the five trials at different interferometer frequencies.

2. LANGMUIR PROBES

To measure the local plasma density and temperature, Langmuir probes are used. The probe is made of a short circular cylindrical wire exposed to the plasma. It is connected to a DC source whose voltage V can bias the probe positive or negative. The plasma density and temperature can be measured from the current response of the probe at different voltages.

Even if Te=Ti the electrons will arrive at an unbiased probe at a much faster rate than the ions because of their higher thermal speeds ($m_e \ll m_i$). This sets up a negative space charge which repels further electrons and attracts more ions. A sheath forms about the probe.

When V is made very negative, effectively all electrons are repelled and only ions are collected. The random current of ions passing through the probe area A is[3]

$$I_i = \frac{A N_i e}{4} \left(\frac{2 K_B T_i}{m_i} \right)^{1/2} \tag{52}$$

However the existence of the sheath increases the effective collecting area of the probe. For Ti≪Te, the current can be corrected as[4]

$$I_i \approx 0.4 A N_i e \left(\frac{2 K_B T_e}{m_i} \right)^{1/2} \tag{53}$$

Knowing the saturated ion current Ii, the physical area of the probe A, and Te would give the density n.

The electron temperature Te can be determined by biasing the probe more and more positively. For a Maxwellian electron distribution the density and thus current should go as

$$I_e = I_o \exp\left(-\frac{eV}{K_B T_e}\right) \tag{54}$$

until electron saturation is reached and space charge limits the electron current to the random electron collection where all ions are repelled.

Thus from the ion saturation current n can be found knowing Te and Te can be found from a log-linear plot of I versus V where the curve is linear.

The obstacle in doing this is the prescence of the strong static magnetic field which limits the random collection of the charged particles. The addition of the magnetic field cannot change the state of thermodynamic equilibrium (provided it exists) so the plot of log I vs. V should still have a linear region to give Te, but the plasma density will tend to be measured as lower than it really is because of the reduced ion saturation current.

By using a very thin probe of radius 0.08 mm and length 2.3 mm, the ion Larmor radius can be made larger than the probe radius. This allows the collection of ions with little effect due to the static magnetic field. For 1/20 ev ions the ion Larmor radius is about 0.3 mm. The problem then arises that the sheath radius becomes much larger than the probe radius and thin sheath theory can no longer be used.

In the case of a thick sheath not all particles entering the sheath will be collected because of orbital motions. From fundamental conservation laws it can be shown that[5]

$$I_i^2 = \frac{4}{\pi} A^2 j_r^2 \left(1 - \frac{eV}{K_B T_i}\right) \tag{55}$$

where A is the physical area of the probe and j_r is the random current density

$$j_r = 0.5 N_i e \left(\frac{2K_B T_i}{\pi m_i}\right)^{1/2} \tag{56}$$

There is thus a linear region where I^2 vs. V has a slope S.

$$S = \frac{2}{\pi^2} A^2 \frac{e^3}{m_i} N_i^2 \qquad (57)$$

This slope is independent of Te or Ti. From the measured slope S the plasma density n can be determined.

Two Langmuir probes were used. One radial probe could be lowered through the waveguide wall at z=0 and sample any position from r=0 to r=4.39 cm (at the waveguide wall.) Alumina insulates the wire from the plasma except at the end. A second axial Langmuir probe was inserted at the end of the chamber. This could be positioned at different axial positions z and was swivelable at the vacuum feed-through so as to be able to sample different radial positions r for different z. The axial probe was given a 1 cm dogleg so the current would be collected with the probe axis perpendicular to the magnetic field.

Figure 41 shows plots of I vs. V and I^2 vs. V both before and after absorption. The radial probe was 1.25 cm from the waveguide wall.

Figure 42 shows plots of log I vs. V both before and after absorption. Electron current alone is plotted here by adding I to the small ion saturation current.

The density before and after absorption was found to be $1.2 \times 10^{+11}$ /cc and $2.1 \times 10^{+11}$ /cc respectively. This does not indicate a doubling of density but only a change in the density profile. By taking the radial average of the ion saturation current , the average density can be seen to change very little from before to after absorption.

The temperature before and after was found to be 6.6 ev and 10 ev respectively. This does represent a 50% heating after the absorption as can be shown from the diamagnetic coil response to be considered in the next section.

The axial Langmuir probe obtained similar results. The average density at the center of the machine is about $2 \times 10^{+11}$ /cc. This is in

FIGURE CAPTIONS

Fig. 41. The radial Langmuir probe current in milliamperes as a function of potential difference applied in volts is plotted both before and after the absorption of the left wave. The ion current squared is also indicated. The probe was located 1.25 cm from the waveguide wall.

Fig. 42. Electron current in milliamperes on a log scale is plotted versus applied potential difference in volts on a linear scale. The points are taken from Fig. 41.

FIG. 41

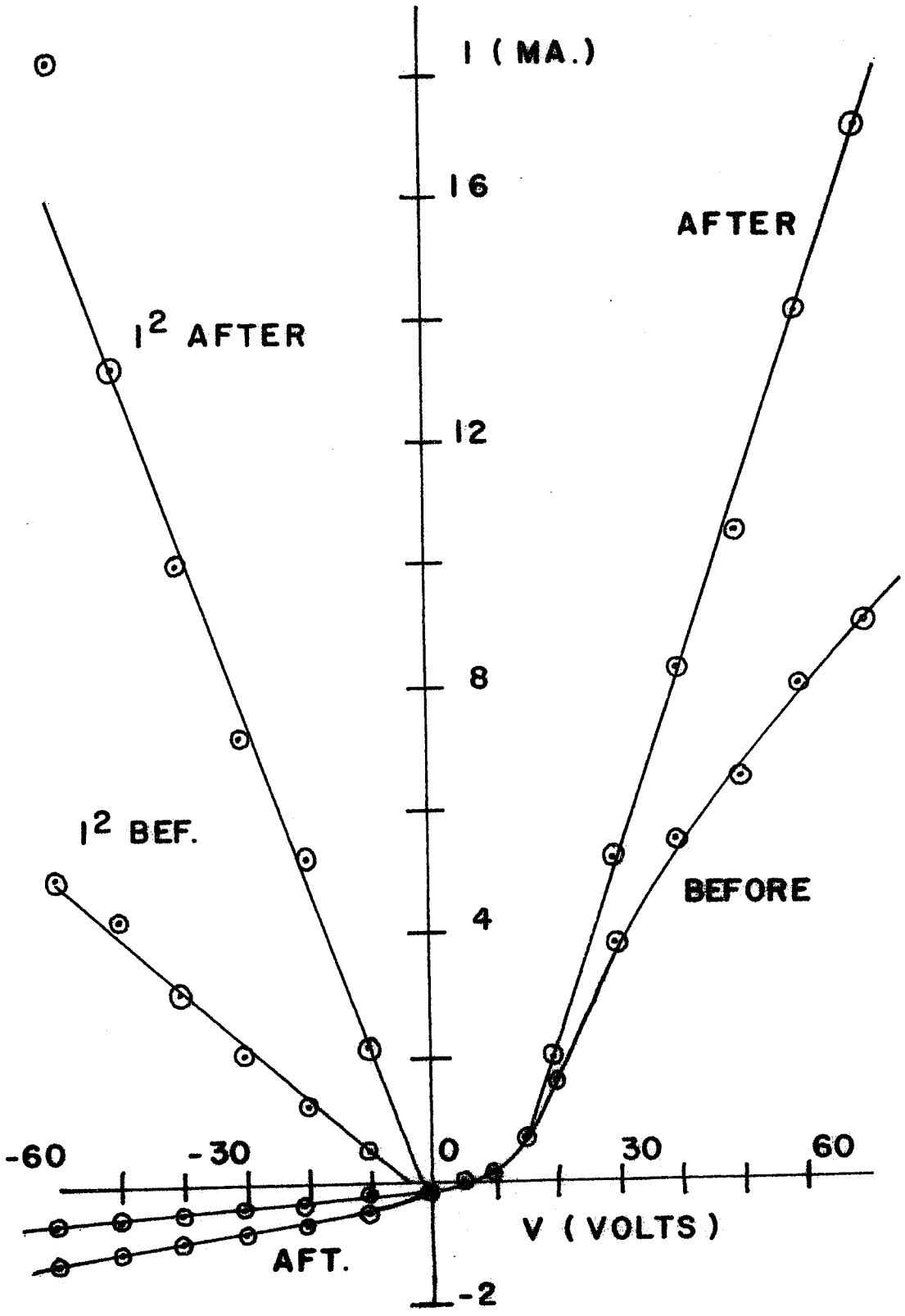
I (MA.)
16
12
8
4
-2
AFTER
I^2 AFTER
I^2 BEF.
BEFORE
-60
-30
0
30
60
V (VOLTS)
AFT.

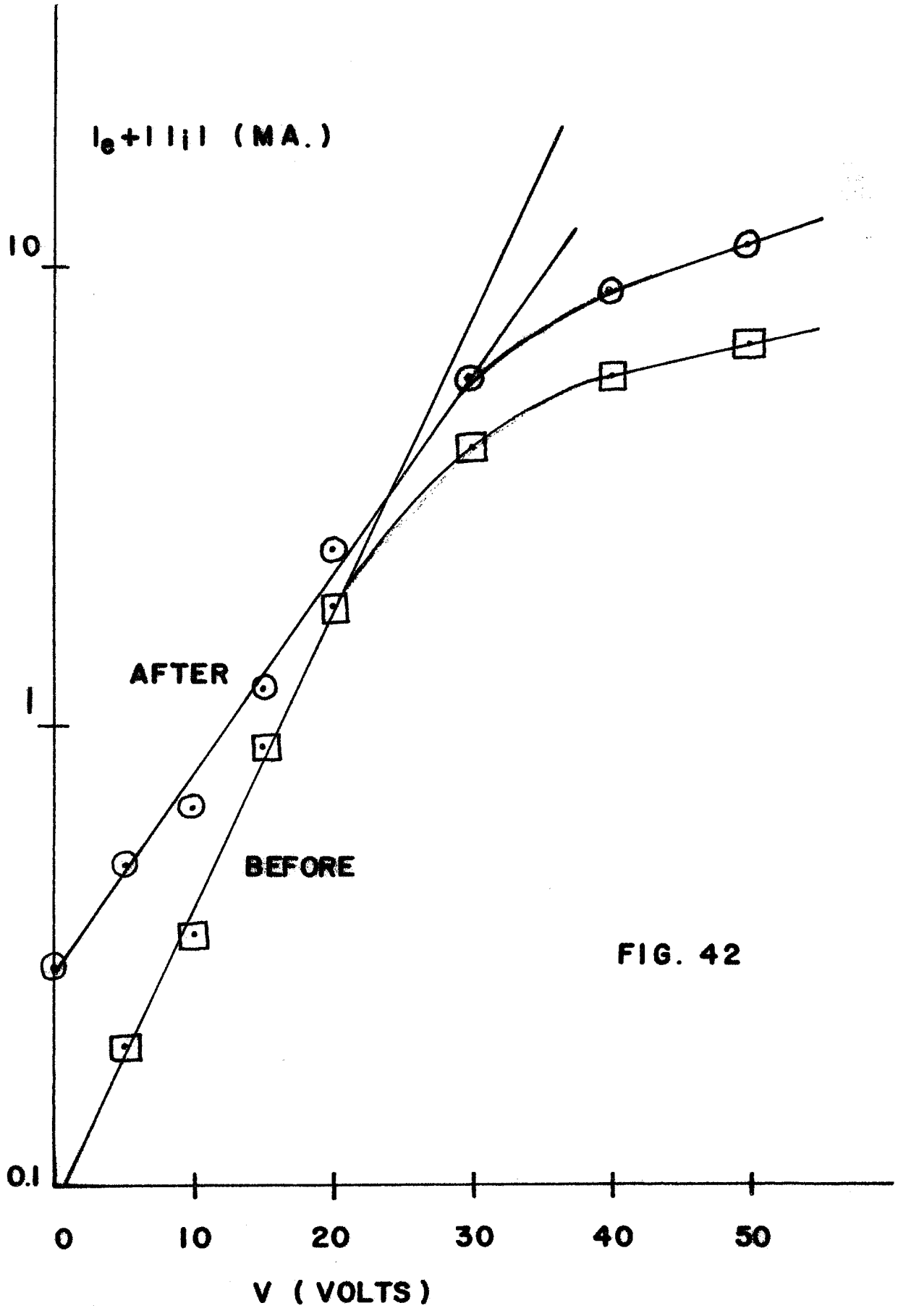

FIG. 42

good agreement with the density obtained from the microwave interferometer and at no radial position does the density fall below the cutoff density for the left wave.

The electron temperature was found to drop off by about 30% from the waveguide axis to the waveguide walls.

3. DIAMAGNETIC COIL

A coil of 100 turns is wrapped around the waveguide at z=0. When the plasma density builds up, electrons gyrating about the static magnetic field induce a diamagnetic change in the magnetic flux threading the coil. An emf results of [6]

$$\mathcal{E}(t) = \mu_0 \frac{NA}{B_0} \frac{d p_\perp(t)}{dt} \tag{58}$$

where N is the number of turns, A is the area of the coil, $p_\perp$ is the perpendicular plasma pressure ($p_\perp = n k_B T_{e_\perp}$) and Bo is the magnitude of the static magnetic field.

This voltage is connected to an RC integrating circuit of resistance R and capacitance C in series. Provided that the self-impedance ωL of the coil is much less than R and that times of interest t are much less than the time constant of the integrating circuit (RC), the output voltage across the capacitor is given as [7]

$$V(t) = \frac{\mu_0 NA}{RC\, B_0} p_\perp(t) \tag{59}$$

Here $\omega L \approx 2500\,\Omega$ at the ion acoustic frequency of 75 KHz. The skin depth of the stainless steel liner at this frequency is several times the liner thickness so that the signal should be little affected by the liner. R is 0.1 MΩ which is 40 times ωL and RC for C=0.001 μf is 0.1 msec. Thus any changes taking place in times less than 0.1 msec (such as the density modulations due to ion acoustic waves) should be well received.

The voltage response before absorption is typically 40 millivolts which gives $p_\perp$ as 0.45 N/M^2 . Using Te of 8 ev from the Langmuir

probe gives the average density as $3.5 \times 10^{+11}$ /cc. By integrating over the waveguide area with the plasma density profile determined by Langmuir probe the lowest density is found to be $2.7 \times 10^{+11}$ /cc with an average density of $3.4 \times 10^{+11}$ /cc.

These values depend on the $Te_{\perp}$ chosen. If $Te_{\perp} > Te_{//}$, as for a mirror machine, than the 8 ev used may be too low and thus the density of $3.4 \times 10^{+11}$ /cc obtained is too high. Still the value for n is close to the previous determinations of the density and acts as a further confirmation that the density of the plasma is well above the cutoff density for the left wave.

After absorption the diamagnetic signal increases up to 50%. With the same average density this indicates a 50% rise in the perpendicular electron temperature which agrees with the temperature rise determined by Langmuir probe.

It is appropriate at this point in the thesis to compare the different values and their uncertainties for the plasma density obtained by the three different methods (Langmuir probe, diamagnetic coil, and microwave interferometer.) The Langmuir probe gives the lowest value of plasma density, typically about 2×10^{11}/cc. This is about three times the cutoff density of the left wave. The ion saturation current collected by the probe should be reduced by the static magnetic field bending the ions around it. This effect leads to a lower density measured than actually exists. The effect can be reduced by making the probe radius (a) much less than the ion Larmor radius ρ_i. Here $\rho_i \approx$ 3 - 4a. The density determined from the probe should be good to about $\pm$50%, but because the magnetic field tends to make the density measured less than it actually is, it is much more likely that the average plasma density is greater than 2×10^{11}/cc than less.

The diamagnetic coil gives an average density of about 3.4×10^{11} /cc when an average perpendicular electron temperature of 8 ev (as determined by Langmuir probe) is used. The temperature from the Langmuir probe should be good to at least $\pm$25%. If the electron temperature is isotropic than the perpendicular temperature is that measured by the Langmuir probe and the density measured by the diamagnetic coil should be good to within $\pm$25%. However, in ECR produced plasmas the perpendicular temperature $T_{\perp}$ is often greater than the parallel temperature

$T_{//}$. If $T_{\perp} \gg T_{//}$, then the current collected by the Langmuir probe is predominantly perpendicular and the temperature determined from the probe data should be $T_{\perp}$. Thus for either $T_{\perp} = T_{//}$ or $T_{\perp} \gg T_{//}$, the probe temperature gives $T_{\perp}$ and $\pm$25% (the uncertainty in measuring T_e from the Langmuir probe data) is a good estimate of the uncertainty in the density determined by the diamagnetic coil.

Another source of error in determining the density with the diamagnetic coil is due to the collisions of the spiralling electrons with the waveguide wall. The reflected electrons can be shown to set up a magnetic flux opposing that of the rest of the electrons. This reduces the induced current in the coil and makes the density obtained slightly less than it actually is. However the effect is of the order of the ratio of the density at the wall to the average density and thus should not be significant for this experiment.

The most reliable determination of the density should be that by the microwave interferometer. The average plasma density from this method was found to be 2.7×10^{11}/cc. The measurement depends on neither the static magnetic field nor the plasma temperatures providing that there is no serious misalignment of the horns. One problem occurs because the plasma acts like a diverging lens of index slightly less than one. This can reduce the transmitted signal through the plasma and can produce a false density shift in the magic tee. This is corrected for by monitoring changes in the transmitted power with a directional coupler. A second problem can occur with this method because of the multiple paths between the transmitting and receiving horns due to reflections in the waveguide. This effect should be minimal because of the directivity of the horns (most of the radiation goes straight across from one horn to the other) and the fact that the reflected paths are of longer distance and thus should have greater spatial attenuation than the direct path. The mean deviation in the density for 5 widely spread frequencies (19 to 25 GHz) is about $\pm$11%.

A check on the accuracy of the density measurements is the situation of Fig. 25 a where the plasma is underdense: the incident wave is of low power and fully penetrates the plasma. The measured and theoretical axial wavenumbers are in good agreenemt for the measured density obtained. (See p. 46.)

4. RADIO FREQUENCY PROBES

To sample the wave electric field an RF dipole probe is used. The probe has a dipole of 1.3 cm connected to 0.9 mm O.D. coaxial cable. The cable and probe are covered with alumina and epoxy so no metal is exposed to the plasma. Like the axial Langmuir probe the RF dipole probe is fed through a vacuum feed-through at the end of the chamber and can be drawn in and out to measure the voltage standing wave pattern and can be swiveled to measure the electric field profile.

In the vacuum guide at 2.45 GHz only the dominant TE_{11} mode can propagate.[9] The theoretical guide wavelength is 20.9 cm or the distance between two minima in the vacuum guide should be 10.5 cm. The measured wavelength from the standing wave pattern was indeed found to be 20.9 cm., so that the probe makes a good measurement of the axial field pattern.

By holding the probe vertical and sweeping in the horizontal direction to the walls E_θ can be measured. By sweeping the probe vertically Er can be profiled although the finite size of the probe keeps the position at the waveguide wall from being taken. Figure 43 shows the theoretical curves for E_θ and Er. The points are experimental. The square root of the power response in millivolts on the microwave crystal connected to the probe is taken as the electric field and has been normalized.

The experimental points for E_θ give a good fit to the curve, going to zero at the walls. The points for Er fall off faster than theoretically predicted but not to zero. The finite size of the probe undoubtably couples the E_θ and Er responses so that picking up just one component alone may be impossible. For the TE_{11} mode there is no Ez.

To sample the wave magnetic field the coax is bent into a single circular loop with the inner conductor welded to the outer jacket. The join is coated with epoxy so no plasma current can be picked up. The loop is 1 cm. in diameter and should couple to the oscillating wave magnetic field vibrating perpendicular to the loop. The probe is inserted in the same way as the RF dipole probe.

Knowing the input power into the vacuum waveguide, the power coupled to the loop at the VSWR maximum can be estimated as 180 milliwatts and compared to the received power of 160 milliwatts. If the probe were responding to the electric fields as well one would expect a greater response than predicted.

The standing wave pattern measured with this probe yields a guide wavelength of 21.6 cm, in reasonable agreement with the theoretical value of 20.9 cm.

The empty guide magnetic field profiles were measured in the same way with the RF loop probe as with the RF dipole probe the electric field profiles were recorded. Figure 44 shows the theoretical curves and the experimental points. Hr makes a good fit except near the wall. H_θ drops off too fast but does not go to zero as indeed it should not. A further complication here is the existence of an Hz for the TE_{11} mode which would tend to couple more off axis as the probe face turns slightly.

To insure that the RF loop probe couples principally to the wave magnetic fields and not to the wave electric fields a microwave cavity was built in which the TM_{010} mode is excited. In the vacuum waveguide with a TE_{11} mode Hr has the same profile as E_θ and one cannot be sure Hr is being profiled. In the TM_{010} mode the only fields are

$$E_z \sim J_0(2.405\, r/a) \tag{60}$$

$$H_\theta \sim J_1(2.405\, r/a) \tag{61}$$

Figure 45 shows the theoretical curves for Ez and H_θ with the experimental points for the probe oriented to couple H_θ. The points are again the square roots of the crystal rectified voltage after normalization. The probe enters from the left. After each insertion further into the cavity the cavity is retuned to account for the frequency shift induced by the prescence of the probe. No account was taken of

FIGURE CAPTIONS

Fig. 43. The normalized square roots of the vacuum response of the RF dipole probe are plotted as the electric field at different radial positions r. a is the guide radius. The curves are the theoretical empty guide fields for the TE_{11} mode.

Fig. 44. The normalized square roots of the vacuum response of the RF loop probe are plotted as the magnetic field at different radial positions r. a is the guide radius. The curves are the theoretical empty guide fields for the TE_{11} mode.

Fig. 45. The normalized square roots of the vacuum response of the loop probe at different radial positions r/a of the microwave cavity built for probe test are shown. The curves are the theoretical TM_{010} cavity fields. The loop probe was oriented to couple to the cavity magnetic field.

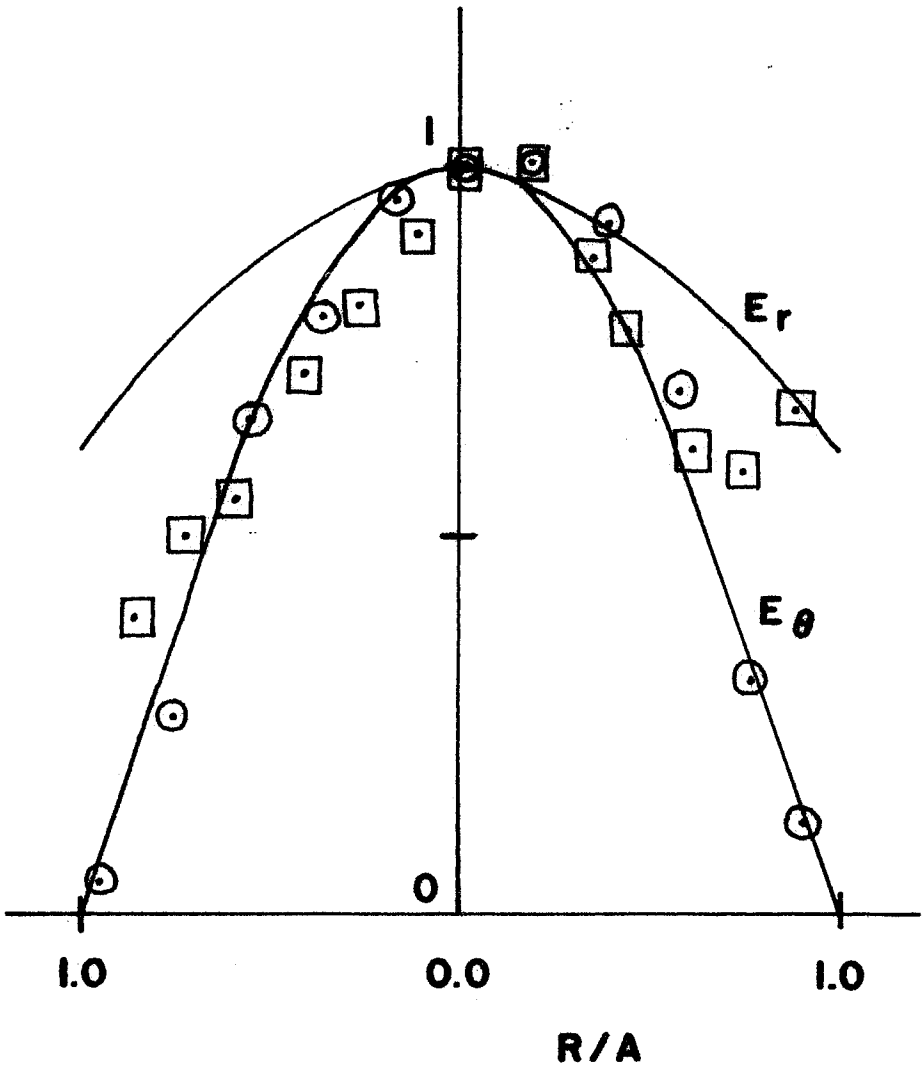

FIG. 43

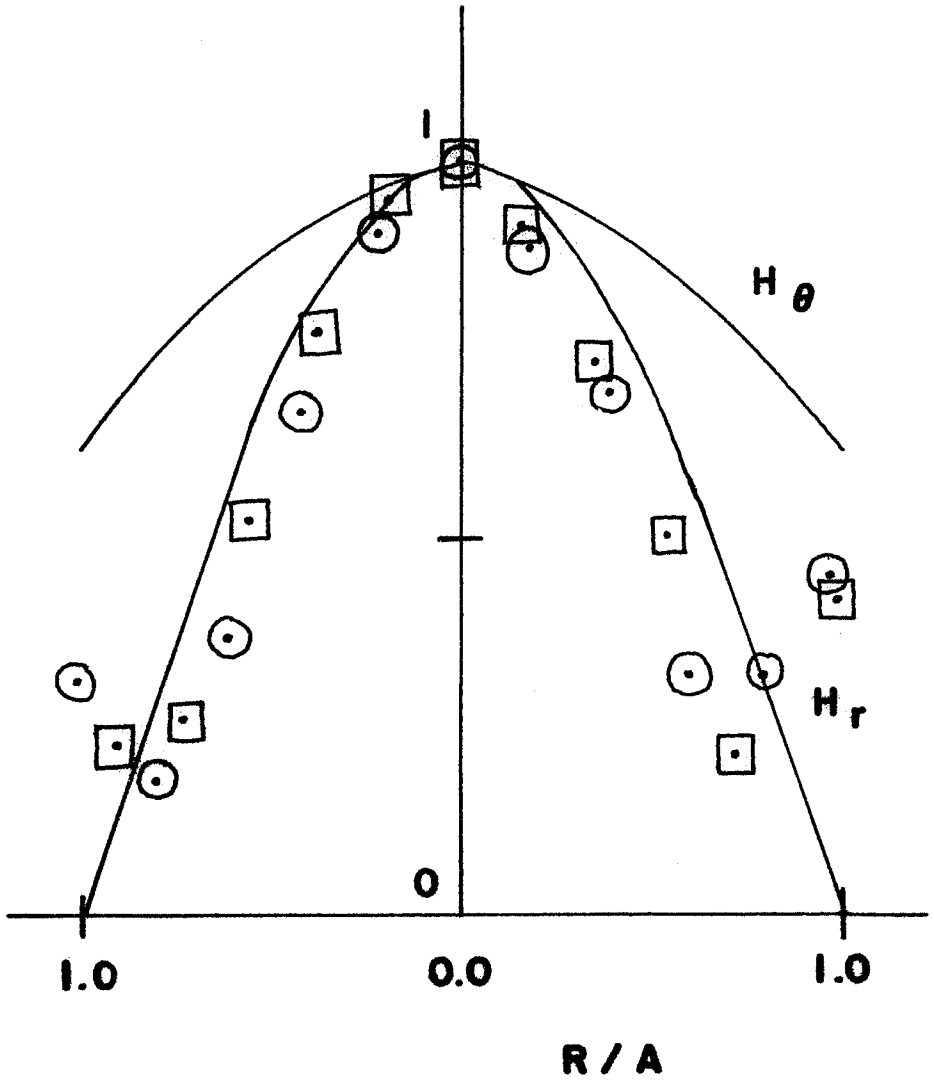

FIG. 44

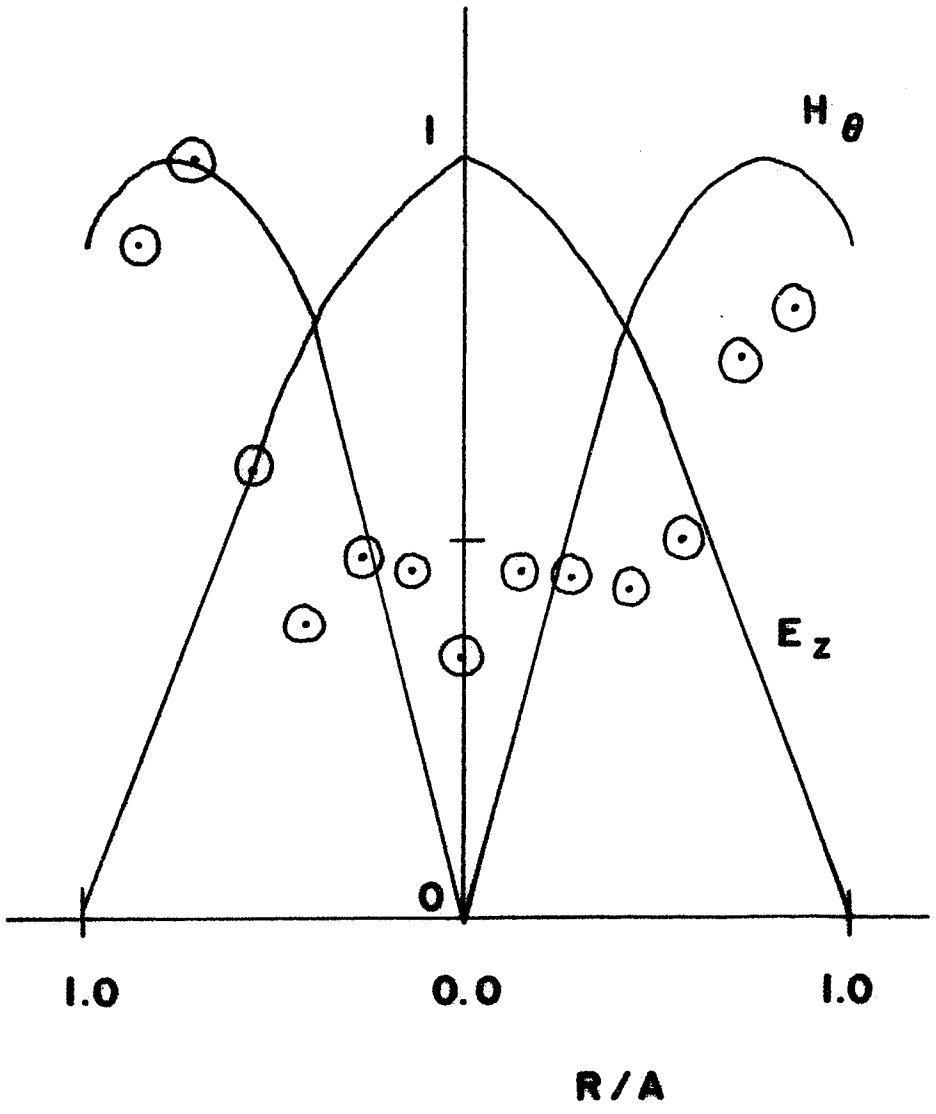

FIG. 45

the effect of the probe on the power coupled to the cavity or the disturbance of the probe on the cavity field structure.

The points are in fair agreement with the theoretical curve for H_θ. The signal drops to about 10% in power at the center of the cavity and not to zero. This may be due to the probe coupling to Ez which is a maximum at the center or to the probe disturbing the local cavity fields. In any case the loop RF probe can be used as an effective magnetic field probe even in the prescence of a strong wave electric field.

To monitor the frequencies being received by the radio frequency probes, the probe signal is fed into a microwave receiver without prior rectification. The video output at different frequency settings can be displayed on the oscilloscope. The receiver was found to be 26 db more sensitive than the crystal and is capable of resolution to $\pm$ 1 MHz.

To verify the reality of the excited waves around the plasma frequency after absorption of the left wave, the probe is moved axially to the region of the guide where the plasma density is down two orders of magnitude and the vacuum guide wavelength can once more be measured. The excited responses are still detected. This means that the plasma does not act as an enhancer of the probe response to weak levels at these frequencies coming out of the magnetron . The responses here are about 15 db above the noise level with no plasma produced.

The question of which wave (right or left) is being transmitted through the plasma can be answered with a spiral antenna consisting of a coaxially fed wire wound on a plexiglass cone (7.6 cm maximum diameter.) The antenna is wound to respond principally to the left wave. The experiment is run and a transmitted signal level from the spiral antenna is recorded. The direction of the static magnetic field is then reversed and the roles of the left and the right waves are switched. The new transmitted signal level drops about 10 db from the previous level, indicating that the left wave is the principal cause of the power transmitted through the plasma.

5. REFERENCES

1. R.E. Collin, Foundations for Microwave Engineering, McGraw-Hill Book Co. (1966) pp. 282-284.

2. M.A. Heald and C.B. Wharton, Plasma Diagnostics with Microwaves, John Wiley and Sons, Inc. (1965) pp. 120-123.

3. Ibid., pp. 378-380.

4. D. Bohm et al, Characteristics of Electrical Discharges in Magnetic Fields, McGraw-Hill Book Co. (1949).

5. R.H. Huddlestone and S.L. Leonard, Plasma Diagnostic Techniques, Academic Press (1965) pp. 128-131.

6. N.A. Krall and A.W. Trivelpiece, Principles of Plasma Physics, McGraw-Hill Book Co. (1973) pp. 628-629.

7. R.H. Huddlestone and S.L. Leonard, pp. 8-9.

8. H. Bradlow, private communication.

9. R.E. Collin, pp. 107-111.

10. J.D. Jackson, Classical Electrodynamics, John Wiley and Sons, Inc. (1962) pp. 252-254.

APPENDIX C - ESTIMATE OF THE ION TEMPERATURE

The ion temperature Ti can be estimated from the rate at which ions gain energy in collisions with electrons of temperature Te.[1]

$$\frac{dT_i}{dt} \approx \nu_{ei} \frac{m_e}{m_i} T_e \qquad (62)$$

ν_{ei} is the collision frequency between electrons and ions.[2] If the ion starts out at the room temperature of 1/40 ev, it will take about 0.050 msec to pass out of the mirror machine and in that time will acquire about 1/10 ev from the 8 ev electrons when $\nu_{ei} = 10^{+6}$ sec^{-1}. However, the increased speed would make the ion pass out of the machine sooner, thus reducing the energy gained. Therefore a conservative estimate of the ion temperature can be made of about 1/20 ev.

1. M.A. Uman, Introduction to Plasma Physics, McGraw-Hill Book Co. (1964) pp. 135-136.

2. N.A. Krall and A.W. Trivelpiece, Principles of Plasma Physics, McGraw-Hill Book Co. (1973) p. 294.